Department of Biotechnology and Chemical Technology

Phase and reaction equilibria in the modelling of hot water extraction, pulping and bleaching

Susanna Kuitunen

Aalto University

DOCTORAL DISSERTATIONS

Aalto University publication series
DOCTORAL DISSERTATIONS 37/2014

Phase and reaction equilibria in the modelling of hot water extraction, pulping and bleaching

Susanna Kuitunen

A doctoral dissertation completed for the degree of Doctor of Science (Technology) to be defended, with the permission of the Aalto University School of Chemical Technology, at a public examination held at the Auditorium KE2 (Komppa Auditorium) of the school on the 9th of May 2014 at 12.

Aalto University
School of Chemical Technology
Department of Biotechnology and Chemical Technology
Research Group of Chemical Engineering

Supervising professor
Professor Ville Alopaeus

Thesis advisor
Professor Ville Alopaeus

Preliminary examiners
Professor Tuomo Sainio, Lappeenranta University of Technology, Finland
Professor Hans Theliander, Chalmers University of Technology, Sweden

Opponent
Professor Tapio Salmi, Åbo Akademi, Finland

Aalto University publication series
DOCTORAL DISSERTATIONS 37/2014

© Susanna Kuitunen

ISBN 978-952-60-5617-3
ISBN 978-952-60-5618-0 (pdf)
ISSN-L 1799-4934
ISSN 1799-4934 (printed)
ISSN 1799-4942 (pdf)
http://urn.fi/URN:ISBN:978-952-60-5618-0

Unigrafia Oy
Helsinki 2014

Finland

441 697
Printed matter

Aalto University

Aalto University, P.O. Box 11000, FI-00076 Aalto www.aalto.fi

Abstract

Author
Susanna Kuitunen

Name of the doctoral dissertation
Phase and reaction equilibria in the modelling of hot water extraction, pulping and bleaching

Publisher School of Chemical Technology

Unit Department of Biotechnology and Chemical Technology

Series Aalto University publication series DOCTORAL DISSERTATIONS 37/2014

Field of research Chemical Engineering

Manuscript submitted 5 December 2013 **Date of the defence** 9 May 2014

Permission to publish granted (date) 12 March 2014 **Language** English

☐ **Monograph** ☒ **Article dissertation (summary + original articles)**

Abstract

This work is part of a joint effort to develop a pulping and bleaching simulator by utilizing fundamental thermodynamic, reaction kinetic, and mass transfer equations extensively. Carbohydrate and lignin polymers are modelled using monomeric pseudo-compounds having different properties and reactivity. Otherwise, well-known chemical compounds are used in the construction of chemical reaction libraries.

The main objective of the present work was to study the importance of modelling reaction and phase equilibria simultaneously with irreversible chemical reactions. Based on the mechanism presented in the literature, libraries consisting of irreversible reactions were constructed for the following cases: the hot water extraction of wood, kraft liquor impregnation into wood, lignin oxidation in oxygen delignification conditions, and alkaline extraction of chlorine dioxide delignified pulp.

By studying the above-mentioned cases, it was noted that many chemicals and substrates in lignin and in carbohydrates dissociate to the extent determined by their pKa value and pH. Depending on whether they are non-dissociated or dissociated, compounds react differently or they do not react at all. The evolution of pH is determined by the chemicals added, the composition of the fibres, and the reactions taking place. Furthermore, due to the cation exchange property of the fibres, the pH in the fibre wall liquid is lower than in the external liquid phase. As a conclusion, simultaneous modelling of all phenomena in a single platform provides the opportunity to study the reaction mechanisms in depth. Furthermore, the model, based on the real physico-chemical phenomena, is supposed to have more capabilities on predicting process behaviour than traditional correlation models.

The implementation of unit operation models (mixer, retention tower, and washer), from which various process sequences can be built, were also introduced. The laboratory experiments were simulated with a batch reactor model, which is capable of reproducing the pressure evolution in addition to chemical composition. Novel method for solving the phase and reaction equilibria was developed and demonstrated.

The simulations produce concentrations of pseudo-units and real chemical compounds thus enabling model validation with sophisticated analytical tools like nuclear magnetic resonance spectroscopy and capillary electrophoresis. In order to use standard every-day analyses (kappa number, intrinsic viscosity, TOC, etc.) for the model validation, the equations converting the chemical composition data into generally used engineering parameters were gathered and implemented.

Keywords modeling, reaction kinetics, mass transfer, phase equilibrium, Donnan equilibrium, reaction equilibrium, hot water extraction, pulping, bleaching

ISBN (printed) 978-952-60-5617-3 **ISBN (pdf)** 978-952-60-5618-0

ISSN-L 1799-4934 **ISSN (printed)** 1799-4934 **ISSN (pdf)** 1799-4942

Location of publisher Helsinki **Location of printing** Helsinki **Year** 2014

Pages 155 **urn** http://urn.fi/URN:ISBN:978-952-60-5618-0

Aalto-yliopisto

Aalto-yliopisto, PL 11000, 00076 Aalto www.aalto.fi

Tiivistelmä

Tekijä
Susanna Kuitunen

Väitöskirjan nimi
Faasi- ja reaktiotasapainojen mallinnuksesta kuumavesiuutossa, keitossa, ja valkaisussa

Julkaisija Kemian tekniikan korkeakoulu

Yksikkö Biotekniikan ja kemian tekniikan laitos

Sarja Aalto University publication series DOCTORAL DISSERTATIONS 37/2014

Tutkimusala Kemian laitetekniikka

Käsikirjoituksen pvm 05.12.2013 **Väitöspäivä** 09.05.2014

Julkaisuluvan myöntämispäivä 12.03.2014 **Kieli** Englanti

☐ **Monografia** ☒ **Yhdistelmäväitöskirja (yhteenveto-osa + erillisartikkelit)**

Tiivistelmä

Tämä työ on osa kokonaisuutta, jonka tavoitteena on kehittää sellun keiton ja valkaisun simulaatiomalli käyttäen perustavanlaatuisia termodynaamikan, reaktiokinetiikan ja aineensiirron yhtälöitä. Hiilihydraatti- ja ligniinipolymeerit kuvataan monomeerisilla pseudokomponenteilla, joilla on toisistaan eriävät ominaisuudet ja reaktiivisuus. Muuten pyritään siihen, että kemiallisista reaktioista kootussa kirjastossa käytetään oikeita kemiallisia yhdisteitä.

Tämän työn ensisijainen tavoite oli tutkia reaktio-ja faasitasapainojen mallinnuksen tärkeyttä mallinnettaessa kineettisiä reaktioita. Käyttäen kirjallisuudessa esitettyjä reaktiomekanismeja, kemiallisten reaktioiden kirjastot muodostettiin seuraaville prosesseille: puun kuumavesiuutto, kraft-keittoliuoksen imeytys puuhun, ligniinin hapetus happidelignifiointi olosuhteissa ja klooridioksidideligniﬁoidun sellun alkaliuutto.

Tutkittaessa edellä mainittuja prosesseja huomattiin, että monet kemikaalit ja ligniinissä ja hiilihydraateissa olevat ryhmät dissosioituvat asteelle, joka riippuu ryhmien pKa arvosta ja pH:sta. Riippuen siitä ovatko ryhmät dissosioituneita vai eivät, ne reagoivat eri tavoin tai eivät reagoi lainkaan. pH:n käyttäytyminen riippuu lisätyistä kemikaaleista, kuitujen kemiallisesta rakenteesta, ja reaktioista. Lisäksi, kuitujen ioninvaihtoilmiön vuoksi, pH kuituseinämään imeytyneessä nesteessä on alhaisempi kuin kuituseinämän ulkopuolella olevassa nesteessä.

Johtopäätöksenä voidaan todeta, että eri ilmiöiden yhtä aikainen mallinnus tarjoaa mahdollisuuden reaktiomekanismien syvälliselle tutkimiselle. Malli, joka perustuu todellisten fysikkalis-kemiallisten ilmiöiden kuvaamiselle, voidaan olettaa olevan parempi ennustamaan prosessin käyttäytymistä kuin perinteiset korrelaatiomallit.

Tässä työssä kuvattiin myös eri yksikköoperaatioiden (sekoitin, retentiotorni, pesuri), joista voidaan koota erilaisia prosessi-sekvenssejä, implementointia. Laboratoriokokeet simuloitiin käyttäen panosreaktorimallia, joka kemiallisen koostumuksen lisäksi simuloi myös paineen käyttäytymisen. Lisäksi esiteltiin uusi menetelmä faasi-ja reaktiotasapainojen ratkaisuun. Simuloinnit tuottavat todellisten rakenteiden ja aineiden konsentraatiot, jolloin mallin validointiin voidaan käyttää sofistikoituneita analyysimenetelmiä, kuten kapillaarielektroforeesia. Korrelaatiot, joiden avulla kemiallinen koostumus voidaan muuttaa yleisesti käytettyihin insinööriparametreihin, mahdollistavat myös jokapäiväisten analyysien (kappa-luku, viskositeetti, TOC, jne.) käytön mallin validoinnissa.

Avainsanat mallinnus, reaktiokinetiikka, aineensiirt, faasitasapaino, Donnan tasapaino, reaktiotasapaino, kuumavesiuutto, keitto, valkaisu

ISBN (painettu) 978-952-60-5617-3 **ISBN (pdf)** 978-952-60-5618-0

ISSN-L 1799-4934 **ISSN (painettu)** 1799-4934 **ISSN (pdf)** 1799-4942

Julkaisupaikka Helsinki **Painopaikka** Helsinki **Vuosi** 2014

Sivumäärä 155 **urn** http://urn.fi/URN:ISBN:978-952-60-5618-0

Preface

This thesis work was carried out at the Aalto University School of Chemical Technology in the research group of Chemical Engineering during 2003-2013.

I would like to thank Professors Juhani Aittamaa, Ville Alopaeus, and Tapani Vuorinen for giving me an opportunity to carry out the simulation model development in different projects. I hope that both industry and academia will find the simulation tool useful.

It has been my pleasure to work with many, many researchers, especially with Ville Tarvo, Tuula Lehtimaa, Anna Kalliola, Olesya Fearon, Vesa Nykänen, Juha Visuri, and Waqar Ahmad. Co-authors Erkki Räsänen, Pekka Tervola, Tarja Tamminen, Kaj Henricson, Tiina Liitiä, Stella Rovio, and Taina Ohra-aho are acknowledged for their advice and contributions.

I want to thank the research group staff for providing a cheerful and inspiring atmosphere. My thanks go to representatives of Metsä-Fibre, Stora Enso, Andritz, and VTT for their valuable encouragement, motivation, feedback, and ideas during the simulation model development.

The financial support from the National Technology Agency of Finland (TEKES), and from the industrial partners of ABLE, and the Finnish Bioeconomy Cluster (FIBIC) is acknowledged with gratitude.

Thanks to my family and relatives for your support. A loving thanks to my husband Tatu and my son Eemeli for your encouragement.

It is all about donating and receiving electrons... How hard can it be?

Espoo, March 23, 2014

Susanna Kuitunen

Contents

Preface i
Contents ii
List of publications iv
The author's contribution to the publications v
Additional publications vi
Notation viii
1.1 Abbreviations viii
1.2 Symbols viii
1.3 Greek letters ix
1.4 Superscripts x
1.5 Subscripts x
1. Introduction 1
2. Modelling of chemical composition 4
2.1 Phases 4
2.2 Chemical compounds 6
2.3 Engineering parameters 7
3. Modelling of equilibria and kinetics 11
3.1 Reversible reactions 12
3.2 Phase equilibrium 12
3.3 Computation of equilibrium constant (K) 14
3.4 Irreversible reactions 16
3.5 Mass transfer 17
3.6 Reaction and mass transfer rates used in unit operation models 19
3.7 Assumption of ideal mixture 20
3.8 Enthalpy 22
3.9 Equation of state 23
4. Unit operation models 24
4.1 Batch reactor 25
4.2 Retention tower 26

4.3 Pump / tank 28
4.4 Displacement washing 29
4.5 Heating and cooling in unit operation models 31
5. Numerical solution methods 33
5.1 Differential equation solver 33
5.2 Solving a unit operation model 33
5.3 Solving reaction and phase equilibria 35
5.3.1 From the system of equations 36
5.3.2 With rate-based approach 39
6. Case studies 45
7. Model parameters 47
8. Results and discussion 49
8.1 Effect of inert compounds on pH 49
8.2 Effect of buffering on pH 53
8.3 Effect of temperature and pressure on the reaction kinetics 55
8.4 Effect of phase and reaction equilibria on irreversible reactions 56
8.5 The reaction kinetic library for lignin and carbohydrate degradation with oxygen chemicals in alkaline conditions 65
9. Conclusions 73
10. Ideas for future research 75
References 76
Errata 83

List of publications

This thesis is based on the following publications, which are referred to in the text by the Roman numerals I-IV.

[I] Tarvo, V., Kuitunen, S., Lehtimaa, T., Tervola, P., Räsänen, E., Tamminen, T., Aittamaa, J., Vuorinen, T., Henricson, K., Modelling of chemical pulp bleaching, Nordic Pulp and Paper Research Journal, 2008. Vol. 23, pp. 91-101.

[II] Kuitunen, S., Vuorinen, T., Alopaeus, V., The role of Donnan effect in kraft liquor impregnation and hot water extraction, Holzforschung, 2013. Vol. 67, pp. 511-521.
DOI: 10.1515/hf-2012-0187

[III] Kuitunen, S., Kalliola, A., Tarvo, V., Tamminen, T., Rovio, S., Liitiä, T., Ohra-aho, T., Lehtimaa, T., Vuorinen, T., Alopaeus, V., Lignin oxidation mechanisms under oxygen delignification conditions. Part 3. Reaction pathways and modeling, Holzforschung, 2011. Vol. 65, pp. 587-599. DOI: 10.1515/hf.2011.100

[IV] Kuitunen, S., Tarvo, V., Liitiä, T., Rovio, S., Vuorinen, T., Alopaeus, V., Modelling of alkaline extraction chemistry and kinetics of softwood kraft pulp, Holzforschung, 2014. Published online ahead of print. DOI: 10.1515/hf-2013-0225

The author's contribution to the publications

[I] The author designed the models and programmed the simulator with the co-authors, and participated in writing the paper.

[II] The author developed the reaction scheme, performed the parameter optimization, analysed the results, and wrote the paper.

[III] The author developed the reaction scheme together with the co-authors, performed the parameter optimization, analysed the results, and wrote the paper.

[IV] The author developed the reaction scheme together with the co-authors, performed the parameter optimization, analysed the results, and wrote the paper.

Additional publications

Kalliola, A., Kuitunen, S., Liitiä, T., Rovio, S., Ohra-aho, T., Vuorinen, T., Tamminen, T., Lignin oxidation mechanisms under oxygen delignification conditions. Part 1. Results from direct analyses, Holzforschung, 2011. Vol. 65, pp. 567-574.

Rovio, S., Kuitunen, S., Ohra-aho, T., Alakurtti, S., Kalliola, A., Tamminen, T., Lignin oxidation mechanisms under oxygen delignification conditions. Part 2. Advanced methods for the detailed characterization of lignin oxidation mechanisms, Holzforschung, 2011. Vol. 65, pp. 575-585.

Kalliola, A., Kangas, P., Kuitunen, S., Simulating A/D stage bleaching chemistry, Poster presentation, 12th European Workshop on Lignocellulosics and Pulp (EWLP), Espoo, Finland, August 27-30, 2012.

Kuitunen, S., Pulkkinen, I., Alopaeus, V., Modeling of fiber swelling, Oral presentation, 5th International Colloquium on Eucalyptus Pulp, Porto Seguro, BA Brazil, May 9-12, 2011.

Kuitunen, S., Alopaeus, V., Robust method for solving reaction and phase equilibrium in aqueous wood fiber systems, Poster presentation, 9th European Congress of Chemical Engineering (ECCE9), Hague, Netherlands, April 21-25, 2013.

Visuri, J. A., Song, T., Kuitunen, S., Alopaeus, V., Model for Degradation of Galactoglucomannan in Hot Water Extraction Conditions, Industrial Engineering and Chemistry Research, 2012. Vol. 51, pp. 10338-10344.

Lehtimaa, T., Kuitunen, S., Tarvo, V., Vuorinen, T., Kinetics of aldehyde oxidation by chlorous acid, Industrial Engineering and Chemistry Research, 2010. Vol. 49, pp. 2688-2693.

Lehtimaa, T., Tarvo, V., Mortha, G., Kuitunen, S., Vuorinen, T., Reactions and kinetics of Cl(III) decomposition, Industrial Engineering and Chemistry Research, 2008. Vol. 47, pp. 5284 – 5290.

Tarvo, V., Lehtimaa, T., Kuitunen, S., Alopaeus, V., Vuorinen, T., Aittamaa, J., The kinetics and stoichiometry of the reaction between hypochlorous acid and chlorous acid in mildly acidic solution, Industrial Engineering and Chemistry Research, 2009. Vol. 48, pp. 6280 – 6286.

Nieminen, K., Kuitunen, S., Paananen, M., Sixta, H., Novel Insight into Lignin Degradation during Kraft Cooking, Industrial & Engineering Chemistry Research, 2014. Vol. 53, pp. 2614-2624.

Notation

1.1 Abbreviations

ACC	Accumulation
AOX	Absorbable organic halogen (mg Cl/kg water)
BR	Brightness (% of ISO)
CAS	Chemical Abstracts Services
COD	Chemical oxygen demand (mg O/kg water)
CSTR	Continuous stirred tank reactor
D_0	Chlorine dioxide delignification stage (1st chlorine dioxide stage)
DP	Degree of polymerization
FSP	Fibre Saturation Point (kg water/kg fibres)
GEN	Generation
GLE	Gas-liquid equilibrium
HexA	Hexenuronic acid
IN	Into
MeGlc	Methylglucuronic acid
OUT	Out
OX	Organic halogen bound to fibres (mg Cl/kg fibres)
OxEq	Oxidation equivalent (mol electrons/mol)
PFR	Plug flow reactor
RPM	Revolutions per minute (1/min)
TOC	Total organic carbon (mg C/kg water)

1.2 Symbols

a	Activity (-)
A	Area (m^2)
A_{457}	Absorbance at wave length 457 nm (-)
b	Width of the drum washer (m)
C_p	Constant pressure heat capacity (J/(K·mol))
d	Diameter (m)
D	Diffusion coefficient (m/s^2)
E	Potential (V)
f	Mass fraction (kg/kg), Fugacity (bars), Function
F	Faraday's constant (96485.309 C/mol)
g	Acceleration due to the gravitational field (m/s^2)
G	Gibbs free energy (J/mol)
h	Total enthalpy (J)
h_l	Height of a CSTR layer in drum washer model (m)
H	Enthalpy (J/mol)
I	Ionic strength (mol/kg water)
k	Reaction rate constant
k_{457}	Overall absorption (at wavelength 457 nm) coefficient

	(m^2/(kg fibres))
$k_{457,i}$	Compound specific absorption (at wavelength 457 nm) coefficient (m^2/mol)
k_La	Combined mass transfer coefficient (computed on liquid side) and mass transfer area (1/s)
K	Equilibrium constant
l	Thickness of the liquid film (m), Cuvette width (1 cm)
m	Molality (mol/kg water)
M	Elastic modulus (Pa)
n	Molar amount (mol)
$\dot{n}$	Molar flow (mol/s)
N	Flux (mol/(m^2·s))
p	Pressure (bar or Pa)
Q	Heating energy (J/s or J/m)
r	Rate (mol/s)
R	Universal gas constant (8.3144 J/(K·mol))
s_{457}	Scattering coefficient (m^2/(kg fibres))
S	Entropy (J/(K·mol))
T	Temperature (K)
u	Circumferential velocity (m/s)
w	Mass (kg)
v	Velocity (m/s)
V	Volume (m^3)
$\dot{V}$	Volume flow (m^3/s)
z	Charge number of an ion (-), Coordinate
x	Mole fraction (-), Coordinate

1.3 Greek letters

γ	Activity coefficient (-)
Δ	Change
ε	Porosity (-)
ε_W	Dielectric constant of water (-)
ε_{457}	Molar absorptivity at a light wavelength of 457 nm (dm^3/(mol·cm))
λ	Donnan lambda (-)
μ	Chemical potential (J/mol)
η	Liquid viscosity (Pa·s), Intrinsic viscosity (ml/g)
κ	Kappa number (ml/g)
ν	Molar volume (m^3/mol)
ξ	Stoichiometric coefficient
$\boldsymbol{\Xi}$	Stoichiometric matrix
π	The ratio of a circle's circumference to its diameter (~3.14159)
Π	Osmotic pressure (Pa)
ρ	Density (kg/m^3)
τ	Tortuosity (-), Retention time (s)
φ	Angle (°)

1.4 Superscripts

E	Liquid external to the fibre wall
F	Liquid bound to the fibre wall
G	Gas phase

1.5 Subscripts

Eff	Effective
F	Fibres
GLMT	Gas-liquid mass transfer
i,j,k,l	Indexing
IR	Irreversible reaction
LLMT	Liquid-liquid mass transfer
MT	Mass transfer
RR	Reversible reaction
W	Water

1. Introduction

Chemical pulp (sulphate or sulphite) is used, for example, in the production of graphic paper, board, and tissue. In 2012, the chemical pulp production in CEPI (*Confederation of European Paper Industry*) countries was 27 Mt, of which 7.5 Mt was produced in Finland (cepi 2013). The number of sulphate pulp mills in CEPI countries is 77, of which 17 are located in Finland.

During the recent years, the call for graphic paper has declined in the Western countries (Pöyry 2013). However, the production of tissue paper and packing board keeps rising and it is predicted to keep rising (Pöyry 2013). The indirect effect of the decline in graphic paper is the reduction in the availability of recycling paper, which also increases the need for virgin fibres, i.e. pulp (Pöyry 2013).

According to the annual report by the Finnish Forest Industries Federation (Jaatinen 2013), graphic paper production during the period of January – June (2013) in Finland was 3.8% less than in the corresponding period of 2012. However, paperboard production increased by 10.9% and pulp production by 4.4%. In the whole world, the production capacity of unbleached and bleached sulphate pulp is estimated to increase from 105.2 Mt (2012) to 112.8 Mt (2017) (FAO 2013).

According to FOEX, the price of PIX pulp, which is a benchmark index based on real trade information, increased during the past year by 14 % (Taloussanomat 2013). In order to obtain a rough estimate of the order of magnitude of the pulp business, the current total pulp production is multiplied by the present pulp price (887.34 USD/t), totalling 93 billion USD i.e. 69 billion € (Finland's budget is 54.1 billion €).

Although traditional pulp production is doing well at the moment, a lot of activities are going on in the field of "biorefinery" development (Ragauskas et al. 2006b). Biorefinery may be considered as a mill which produces biomass chemicals, transportation fuels, and energy in addition to traditional pulp and paper products. Biomass-based chemicals and fuels could replace products made from fossil raw materials. Ideas on integrating biofuel and pulp production have been reviewed, for instance, by Ragauskas et al. (2006a).

The design of modern pulp mills is based on the best available technology guidelines (BAT). Furthermore, during the last 20 years, a substantial reduction in the environmental load has taken place in pulp and paper mills: BOD reduction 80.5%, COD reduction 73.4%, and AOX reduction 92.6% (cepi 2013). These reductions are mainly due to the invention of the oxygen delignification stage, and the replacement of chlorine with chlorine dioxide.

Considering the fact that pulp mill performance has been developed for decades, it is likely that further development of the processes will become more and more difficult. It also seems that processes are becoming increasingly complicated, as the new biorefinery ideas are put into practice. To tackle the challenges, process simulation tools are often used for the optimization and design of existing and new processes.

The main constituents of wood are cellulose, hemicelluloses, and lignin. The goal of chemical pulping is to remove the lignin that glues the wood fibres together, with minimal cellulose and hemicellulose degradation. After pulping, the disintegrated fibres (i.e. pulp) contain some brownish-coloured lignin to be removed in bleaching by applying different chemicals consecutively and/or simultaneously. A number of reactions take place in the different bleaching stages, which determine the final pulp properties, the economy of the process, and the environmental load. The traditional approach to model the very complex set of reactions is to use correlation models. Usually, only the pulp properties, like kappa number and intrinsic viscosity, have been modelled and the changes in the filtrate composition have been ignored (Susilo and Bennington 2007). However, a few models that take changes in filtrate composition into consideration have also been developed (Zhang et al. 2007; Jain et al. 2008). In some studies, reaction and phase equilibria modelling have been combined with reaction kinetic modelling (Salminen et al. 2000; Räsänen et al. 2005; Ji 2007).

On the other hand, an extensive amount of knowledge concerning the lignin and carbohydrate reaction mechanism has been accumulated during several decades. This knowledge is based on experimental studies conducted with lignin and carbohydrate model compounds, which have a structure and properties similar to the actual structures in the fibres. Usage of model compounds in the experiments enables studies concerning a single reaction as well as other phenomena or properties.

On the basis of the discussion above, there is a need and opportunity for more comprehensive chemistry modelling of fibre line operations. In the present work, rigorous reaction chemistry modelling is combined with modelling of reaction and phase equilibria. The following case studies demonstrate different model features:

- Hot water extraction aims to extract hemicelluloses from wood using heat and water. Although an old existing technology, hot water extraction is one of the options in the new biorefinery designs.
- Kraft liquor impregnation is a process step before actual pulping. Wood chips are homogenously impregnated at low temperature with pulping chemicals.
- Lignin removal in oxygen delignification stage takes place through oxidation of lignin by oxygen. After pulping to a certain kappa number, the removal of lignin can be continued in a more selective way in the oxygen delignification stage. In order to better understand the lignin oxidation mechanism, oxidation of kraft lignin was studied.
- Alkaline extraction of chlorine dioxide delignified pulp removes the reacted lignin and improves the reactivity of the residual lignin in the following chlorine dioxide stage.

This thesis starts with a description of the approach used in modelling the chemical composition of wood/pulp and water systems, and how the chemical composition can be converted into generally used engineering parameters. After that, equations for solving the reaction and phase equilibria, in addition to reaction kinetics and mass transfer, are presented. Then, the practical aspects concerning the modelling, implementing, and solving of unit operation models are discussed. Finally, the case studies demonstrate the importance of including all the different models in one single simulation tool.

Previously, this modelling approach has been applied to the modelling of the chemistry of chlorine chemicals as presented in theses by Ville Tarvo (Tarvo 2010) and Tuula Lehtimaa (Lehtimaa 2010). The present work expands the model application to alkaline conditions and low ionic strength systems, in which the ion exchange effect is more pronounced. Furthermore, the oxygen/peroxide chemistry library and the unit operation models developed in the present work complement the previous work so that whole bleaching sequence can now be simulated.

2. Modelling of chemical composition

Wood fibres, which are the cells of trees, consist of three different kinds of polymer: cellulose, hemicelluloses, and lignin. Other minor chemical compounds are, for instance, extractives and metals. In wood, the fibres are bound together by lignin. In kraft pulping, the lignin holding the fibres together is solubilised and fibres are disintegrated. The kraft pulping chemicals are dissolved in water, and thus the product from kraft pulping is a suspension consisting of disintegrated wood fibres, water, residual chemicals, and the degradation products of wood. The mixture consisting of fibres and water is often called a pulp suspension. Pulp bleaching, which aims to remove the residual lignin from the pulp and convert the coloured structures into colourless ones, is conducted with a mixture of water and various chemicals. Oxygen is the only commonly used gaseous chemical.

In short, this chapter deals with the concept chosen for modelling the chemical composition of the pulp suspension. This topic is discussed in detail in paper [I], but is also dealt with in other papers ([II]-[IV]).

2.1 Phases

Based on previous modelling studies, for example Towers and Scallan (1996), the suspension of wood fibres, water, and gas is modelled to consist of the following phases (Figure 1):

A. Water bound to the fibre wall (***Fibre bound liquid phase***). The wood fibre wall is porous and absorbs a certain amount of water depending on its processing history. The solid fibre wall material (carbohydrates and lignin) is assumed to be present in this phase. Acids and phenols covalently bound to the fibre wall dissociate to different degrees, depending on the pH of the fibre bound liquid. The stagnant negative charge in the fibre bound liquid induces a cation exchange.
B. Liquid external to the fibre wall (***External liquid phase***). Water external to the fibre wall including the water in the lumen.
C. ***Gas phase***.

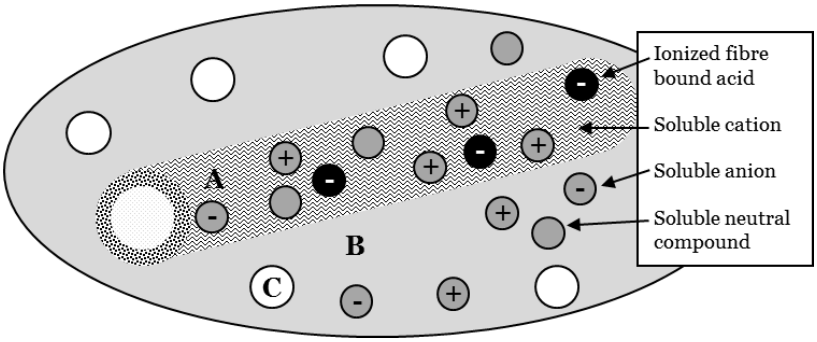

Figure 1. Schematic presentation of wood fibre + water + gas suspension. A: Fibre + water absorbed by the fibre; B: Liquid external to the fibre wall; C: Gas bubble.

The division of the system into several phases enables the modelling of the variations in chemical composition due to phase equilibrium. The variations in chemical composition, in turn, have an influence on the progress of the chemical reactions and the outcome of the processing steps, as will be discussed later in this thesis in more detail.

The phases have a different chemical composition and state (gaseous, liquid, or solid), but no variations in composition within the phase, i.e. each of them are assumed to be homogenously mixed. The estimation of how and how quickly the chemical compounds are distributed between the phases is the topic of Chapter 3. Only the determination of the amount of water in phases A and B is discussed here.

The amount of water in phases A and B is obtained from the consistency of the pulp suspension and the fibre saturation point (FSP). Consistency (kg/kg · 100%) is the mass of dry fibres divided by the total mass of the suspension. FSP is a laboratory analysis giving the amount of water bound to the fibre wall (Stone and Scallan 1968).

FSP for untreated wood has been reported to be 0.3 kg water/kg fibres (Sixta et al. 2006a). It has been shown that the FSP increases during kraft pulping (Scallan and Tigerstrom 1992). Analysis of the data reported in Scallan and Tigerstrom (1992) shows that the total volume (water + solid) of the fibre wall is roughly constant throughout the pulping (Figure 2). The volume of the fibre wall is obtained from:

$$V_{FibreWall} = \frac{w_{Lignin}}{\rho_{Lignin}} + \frac{w_{Carbohydrates}}{\rho_{Carbohydrates}} + \frac{\left(w_{Lignin} + w_{Carbohydrates}\right) \cdot FSP}{\rho_{Water}} \qquad (2.1)$$

For the density of lignin (Sixta et al. 2006a), carbohydrates (Sixta et al. 2006a), and water, the following values were used: 1400, 1580 and 1000 kg/m^3 respectively.

In the model, the volume of the material removed from the fibre wall is replaced by the equal volume of water.

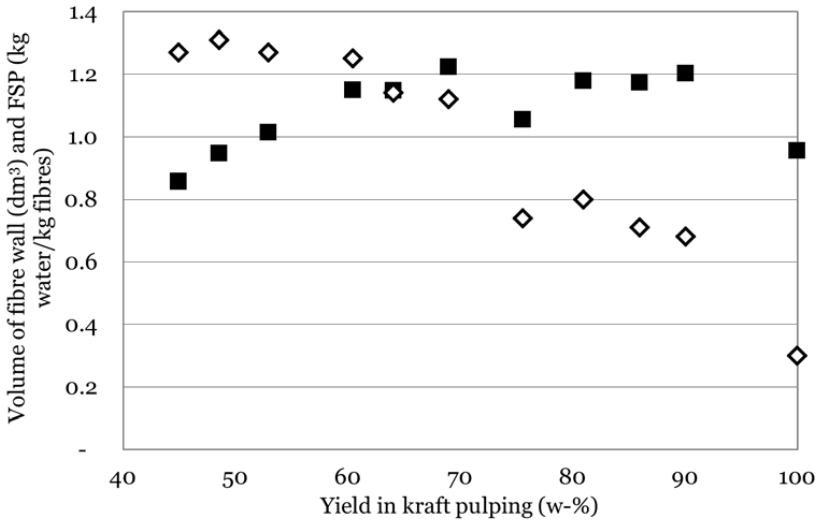

Figure 2. Estimated fibre wall volume (■) of 1 kg of o.d. wood based on the yield, lignin content, and FSP (◇) reported in Scallan and Tigerstrom (1992).

2.2 Chemical compounds

The chemical composition is modelled by using well-known chemical compounds having a CAS number (Chemical Abstracts Service), for instance HS^-, OH^-, Na^+, ClO_2, H_2O_2, and SO_4^{2-}. The advantage of using well-known chemical compounds is that many of the properties of the compounds needed in the model equations are available in the literature.

The wood polymers, in turn, are modelled using different monomeric pseudo-units having differences in their properties and reactivities. The term 'pseudo' is used to distinguish these compounds from those having a CAS number.

The selection of the pseudo-units was done based on the structures that have been analysed from the wood and fibre samples, and the reaction kinetic and mechanistic experiments with model compounds. The modelling of lignin is discussed in papers [III] and [IV], and the modelling of cellulose in paper [IV]. In addition to lignin and cellulose, methyl glucuronic acid (MeGlc) and hexenuronic acid (HexA) are relevant fibre wall compounds since they contribute to the ion exchange and also take part in chemical reactions.

As a general guideline, a chemical compound should be included in the simulation, if the following conditions hold:

- compound participates in reactions (reactant or product)
- compound has an effect on pH (neutralization or buffering)
- compound has an effect on the ionic strength and consequently on the ion exchange

2.3 Engineering parameters

Due to the difficulties in directly analysing the concentrations of the pseudo-units in the fibre wall, several correlations for the estimation of engineering parameters were sought from the literature. These engineering parameters are equivalent to the generally used standard characterization methods applied to pulp and filtrate samples. The most common analyses from pulp samples are kappa number, intrinsic viscosity, and ISO brightness. Filtrate samples are usually analysed for total organic carbon (TOC), chemical oxygen demand (COD), and absorbable organic halogen (AOX).

The kappa number correlates with the lignin and HexA content of the pulp. It is used, for instance, for estimating the chemical consumption by lignin and HexA in the bleaching stages. The kappa number is, according to ISO 302, the amount (in ml) of 20 mmol/dm^3 potassium permanganate consumed by 1 g of oven dry pulp in the reaction conditions specified in the standard. The number of electrons needed to oxidize 1 mol of a pseudo-unit (OxEq), reported in paper [IV], was obtained from the literature (Li and Gellerstedt 1997; Li and Gellerstedt 1998; Brogdon 2001; Li et al. 2002). The oxidizing power of one potassium permanganate is 5 electrons, and thus the kappa number is obtained from the following correlation:

$$\kappa = \frac{\sum_i OxEq_i \cdot c_i^F}{5\ mol\ e / 1\ mol\ KMnO_4 \cdot 0.02\ mol\ KMnO_4 / L} = \frac{\sum_i OxEq_i \cdot c_i^F}{0.1\ mol\ e / L} \quad (2.2)$$

The above equation is a modification of our earlier version of the kappa number model (Tarvo et al. 2010) as explained in paper [IV].

Similarly, permanganate consumption could be measured and modelled for filtrate samples (filtrate kappa, $\kappa_{Filtrate}$). The filtrate kappa could be measured for 1 ml of filtrate sample, and the resulting correlation is then the amount (in ml) of 20 mmol/dm^3 potassium permanganate consumed by 1 ml of filtrate sample:

$$\kappa_{Filtrate} = \frac{\sum_i \left(OxEq_i \cdot m_i^E\right)}{0.10\ mol\ e / L} \quad (2.3)$$

The filtrate kappa would probably be more useful for the estimation of chemical consumption by organic carry-over in the bleaching stages than COD. In COD analysis, almost all the organic material is oxidized by the dichromate ion. In practice, however, all compounds contributing to COD do not necessarily react with bleaching chemicals (Sankari et al. 2004). In Table 1, the change in COD measured by dichromate (COD(Cr)) and permanganate (COD(Mn)) is given. The samples came from softwood lignin oxidation experiments (Kalliola et al. 2011). These measured reductions,

both in COD(Mn) and COD(Cr), were well in line with the estimated filtrate kappa and COD, respectively. However, further testing is suggested regarding the usability of filtrate kappa in the estimation of bleaching chemical consumption by carry-over.

Table 1. Change in dichromate (Kalliola et al. 2011) and permanganate consumption of samples from softwood kraft lignin oxidation experiments after 240 min.

	Change in COD(Cr) ISO/DIS 15705	**Change in COD(Mn) SFS 3036**
0.9 MPa, 90 ℃	-15 %	-22%
0.9 MPa, 110 ℃	-15 %	-33%
0.6 MPa, 90 ℃	-8 %	-27%
0.6 MPa, 110 ℃	-15 %	-21%

The intrinsic viscosity, which correlates with the strength properties of the paper made from the pulp, is obtained from the equation presented by van Heiningen et al. (2004):

$$\eta = \frac{DP^{1/1.111} f_{Cellulose} + 116 f_{Hemicelluloses}}{1.65} \tag{2.4}$$

The average degree of polymerization (DP) of cellulose is obtained from the amounts of different cellulose pseudo-units in the fibre wall. The average DP is the sum of all cellulose pseudo-units divided by the molar amount of cellulose chains. The molar amount of cellulose chains is obtained by dividing the molar amount of the pseudo-units at the ends of the cellulose chains by two. More details of the intrinsic viscosity computation are given in paper [IV].

The ISO brightness (ISO 2470), an optical quality property of pulp, is estimated from the Kubelka-Munk equation (Kubelka and Munk 1931; Schmidt and Heitner 1999):

$$BR = 100\% \left\{ 1 + \left(\frac{k_{457}}{s_{457}} \right) - \sqrt{\left(\frac{k_{457}}{s_{457}} \right)^2 + 2\left(\frac{k_{457}}{s_{457}} \right)} \right\} \tag{2.5}$$

The overall absorption coefficient, used in the above equation, is obtained by summation using the compound specific absorption coefficients and concentrations of the compounds in the fibre wall (Zawadzki et al. 1998):

$$k_{457} = \sum_i c_i^F \cdot k_{457,i} \tag{2.6}$$

Particularly useful is the correlation between the specific absorption coefficient (compound absorbed on the solid material) and molar absorptivity (compound dissolved in the solvent) (Boroumand et al. 1992):

$$k_{457,i} = 2 \cdot \ln(10) \cdot \varepsilon_{457,i} \cdot 10^{-3} \frac{m^3}{dm^3} \cdot 100 \frac{cm}{m} \tag{2.7}$$

Equation (2.7) enables the estimation of the compound specific absorption coefficients of pseudo-units by using the molar absorptivities of the model compounds.

Equation (2.7) was validated with sheet impregnation experiments in paper [IV]. The molar absorptivity of 3,5-di-tert-butyl-o-quinone was first measured, after which Equation (2.7) was used for the prediction of the specific absorption coefficient. In Figure 3, the predicted (line) overall absorption coefficient is compared to the measured (symbols) overall absorption coefficient showing reasonable agreement between measured and estimated values and confirming the validity of Equation (2.7).

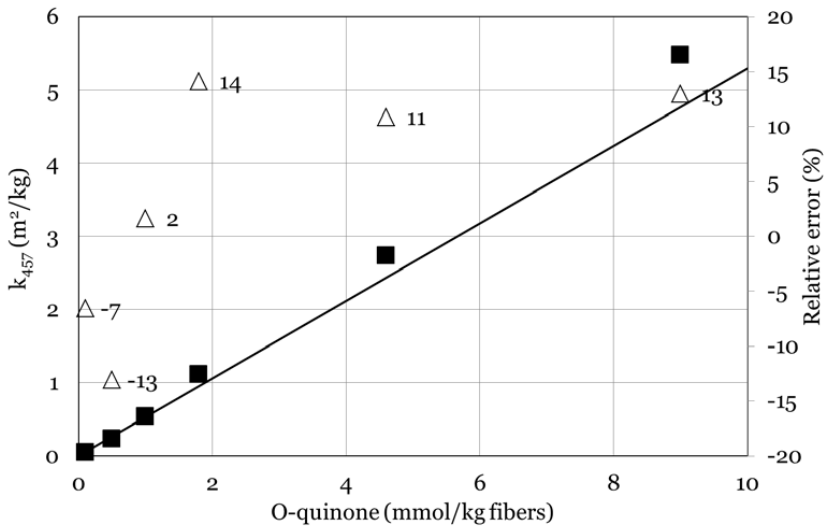

Figure 3. Measured (■) and predicted (line) k_{457} value of the cotton linter sheet impregnated with varying amounts of 3,5-di-tert-bu-o-quinone. Relative error between the measured and predicted value shown with Δ together with the numerical value. The base k_{457} value (0.1205 m²/kg fibres) of the cotton linter sheet without addition of 3,5-di-tert-butyl-o-quinone model compound was subtracted from the measured k_{457} values.

The filtrate absorbance is obtained from the Beer-Lambert law (1 cm is the width of the cuvette, and 1 kg/dm³ is the density of water at room temperature):

$$A_{457} = \sum_i \varepsilon_{457,i} \cdot m_i^E \cdot 1cm \cdot 1 \, {}^{kg}\!/_{dm^3} \tag{2.8}$$

AOX and TOC are obtained as a straightforward summation using the amount of chlorine (AOX), and carbon (TOC) atoms in the molecular formulas of the compounds. In the estimation of COD, it is assumed that carbon is oxidized into carbon dioxide and hydrogen into water. The oxygen content of the compound reduces the COD value. More details are given in paper [IV]. The OX parameter (the organic chlorine bound to the structures

still attached to the fibre wall) is obtained in a similar manner as AOX (Tarvo et al. 2010).

To summarize, in the estimation of engineering parameters, the following properties are needed for each compound:

- $OxEq_i$ – for the kappa number and filtrate kappa
- $k_{457,i}$ – for the ISO brightness and liquid absorbance
- molecular formula – for AOX, OX, TOC, and COD

As explained above, both $OxEq_i$ and $k_{457,i}$ were obtained from the literature reporting experimental results for the model compounds. For one pseudo-component, the $k_{457,i}$ was determined in paper [IV].

3. Modelling of equilibria and kinetics

As explained in Chapter 2, a pulp suspension consists of 3 phases (Figure 4). The topic of this chapter is the modelling of the phase and reaction equilibria, reaction kinetics, and mass transfer. Modelling of equilibrium and rate processes (reaction kinetics and mass transfer) are connected, as the driving force in rate processes is the deviation from the equilibrium state.

In the model, the following phenomena are considered (Figure 4):

1. A ↔ B: equilibrium between ***Fibre bound liquid phase*** and ***External liquid phase***. Mass transfer takes place between phases A and B
2. B ↔ C: equilibrium between ***External liquid phase*** and ***Gas phase***. Mass transfer takes place between phases B and C.
3. Reversible reaction equilibrium in both liquid phases.
4. Irreversible reactions in both liquid phases.

Compounds covalently bound to the fibre wall react only with compounds in the fibre wall liquid. The reaction products of the fibre wall compounds dissolve into the fibre wall liquid, after which they are able to diffuse into the external liquid phase. No reactions take place in the gas phase.

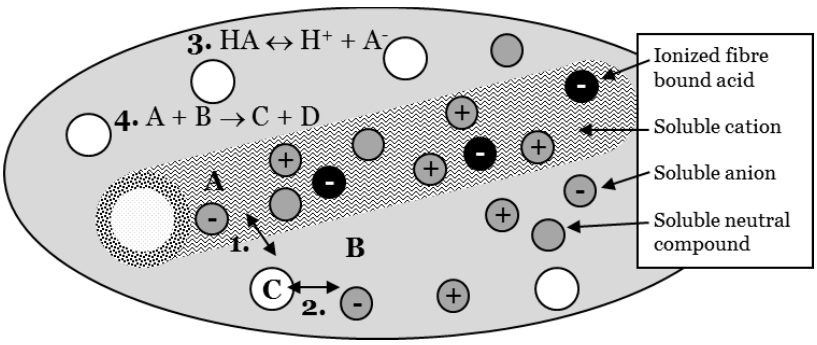

Figure 4. Schematic presentation of phenomena in wood fibre + water + gas suspension. 1: Equilibrium and mass transfer between fibre bound and external liquid; 2. Equilibrium and mass transfer between external liquid and gas phase; 3. Reversible reaction equilibrium; 4. Irreversible reactions.

Modelling of these phenomena was introduced in paper [I]. More details on modelling the gas-liquid equilibrium and estimation of the equilibrium

constant are given in this chapter. Additionally, the consequences of assuming ideal mixture in papers [I]-[IV] are discussed.

Gibbs energy minimization approach has been adopted for solving phase and reaction equilibrium (Sandler 1989). In the context of pulp suspension, the approach has been discussed earlier by Koukkari et al. (2002).

3.1 Reversible reactions

In aqueous electrolyte solutions, a great number of reversible equilibrium reactions may take place simultaneously. In equilibrium, Gibbs free energy has attained its minimum value. From the minimization of the total Gibbs free energy of the system, it follows that all the reaction equilibria need to fulfil the equation:

$$K = \prod_i a_i^{\xi_i} \tag{3.1}$$

For reactants, the stoichiometric coefficients (ξ) are negative and for products they are positive. K, the equilibrium constant, is obtained from the Gibbs free energies of the compounds involved in the equilibrium reaction as is explained in Chapter 3.3.

As introduced in paper [II], in modelling unit operations, each equilibrium reaction is treated as two kinetic reactions (a forward and a backward reaction). The kinetics of these reactions are assumed to be fast: the rate constant for the reaction of base (A^-) with H^+ can be assumed to be $k_{b,RR} = 10^{10}$ M^{-1} s^{-1}, (Grenthe et al. 1997). For acid-base equilibrium, Equation (3.1) becomes:

$$K_{RR} = \frac{a_{H^+} a_{A^-}}{a_{HA}} \tag{3.2}$$

In order to obtain the rate constant for the dissociation of acid (HA), Equation (3.2) is multiplied by $k_{b,RR} a_{HA}$:

$$K_{RR} k_{b,RR} a_{HA} = k_{b,RR} a_{H^+} a_{A^-} \tag{3.3}$$

The right-hand side of Equation (3.3) represents the rate law for the reaction of H^+ with A^-, and the left-hand side of Equation (3.3) is the rate law for the dissociation of HA. Thus the rate constant for the dissociation of HA into A^- and H^+ is:

$$k_{f,RR} = K_{RR} \cdot k_{b,RR} \tag{3.4}$$

3.2 Phase equilibrium

Equilibrium between external and fibre bound liquid phase is modelled using the Donnan potential (Helfferich 1962):

$$E_{Donnan} = \frac{1}{z_i F} \left(RT \ln \frac{a_i^E}{a_i^F} - \Pi v_i \right) \tag{3.5}$$

The equation for the osmotic pressure, causing the swelling of the fibres, can be derived from Equation (3.5) by first multiplying both sides of the equation by the charge number (z). The charge number of water is zero, thus the equation becomes (Kuitunen et al. 2011):

$$\Pi = \frac{RT}{v_W} \ln \frac{a_W^E}{a_W^F} \tag{3.6}$$

The mechanical force of the fibre wall, resisting the swelling, is modelled with Hooke's law (Scallan and Tigerstrom 1992). In equilibrium, the chemical and mechanical forces are equal to each other, and the FSP of the swollen fibres is obtained from:

$$FSP = \frac{\Pi\left(\frac{\rho_w}{\rho_f} + FSP_0\right) + M \cdot FSP_0}{M} \tag{3.7}$$

Two parameters are needed, namely the FSP of the non-swollen fibres (FSP_0) and elastic modulus (M) of the fibre wall. They can be regressed by using experimental FSP data at different chemical compositions.

Using the data given in Scallan and Tigerstrom (1992):

- FSP_0 = FSP(H) = 1.27 kg water/kg fibres
- FSP = FSP(Na) = 1.37 kg water/kg fibres
- M = 2 MPa

The osmotic pressure, calculated from Equation (3.7) for the fibres in sodium form, is 0.1 MPa. By using the volume of hydrated sodium ion (115.8 cm^3, Horvath (1985)) and the osmotic pressure of 0.1 MPa, it is noted that, if the activity of ion in the external liquid phase is 90% of the activity of the ion in the fibre bound liquid, the value for the term Πv_i is only 0.7% of the value for the term $RT \ln \frac{a_i^E}{a_i^F}$ at 25°C. If the differences in the activities and temperature are higher, the contribution of the term Πv_i further diminishes.

Thus the term Πv_i is neglected, and the commonly used form of the Donnan equation is obtained:

$$\left\{\exp\left[-\frac{F}{RT} E_{Donnan}\right]\right\}^{z_i} = \lambda^{z_i} = \frac{a_i^F}{a_i^E} \tag{3.8}$$

In modelling the gas-liquid equilibrium (GLE), the chemical potential / Gibbs energy minimization approach was used as well. In the chemical equilibrium, the chemical potential of compound i is the same in all the phases in which it exists. In the gas phase, the chemical potential is written as:

$$\mu(i,g,T) = \mu^{\circ}(i,g,T_0) + RT\ln(f_i) \tag{3.9}$$

In the liquid phase, compounds can be considered as solutes:

$$\mu(i,aq,T) = \mu^{\circ}(i,aq,T_0) + RT\ln\left(\frac{\gamma_i^* m_i}{m^{\circ}}\right) \tag{3.10}$$

or as solvents (this will be explained below):

$$\mu(W,lq,T) = \mu^{\circ}(W,lq,T_0) + RT\ln(\gamma_W x_W) \tag{3.11}$$

As stated above, in equilibrium chemical potentials are equal in each phase:

$$\mu(i,g,T) = \mu(i,aq,T) \tag{3.12}$$

$$\mu(i,g,T) = \mu(i,lq,T) \tag{3.13}$$

After substituting Equations (3.9) and (3.10) into Equation (3.12), and similarly Equations (3.9) and (3.11) into (3.13), the following equations are obtained:

$$\exp\left[\frac{\mu^{\circ}(i,aq,T_0) - \mu^{\circ}(i,g,T_0)}{RT}\right] = \frac{f_i}{a_i} \tag{3.14}$$

$$\exp\left[\frac{\mu^{\circ}(W,lq,T_0) - \mu^{\circ}(i,g,T_0)}{RT}\right] = \frac{f_i}{a_W} \tag{3.15}$$

It can be noted that the left-hand sides of Equation (3.14) and (3.15) equal the equation for the equilibrium constant (K), because the standard state potential of a compound is actually equal to the Gibbs energy of formation of a compound.

Thus, GLE can be treated in a similar manner as reaction equilibrium: Compound in the external liquid phase $\leftrightarrow$ Compound in the gas phase

$$K_{E\leftrightarrow G,k} = \frac{f_k}{a_k^E} \tag{3.16}$$

3.3 Computation of equilibrium constant (K)

Whether the equilibrium constant is for the reaction equilibrium or for GLE, it is obtained from (as a consequence of the total Gibbs free energy minimization):

$$K = \exp\left[\frac{-\Delta_r G}{R \cdot T}\right] \tag{3.17}$$

The Gibbs free energy change in the reaction/GLE is obtained from the heat of formation, entropy of formation, and constant pressure heat capacity functions of compounds involved in the reaction/GLE.

$$\Delta_r G^\circ = \Delta_r H^\circ - T \cdot \Delta_r S^\circ =$$

$$\Delta_r H^\circ(T_0) + \int_{T_0}^{T} \Delta_r C_p^\circ dT - T \cdot \left(\Delta_r S^\circ(T_0) + \int_{T_0}^{T} \frac{\Delta_r C_p^\circ}{T} dT \right) \tag{3.18}$$

$$\Delta_r H^\circ(T_0) = \sum_i \xi_i \Delta_f H^\circ(i, T_0) \tag{3.19}$$

$$\Delta_r C_p^\circ = \sum_i \xi_i C_p^\circ(i) \tag{3.20}$$

$$\Delta_r S^\circ(T_0) = \sum_i \xi_i \Delta_f S^\circ(i, T_0) \tag{3.21}$$

The absolute values of most of the thermodynamic parameters cannot be determined experimentally. A well-defined standard state is needed, a "base line", to which variations can be referred. For the data used in this thesis, the following standard state is applied (Grenthe and Puigdomenech 1997):

- Pressure, p^o=0.1 MPa
- Liquid and solid: pure substance at standard state pressure. In the aqueous phase computation, this is applied to water i.e. solvent
- Gaseous substance: pure substance at standard state pressure in a hypothetical state, in which it exhibits ideal gas behaviour
- Solute: hypothetical solution at standard state pressure, in which m_i = m^o=1 mol/kg, and in which the activity coefficient equals unity. Thermodynamic parameters for hydrogen ion are set to zero.
- Reference temperature (T_o) is 298.15 K

By applying the equations above, the effect of temperature on the reaction and phase equilibria is inherently taken into account through the value for the equilibrium constant (K).

It is worth noting that using either standard state entropy or entropy of formation, the same reaction entropy is obtained from Equation (3.21) (Puigdomenech et al. 1997). In the model, standard state entropy was chosen, because this is usually reported instead of entropy of formation.

The pseudo-units in the fibre wall are treated as solutes, which are evenly distributed in the fibre bound liquid. The molality of the fibre bound compounds is obtained by dividing the molar amount by the mass of water in the fibre bound liquid. This approach has been used earlier by van der Stegen et al. (1999) in modelling ion-selective membranes.

For the pseudo-units in the fibre wall, and also for a few CAS-compounds, the whole set of thermodynamic parameters required in the computation of the equilibrium constant as a function of temperature are missing. Usually, only the pKa value at 25°C has been reported. For instance, in the case of phenolic lignin units, Ragnar et al. (2000) have reported the pKa for several different structures. In order to obtain the temperature dependency of the

pKa value, the heat of reaction of phenol was assumed and the constant pressure heat capacity was set to zero. In the simulator, the fact that part of the thermodynamic data is missing is resolved by assigning zero values to the data of some compounds ("reduced compounds" will be introduced later) and assigning a change in the reaction enthalpy and entropy to some compounds ("dependent compounds"). More details about this are given in paper [III].

3.4 Irreversible reactions

The selection of irreversible reactions for the model was one of the most challenging tasks. Guidance was sought from the literature, especially from the experimental studies conducted with model compounds. This task was closely linked to the modelling of the structure of lignin and carbohydrates. For a chosen reaction, both reactants and products need to be included in the simulation in order to model the mass and charge balance. The main principle was to include only elementary reactions in the model. However, this was not always possible, because in that case the number of compounds to be included in the simulation would have been too high.

In the sequence of elementary reaction steps, the slowest reaction is often called the rate-determining step. The reactants of that reaction are fairly stable, i.e. their amounts can be analysed and consequently the kinetics of the rate-determining step can be followed. Thus, in the modelling, the aim was to identify the rate-determining reactions and to include their reactants (A and B) in the simulation. The final stable products (C and D) of several fast elementary reaction steps were included as well.

$$aA + bB \rightarrow\rightarrow\rightarrow cC + dD$$

Sometimes model compound studies suggest that several parallel reaction paths are possible, yielding different final products. In such cases, both of these approaches were applied.

1. If a short-lived compound reacts with more than one other compound, the short-lived compound needs to be included in the simulation. For example, a phenoxy radical might react (paper [III]):
    a. with another phenoxy radical, yielding condensed phenol
    b. with a superoxide leading to the destruction of the aromatic ring or yielding phenolate and oxygen
2. If the ratio of these paths does not depend on the temperature or the composition of the system, it is not necessary to include the short-lived compound in the simulation. As the rate laws for these parallel paths are written, the ratio of these parallel paths is taken into account in the value for the frequency factor of the Arrhenius

law. An example of this case is the modelling of HexA hydrolysis (paper [I]).

3.5 Mass transfer

In electrolyte systems, the mass transfer between the two liquid phases is modelled with the Nernst-Planck equation, which maintains the electroneutrality condition (Newman 1991):

$$r_{i,LLMT} = \frac{A_{MT} \cdot w_F \cdot \rho_W \cdot D_{i,eff}}{l} \left(\Delta a_i - \overline{a}_i \cdot z_i \left(\frac{\sum_{j=1}^{n} z_j \cdot D_{j,eff} \cdot \Delta a_j}{\sum_{j=1}^{n} z_j^2 \cdot D_{j,eff} \cdot \overline{a}_j} \right) \right) \quad (3.22)$$

A liquid film, located on the fibre bound liquid side, is assumed to be on the boundary of the fibre bound liquid and external liquid. All mass transfer resistances are assumed to be in this liquid film.

The assumption of a linear profile in the liquid film leads to the following equations for the activity difference across the film and the average activity in the film (Ala-Kaila 1998; paper [I]):

$$\Delta a_i = a_i^{E \leftrightarrow F} - a_i^{E} \quad (3.23)$$

$$\overline{a}_i = \frac{a_i^{E \leftrightarrow F} + a_i^{E}}{2} \quad (3.24)$$

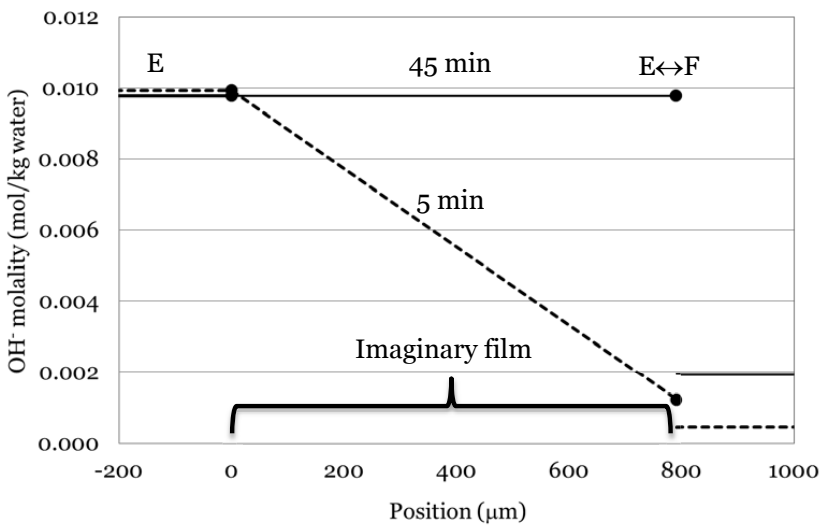

Figure 5. Hydroxide ion profile in imaginary film that is between external liquid and fibre bound liquid. Simulation time 5 min (ticked line) and 60 min (solid line), with NaCl charge of 0.19 mol/kg water and NaOH charge 0.01 mol/kg water. Adopted from paper II.

The activities on the other interface of the liquid film and the external liquid phase are equal to each other (Figure 5). At the other interface, the liquid film (E↔F) and the fibre bound liquid phase are in the Donnan equilibrium (Ala-Kaila 1998):

$$\lambda^{z_i} = \frac{a_i^F}{a_i^{E\leftrightarrow F}} = \frac{a_i^F}{\gamma_i^{E\leftrightarrow F} m_i^{E\leftrightarrow F}} \tag{3.25}$$

The electroneutrality condition needs to hold as well:

$$\sum_i z_i m_i^{E\leftrightarrow F} = 0 \tag{3.26}$$

Combining the two equations above gives:

$$\sum_i z_i \frac{a_i^F}{\gamma_i^{E\leftrightarrow F} \lambda^{z_i}} = 0 \tag{3.27}$$

Both sides of the equation can be multiplied by $\lambda^{z_{MAX}}$ leading to the polynomial:

$$\sum_i z_i \frac{a_i^F}{\gamma_i^{E\leftrightarrow F}} \lambda^{z_{MAX}-z_i} = \sum_i z_i \frac{a_i^F}{\gamma_i^E} \lambda^{z_{MAX}-z_i} = 0 \tag{3.28}$$

The highest order of the polynomial (Equation 3.28) depends on the difference between the highest and the lowest charge number among the soluble ions included in the simulation. For instance, if the charge number of Ca^{2+} represents the highest and the charge number of CO_3^{2-} the lowest charge number, then the polynomial order is 4. In the simulation model, an analytical solution for the roots of the polynomial exists for the polynomial of order 4 and lower. If the polynomial order is higher, λ is solved with Newton-Raphson iteration. When the stagnant charge in the fibre wall is negative, then values higher than unity for λ are acceptable. If the stagnant negative charge is positive, then λ is in the range of zero and unity. Among the real numbers roots, the smallest one is chosen for value of λ.

For simplicity, activity coefficients (γ) estimated on the basis of the external liquid phase (E) composition, rather than liquid film (E↔F) composition, are used in Equation (3.28).

The effective diffusion coefficients were obtained from data found at 25°C in free water (D_i) by correcting them with the equation (Reid et al. 1987):

$$D_{i,Eff} = \frac{\varepsilon}{\tau} D_i \frac{T}{298.15K} \frac{\eta(298.15K)}{\eta(T)} \tag{3.29}$$

Liquid viscosity was estimated from the correlation presented by Laliberte (2007a) and Laliberte (2007b). The porosity of the fibre wall (ε) is obtained from the FSP value. For tortuosity, the value of 7 reported by Zhang et al. (1998) is used.

For *l*, the diffusion length, the fibre wall thickness of 4 μm has been used (Sixta et al. 2006b).

For pulp, the effective mass transfer area (A_{MT}) has been found to be 1-10 m^2/kg fibres (Maja 2006). This is order of magnitude lower than the theoretical estimate, 254 m^2/kg fibres, obtained using the following data:

- FSP = 1.5 kg water/kg fibres
- Fibre wall thickness 4 μm (Sixta et al. 2006b)
- Fibre diameter 65 μm (Sixta et al. 2006b)
- → Fibre lumen width = Fibre diameter – two times the fibre wall thickness = 57 μm

For small wood particles (paper [II]), the effective mass transfer area was estimated from the given particle dimensions, and then the diffusion length was estimated along with other model parameters.

The diffusion coefficients of ions in free water at 25°C can be found from several handbooks like Lide (1994). For polymers, the Wilke-Chang estimation method was used (Reid et al. 1987). The molar volume of a polymer at its boiling point, needed in Wilke-Change equation, was estimated using the Le Bas method (Reid et al. 1987).

In the modelling of gas-liquid mass transfer, a simple k_La approach was adopted.

$$r_{GLMT,i} = k_L a\left(a_i^{E\leftrightarrow G} - a_i^E\right)w_W^E \tag{3.30}$$

In the model, it was assumed that the mass transfer restrictions are in the liquid film, which is on the boundary of the gas and liquid interface. The other end of the film (next to the gas phase) is in equilibrium with the gas phase.

In paper [III], k_La was estimated from experimental results and in paper [IV] it was estimated from the correlation presented by Rewatkar and Bennington (2000). In paper [III], the value for k_La, obtained experimentally, was 0.012 s^{-1} and in paper [IV], the resulting value for k_La was estimated to be 0.19 s^{-1}. For the laboratory reactor used in paper [III] experiments, the power dissipation, needed in k_La correlations, was not available. Thus, it was considered easier to determine it from a separate experimental setup. In that setup, the reactor was filled with water, pressurized with oxygen, sealed, and mixing was started. After the mixing was started, recording the pressure decrease as a function of time was started. From the pressure vs. time data, the k_La was estimated.

3.6 Reaction and mass transfer rates used in unit operation models

In order to simplify the equations presented in Chapter 4 for unit operation models, the rates from the individual phenomena are summed together.

$$r_{i,ALL}^E = r_{i,RR}^E + r_{i,IR}^E + r_{i,LLMT} + r_{i,GLMT} \tag{3.31}$$

$$r_{i,ALL}^{F} = r_{i,RR}^{F} + r_{i,IR}^{F} - r_{i,LLMT} \quad (3.32)$$

$$r_{i,ALL}^{G} = -r_{i,GLMT} \quad (3.33)$$

The rates due to reversible reactions ($r_{i,RR}$) include a contribution from all reactions in which the compound i is involved. For example (AcH = acetic acid, Ac^- = acetate):

RR1: $H_2O \leftrightarrow OH^- + H^+$

RR2: $AcH \leftrightarrow Ac^- + H^+$

$$r_{H_2O,RR} = \left(-k_{f,RR1}a_{H_2O} + k_{b,RR1}a_{OH^-}a_{H^+}\right)w_W \quad (3.34)$$

$$r_{OH^-,RR} = \left(k_{f,RR1}a_{H_2O} - k_{b,RR1}a_{OH^-}a_{H^+}\right)w_W \quad (3.35)$$

$$r_{H^+,RR} = \left(k_{f,RR1}a_{H_2O} - k_{b,RR1}a_{OH^-}a_{H^+} + k_{f,RR2}a_{AcH} - k_{b,RR2}a_{Ac^-}a_{H^+}\right)w_W \quad (3.36)$$

$$r_{AcH,RR} = \left(-k_{f,RR2}a_{AcH} + k_{b,RR2}a_{Ac^-}a_{H^+}\right)w_W \quad (3.37)$$

$$r_{Ac^-,RR} = \left(k_{f,RR2}a_{AcH} - k_{b,RR2}a_{Ac^-}a_{H^+}\right)w_W \quad (3.38)$$

Similarly for irreversible reactions (acid catalyzed deacetylation is the example here):

IR: $OAc + H^+ + H_2O \rightarrow AcH + H^+$

$$r_{OAc,IR} = \left(-k_{IR1}a_{OAc}a_{H^+}\right)w_W \quad (3.39)$$

$$r_{H^+,IR} = \left(-k_{IR1}a_{OAc}a_{H^+} + k_{IR1}a_{OAc}a_{H^+}\right)w_W \quad (3.40)$$

$$r_{AcH,IR} = \left(k_{IR1}a_{OAc}a_{H^+}\right)w_W \quad (3.41)$$

Both reversible and irreversible reactions take place in both liquid phases. In the external liquid phase, the amount of fibre bound compounds is zero, thus, the rates of reactions involving fibre bound compounds equal zero in the external liquid phase.

3.7 Assumption of ideal mixture

For simplicity, in the systems studied for this thesis, the assumption of ideal mixture was used. Thus, the activity coefficients were set equal to unity, and instead of activities (a), molalities (m) were used for the solutes, and mole fractions (x) for the solvent (water). Furthermore, partial pressures (p) were used instead of fugacities (f). In the following, the inaccuracies caused by this assumption are discussed.

Usually the interactions between ions become increasingly important when the ionic strength of the mixture increases. When the interactions between compounds are strong, mixtures are called non-ideal. The ionic strength is obtained from:

$$I = \frac{1}{2}\sum_i m_i z_i^2 \quad (3.42)$$

The ionic strength in the cases studied for this thesis, are the following:

- Hot water extraction: in the beginning close to zero, at the end ~10^{-3} M (estimated from the pH)
- Kraft cooking liquor impregnation: 0.01 – 0. 2 M (estimated from the added amount of sodium hydroxide and sodium chloride)
- Lignin oxidation by oxygen: 0.1 M (estimated from the added amount of sodium hydroxide)
- Alkaline extraction of D_0 pulp: 0.033 – 0.083 M (estimated from the added amount of sodium hydroxide)

A simple model for the estimation of activity coefficients is the Davies model (applicable up to an ionic strength of 0.1 M):

$$\log_{10} \gamma_i = -0.51 z_i^2 \left(\frac{\sqrt{I}}{1+\sqrt{I}} - 0.3I \right) \tag{3.43}$$

The temperature dependency of the activity coefficients are obtained from (Stumm and Morgan 1996):

$$\log_{10} \gamma_i = -1.82 \cdot 10^6 \cdot (\varepsilon_W T)^{-3/2} z_i^2 \left(\frac{\sqrt{I}}{1+\sqrt{I}} - 0.2I \right) \tag{3.44}$$

The activity coefficients of neutral compounds can be estimated from (Morel and Hering 1993):

$$\log_{10} \gamma_i = 0.1I \tag{3.45}$$

When plotting the activity coefficient of a neutral compound, monovalent ion, and divalent ion as a function of ionic strength, it can be noted that the effect of ionic strength on the divalent ion activity coefficient is much higher than on the neutral compound and monovalent ion (Figure 6).

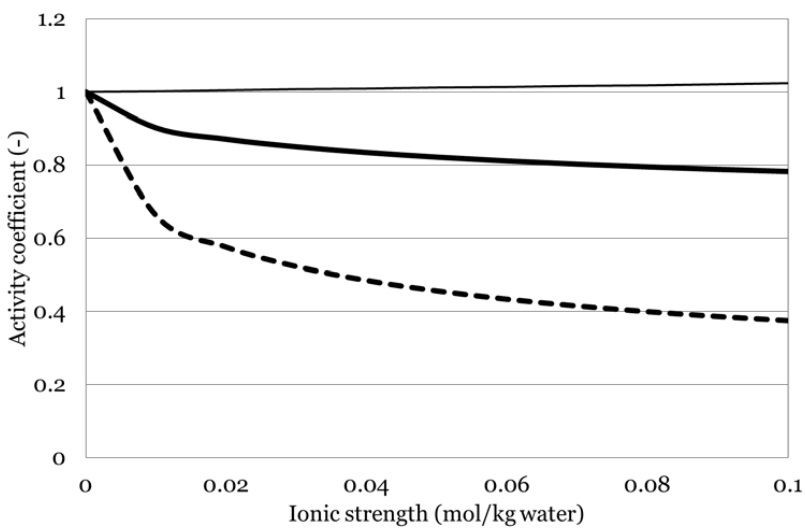

Figure 6. Activity coefficient of neutral compound (thin solid line), monovalent ion (thick solid line), and divalent ion (dashed line) estimated with Equations (3.44) and (3.45).

The amount of divalent ions in the studied cases was rather low, and divalent ions were not used as reactants in irreversible reactions.

For instance, Lindgren and Öhman (2000) have used the Davies model and Bygrave and Englezos (2000) have used the Pitzer model (Pitzer 1991) for predicting the partitioning of metal ions between the fibre bound liquid and external liquid. Accurate prediction of metal ion partitioning is important in the context of pulp washing.

Concerning the kinetics of irreversible reactions, La Mer (1932) has found the following (reaction of A+B→):

1. A and B have a charge number of the same sign (A and B are cations or A and B are anions): the rate constant increases when the ionic strength increases
2. A and B have a charge number of the opposite sign (one is a cation and the other one is an anion): the rate constant decreases when the ionic strength increases
3. A or B is neutral: the ionic strength has no effect

Considering the irreversible reactions modelled in this thesis, most of them fall into category 3 (ionic strength has no effect).

One example of an irreversible reaction in which two anions react, is pQO^- + HOO^- (paper [IV]). This reaction is supposed to be accelerated by increasing ionic strength.

It is likely that the ignoring the non-idealities limits the usage of the model at other ionic strengths. The expected error, based on the evolution of monovalent ion activity coefficient as a function of ionic strength, is 10-20 %. In the future, the Davies model should be incorporated into the simulation model, if the ionic strength of the studied system is below 0.1 M.

3.8 Enthalpy

The total enthalpy of a flow is obtained from the following equation:

$$h = \sum_i n_i \cdot \Delta_f H(i,T) + w_{fibers} \cdot \hat{H}_{fibers} \tag{3.46}$$

For solutes, solvents, and gaseous compounds, the enthalpy of formation is used in Equation (3.46). This enables the estimation of the temperature increase/decrease due to exothermic/endothermic reactions. The temperature dependency of the heat of formation is obtained from:

$$\Delta_f H(i,T) = \Delta_f H^\circ(i,T_0) + \int_{T_0}^{T} C_p^\circ(i)dT \tag{3.47}$$

For solid material in the fibre wall, the correlation presented by Ganster and Fink (2005) are used:

$$\hat{H}_{fibers} = 5949.7\,{}^{kJ}\!/_{kg} + 1.364\,{}^{kJ}\!/_{kg \cdot K}\left(T - 350K\right) + 5.06 \cdot 10^{-3}\,{}^{kJ}\!/_{kg \cdot K^2}\left(T^2 - \left(350K\right)^2\right) \tag{3.48}$$

The above correlation is actually intended for cellulose only, but in the model, it is also used for lignin and hemicelluloses in the fibre wall.

3.9 Equation of state

The volume of the pulp flow is obtained by summing together the volume of the gas phase, the volume of the water, and the volume of the fibres. The volume of the gas phase is obtained from the ideal gas law:

$$V^G = \frac{\sum_i n_i^G \cdot R \cdot T}{p} \tag{3.49}$$

The density of water is obtained from Laliberte and Cooper (2004). The density of lignin and carbohydrates were taken from Sixta et al. (2006a) as presented in Chapter 2.

The effect of solutes on the total volume of the flow is omitted.

4. Unit operation models

For simulation of industrial bleaching sequences and laboratory set-ups, equations for unit operations were derived and implemented. Unit operation models account for the hydrodynamics (evolution of pressure) and the different arrangements of the flows into, out, and within the unit. The arrangement of feed and product flows in the ideal unit operation models is shown in Figure 7. The word "ideal" refers to the fact that certain assumptions are made concerning the flow pattern and mixing conditions. The plug flow reactor (PFR) is modelled assuming no radial variation in the velocity, and no dispersion in the radial or longitudinal direction. The tank (CSTR) and batch reactors are modelled assuming perfect mixing inside the reactor.

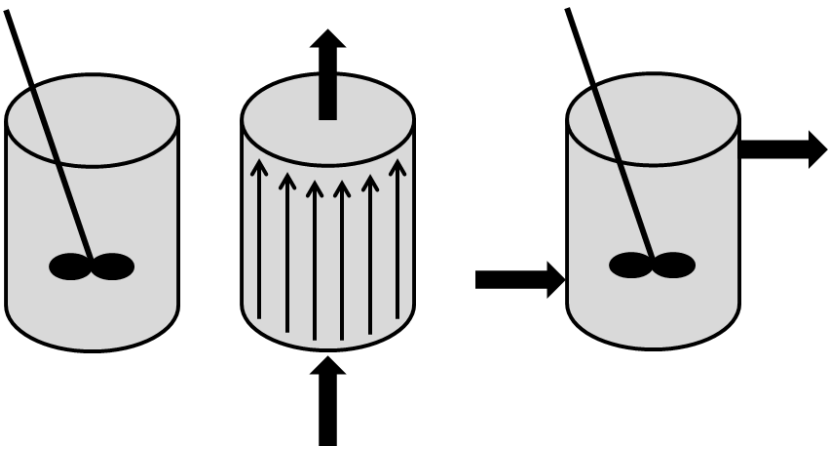

Figure 7. Schematic representation of the ideal reactor models: batch reactor, plug flow reactor (PFR), and continuous stirred tank reactor (CSTR).

The bleaching sequences usually consist of pumps, pipes, retention towers, drum washers, and filtrate tanks. In this work, it is assumed that the pumps and filtrate tanks can be modelled as CSTR units, and pipes and retention towers as PFR units. These assumptions were also made by van Heiningen et al. (2003) in the modelling of the oxygen delignification stage (mixing+retention tower). A batch reactor unit is needed in the modelling of laboratory experiments.

The modelling of unit operations is based on the conservation of mass and energy. The general balance equation applied to both mass and energy is:

ACC = IN – OUT + GEN (4.1)

where:

ACC = accumulation of mass or energy inside the control volume

IN = flow of mass or energy into the control volume

OUT = flow of mass or energy from the control volume

GEN = generation of mass or energy inside the control volume. The phenomenon models introduced in the previous chapter are included in this term.

Obviously, the GEN term for the total mass of the system equals zero (no nuclear reactions), but because the balance equations are written for each compound in each phase, the chemical reactions converting compounds to other compounds and mass transfer between the phases make the GEN term deviate from zero.

While simulating a bleaching sequence, steady state is assumed, thus, the accumulation (ACC) equals zero and Equation (4.1) becomes:

0=IN – OUT + GEN (4.2)

Equation (4.2) is applied in the modelling of the retention tower.

The mixer/tank is modelled as a continuous stirred tank reactor (CSTR) using a time-dependent approach with Equation (4.1). The final value of the independent variable, i.e. time, is increased until steady state is approached. In steady state, ACC becomes equal to zero, and the unit is considered to be solved.

The washer unit is modelled by applying both the CSTR and PFR concepts.

The batch reactor is a dynamic model (variations as a function of time), so ACC≠0. On the other hand, IN=0 and OUT=0 and Equation (4.1) becomes:

ACC = GEN (4.3)

The batch reactor unit model was introduced in paper [III]. The other unit operation models are introduced for the first time in this thesis, and have been used in the study by (Kalliola et al. 2012).

4.1 Batch reactor

For the modelling of a batch reactor, a mass balance equation is written for the molar amount of every compound in both liquid phases and in the gas phase:

$$\frac{dn_i^E}{dt} = r_{i,ALL}^E \tag{4.4}$$

$$\frac{dn_i^F}{dt} = r_{i,ALL}^F \tag{4.5}$$

$$\frac{dn_i^G}{dt} = r_{i,ALL}^G \tag{4.6}$$

For the usage of a batch reactor, two options exist:

- Simulation of the batch reactor at constant pressure (isobaric). Variations in the gas phase composition are reflected in the changes in reactor volume. This behaviour corresponds to the behaviour of a batch reactor with a sliding lid or a batch reactor attached to a gas bottle through a pressure controller.
- Simulation of the batch reactor at constant volume (isochoric). When the total molar amount of compounds in the gas phase changes, the changes are reflected in the reactor pressure. The ideal gas law is used as the equation of state for the gas phase. Reactor pressure is driven to the pressure obtained from the ideal gas law (weighting factor 10^{10}):

$$\frac{dp}{dt} = \left(p - \frac{\sum_i n_i^G \cdot R \cdot T}{V^G} \right) \cdot 10^{10} \tag{4.7}$$

More details are given in paper [III].

In papers [III] and [IV], isochoric operation was used. Isobaric operations were applied in the simulation of cases presented in papers [I,II,IV]. The simulation of isobaric reactor is faster. If gas phase is not relevant, this option should be used.

4.2 Retention tower

The retention tower unit is modelled assuming an ideal plug flow i.e. ignoring axial and radial dispersion. The equations are derived by starting from the mass balance for a slice of the tower (Figure 8).

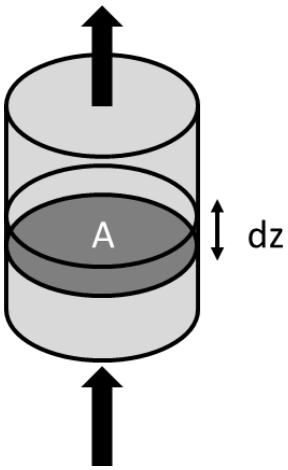

Figure 8. Mass balance for a slice in the retention tower.

$$0 = \dot{n}_{i,z}^{E} - \left[\dot{n}_{i,z}^{E} + \frac{\partial\left(\dot{n}_{i,z}^{E}\right)}{\partial z} \right] \cdot dz + r_{i,ALL}^{E}\left(n_{i,z}^{E}, n_{i,z}^{F}, T_z, p_z\right) \tag{4.8}$$

$$0 = \dot{n}_{i,z}^{F} - \left[\dot{n}_{i,z}^{F} + \frac{\partial\left(\dot{n}_{i,z}^{F}\right)}{\partial z} \right] \cdot dz + r_{i,ALL}^{F}\left(n_{i,z}^{E}, n_{i,z}^{F}, T_z, p_z\right) \tag{4.9}$$

The term for outflow comes from Taylor series expansion of a function f around z (Luyben 1990):

$$f_{(z+dz)} = f_{(z)} + \left(\frac{\partial f_{(z)}}{\partial z}\right)_{(z)} dz + \left(\frac{\partial^2 f_{(z)}}{\partial z^2}\right)_{(z)} \frac{(dz)^2}{2!} + \ldots + \left(\frac{\partial^n f_{(z)}}{\partial z^n}\right)_{(z)} \frac{(dz)^n}{n!} \tag{4.10}$$

If dz is small, as it is assumed here, the series can be truncated after the second term.

In order to use the molar flows instead of molar amounts in the computation of r_{ALL}, it is noted that:

$$n_z = \frac{\dot{n}_z}{v} dz \tag{4.11}$$

Thus, the mass balance equations become:

$$0 = -\frac{\partial\left(\dot{n}_{i,z}^{E}\right)}{\partial z} dz + r_{i,ALL}^{E}\left(\dot{n}_{i,z}^{E}, \dot{n}_{i,z}^{E}, T_z, p_z\right)\frac{dz}{v} \tag{4.12}$$

$$0 = -\frac{\partial\left(\dot{n}_{i,z}^{F}\right)}{\partial z} dz + r_{i,ALL}^{F}\left(\dot{n}_{i,z}^{E}, \dot{n}_{i,z}^{F}, T_z, p_z\right)\frac{dz}{v} \tag{4.13}$$

Division of both sides by dz and reorganizing gives:

$$\frac{d\dot{n}_{i,z}^{E}}{dz} = r_{i,ALL}^{E}\left(\dot{n}_{i,z}^{E}, \dot{n}_{i,z}^{E}, T_z, p_z\right) \Big/ v \tag{4.14}$$

$$\frac{d\dot{n}_{i,z}^{F}}{dz} = r_{i,ALL}^{F}\left(\dot{n}_{i,z}^{E}, \dot{n}_{i,z}^{F}, T_z, p_z\right) \Big/ v \tag{4.15}$$

Superficial velocity is obtained from:

$$v = \frac{\dot{V}}{A} \tag{4.16}$$

And the cross-sectional area of the tower from:

$$A = \pi\left(\frac{d}{2}\right)^2 \tag{4.17}$$

In order to account for the changes in volume flow due to the changes in hydrostatic pressure, the derivative for the volume flow is obtained by applying the chain rule of differentiation:

$$\frac{d\dot{V}}{dz} = \frac{d\dot{V}}{dp} \cdot \frac{dp}{dz} \tag{4.18}$$

The pressure derivative of the volume flow is approximated with the following equation ($\Delta p = 0.01 \cdot p$):

$$\frac{d\dot{V}}{dp} \approx \frac{\dot{V}(p+\Delta p)-\dot{V}(p)}{\Delta p} \tag{4.19}$$

The derivate for the pressure is obtained by starting from the equation for the hydrostatic pressure:

$$p = \rho \cdot g \cdot z = \frac{\dot{w}}{\dot{V}} \cdot g \cdot z \tag{4.20}$$

The differential of the above equation gives (mass flow is constant because of the steady state and the law for the conservation of total mass):

$$\frac{dp}{dz} = g \cdot \left(\frac{\dot{w}}{\dot{V}} \cdot \frac{dz}{dz} - \frac{\dot{w} \cdot z}{\dot{V}^2} \cdot \frac{d\dot{V}}{dz} \right) = g \cdot \left(\frac{\dot{w}}{\dot{V}} - \frac{\dot{w} \cdot z}{\dot{V}^2} \cdot \frac{d\dot{V}}{dp} \cdot \frac{dp}{dz} \right) \tag{4.21}$$

Solving for dp/dz, gives:

$$\frac{dp}{dz} = \frac{g \cdot \dot{w}}{\dot{V} \cdot \left(1 + g \cdot \frac{\dot{w} \cdot z}{\dot{V}^2} \cdot \frac{d\dot{V}}{dp} \right)} \tag{4.22}$$

The derivative is then multiplied by the direction of flow (*f*), so that when the flow is upwards (*f=-1*), pressure decreases, when the flow is downwards (*f=1*), pressure increases, and in the case of a horizontal flow (*f=0*), pressure remains constant.

$$\frac{dp}{dz} = f \cdot \frac{g \cdot \dot{w}}{\dot{V} \cdot \left(1 + g \cdot \frac{\dot{w} \cdot z}{\dot{V}^2} \cdot \frac{d\dot{V}}{dp} \right)} \tag{4.23}$$

The retention time is computed along the integration of the retention tower. The derivative for the retention time is obtained from:

$$\frac{d\tau}{dz} = \frac{d}{dz}\left(\frac{A \cdot z}{\dot{V}} \right) = \frac{A}{\dot{V}} - \frac{A \cdot z}{\dot{V}^2} \frac{d\dot{V}}{dz} = \frac{1}{v} - \frac{z}{v^2 \cdot A} \frac{d\dot{V}}{dz} \tag{4.24}$$

4.3 Pump / tank

A pump or tank unit can be operated in two modes:

- The volume of the unit is zero (in practice very small). Two or more flows are mixed together so that the external liquid phases of the flows are mixed together. If more than one of the feed flows is a fibre flow, then the fibre bound liquids are also mixed together. After mixing, the reaction equilibrium and the temperature (from the enthalpy balance) are solved.
- The volume of the unit is higher than zero. Flows are mixed as described above, after which the unit is solved as a continuously stirred tank reactor (CSTR).

Since the mixer is considered to be a pump, the pressure inside the mixer needs to be given in the simulation specifications. This will also be the pressure of the product flow.

The mass balance for the unit is:

$$\frac{dn_i^E}{dt} = \dot{n}_{i,IN}^E - \dot{n}_{i,OUT}^E + r_{i,ALL}^E\left(n_i^E, n_i^F, T, p\right) \tag{4.25}$$

$$\frac{dn_i^F}{dt} = \dot{n}_{i,IN}^F - \dot{n}_{i,OUT}^F + r_{i,ALL}^F\left(n_i^E, n_i^F, T, p\right) \tag{4.26}$$

A characteristic feature of a CSTR is that the composition of the flow coming out from the reactor has the same composition as that of the reactor content, i.e. the CSTR is thoroughly mixed. Thus, for the reactor content:

$$\frac{n}{V} = \frac{\dot{n}_{OUT}}{\dot{V}_{OUT}} \Rightarrow n = \dot{n}_{OUT}\frac{V}{\dot{V}_{OUT}} = \dot{n}_{OUT}\tau \tag{4.27}$$

Thus, the mass balance equations become:

$$\frac{d\dot{n}_{i,OUT}^E}{dt} = \left(\dot{n}_{i,IN}^E - \dot{n}_{i,OUT}^E\right)\Big/\tau + r_{i,ALL}^E\left(\dot{n}_i^E, \dot{n}_i^F, T, p\right) \tag{4.28}$$

$$\frac{d\dot{n}_{i,OUT}^F}{dt} = \left(\dot{n}_{i,IN}^F - \dot{n}_{i,OUT}^F\right)\Big/\tau + r_{i,ALL}^F\left(\dot{n}_i^E, \dot{n}_i^F, T, p\right) \tag{4.29}$$

4.4 Displacement washing

The axial dispersion of the liquid flowing through the pulp mat is modelled with a series-of-CSTRs approach (Levenspiel 1972). Thus, in vertical direction pulp mat is divided into CSTR layers whereas in horizontal direction the pulp mat is assumed to behave as in plug flow reactor. Earlier, the series-of-CSTRs approach to model liquid dispersion to washing of pulp mats has been applied by Räsänen (2003). Schematic presentation of a drum washer, and the pulp mat is given in Figure 9.

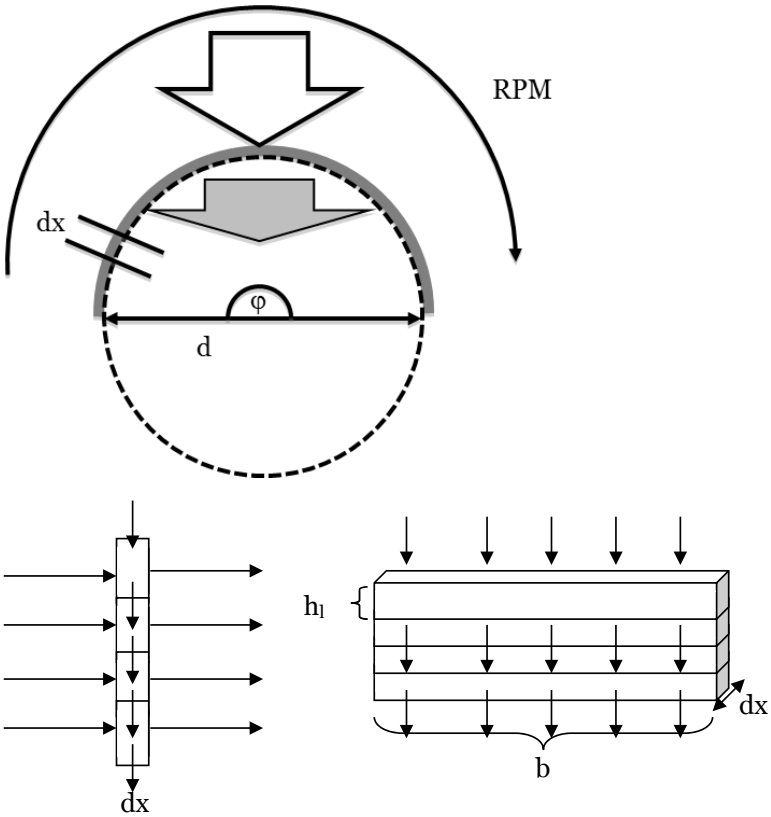

Figure 9. Schematic presentation of the displacement washer model.

Considering the mass balance for a slice of a layer of the pulp mat (dx × b × h_l), the equations developed for a slice of a plug flow reactor can be applied. The pulp mat thickness is assumed to be small in comparison to the drum diameter. The washing water (and possibly some filtrate due to changes in the consistency of the pulp mat) flows through the mat.

$$0 = \dot{n}^E_{i,x,l} - \left[\dot{n}^E_{i,x,l} + \frac{\partial\left(\dot{n}^E_{i,x,l}\right)}{\partial x} \right] \cdot dx + b \cdot dx \cdot \left(N^E_{i,x,l-1} - N^E_{i,x,l} \right) + r^E_{i,x,l,ALL}\left(n^E_{i,x,l}, n^F_{i,x,l}, T, p\right) \tag{4.30}$$

In order to use molar rates in the above equation, it can be noted that:

$$n_x = \frac{\dot{n}_x}{u} dx \tag{4.31}$$

The circumferential velocity (u) is obtained from the revolutions per minute using the equation:

$$u = RPM \Big/ \left(60\, {}^{s}\!/_{\min}\right) \cdot \pi \cdot d \tag{4.32}$$

The first two terms on the right hand side in Equation (4.30) cancel each other and the third term is moved to the left hand side:

$$\frac{\partial\left(\dot{n}_{i,x,l}^{E}\right)}{\partial x}dx = b \cdot dx \cdot \left(N_{i,x,l-1}^{E} - N_{i,x,l}^{E}\right) + r_{i,x,l,ALL}^{E}\left(\dot{n}_{i,x,l}^{E}, \dot{n}_{i,x,l}^{F}, T, p\right)\frac{dx}{u} \tag{4.33}$$

The multiplication of both sides of the equation by u/dx gives:

$$u\frac{\partial\left(\dot{n}_{i,x,l}^{E}\right)}{\partial x} = u \cdot b \cdot \left(N_{i,x,l-1}^{E} - N_{i,x,l}^{E}\right) + r_{i,x,l,ALL}^{E}\left(\dot{n}_{i,x,l}^{E}, \dot{n}_{i,x,l}^{F}, T, p\right) \tag{4.34}$$

The independent variable can be changed from the spatial variable (x) to time (t):

$$u = \frac{dx}{dt} \Rightarrow dt = \frac{dx}{u} \tag{4.35}$$

$$\frac{d\left(\dot{n}_{i,x,l}^{E}\right)}{dt} = u \cdot b \cdot \left(N_{i,x,l-1}^{E} - N_{i,x,l}^{E}\right) + r_{i,x,l,ALL}^{E}\left(\dot{n}_{i,x,l}^{E}, \dot{n}_{i,x,l}^{F}, T, p\right) \tag{4.36}$$

The time needed for a pulp mat slice (of thickness of dx) to travel from the beginning of a sector to the end of a sector is obtained from:

$$t = \frac{\pi \cdot d \cdot \frac{\varphi}{360^{\circ}}}{u} = \frac{A_{Eff}}{b \cdot u} \tag{4.37}$$

The effective area of the drum used for washing is obtained from the equation:

$$A_{Eff} = \pi \cdot d \cdot b\frac{\varphi}{360^{\circ}} \tag{4.38}$$

In the fibre bound liquid phase, the mass balance is simply:

$$\frac{d\left(\dot{n}_{i,x,l}^{F}\right)}{dt} = r_{i,x,l,ALL}^{F}\left(\dot{n}_{i,x,l}^{E}, \dot{n}_{i,x,l}^{F}, T, p\right) \tag{4.39}$$

4.5 Heating and cooling in unit operation models

The unit operation models can be simulated

- at constant temperature (isothermal)
- at constant enthalpy (adiabatic)
- with constant cooling or heating power (J/s or J/m)
- with constant temperature ramp (K/s)
- so that they are heated or cooled to target temperature.

As the **isothermal** operation is chosen, the enthalpy balance is not considered at all. Choosing this option speeds up the simulations. An isothermal assumption is a quite adequate assumption since usually the energy released in the reactions is rather small, and the mass of water is high. Furthermore, the heat capacity of water is high, thus, a relatively high amount of energy is needed to raise the temperature of the water. In all the cases studied in this thesis, an isothermal assumption was applied.

In the **adiabatic** operation, the enthalpy balance is:

$$\frac{dh}{dt} = 0 \tag{4.40}$$

In the case of heating (positive Q) or cooling (negative Q), the enthalpy balance becomes:

$$\frac{dh}{dt} = Q \tag{4.41}$$

Temperature is solved iteratively from the equation of the total enthalpy of a flow (Equation 3.46).

5. Numerical solution methods

This chapter introduces the practices employed in solving differential equations, the unit operation models, and simultaneous phase and reaction equilibria.

5.1 Differential equation solver

The system of differential equations for unit operation models is stiff. This is due to the simultaneous fast (reversible reactions) and slow phenomena (mass transfer, and most of the irreversible reactions). The appropriate numerical solver for this kind of system was found to be DASSL (Petzold 2011).

DASSL solves a system of implicit differential and algebraic equations using backward differentiation formulas. In this work, all differential equations were written in explicit form and the option to provide algebraic equations for DASSL was not used.

It is also possible to implement a routine for the computation of the analytical Jacobian of the system of differential equations, but due to the complexity of the system, the option to estimate the Jacobian numerically was chosen.

The default settings of DASSL were found to be appropriate for the studied cases. The only changed default setting was that the integrator returns to the routine, from which DASSL was called, after each successful step. Thus, it was possible to follow the evolution of composition, temperature, and pressure by printing the intermediate results to text file.

5.2 Solving a unit operation model

Solving a unit operation model as an initial value problem involves:

- Implementation of the ordinary differential equations (right-hand side of dy/dt, where y is a dependent variable and t is the independent variable)
- Setting initial values for all dependent variables
- Setting initial and final value for the independent variable
- Selection of scaling and tolerances in order to obtain an accurate solution in a reasonable computational time

The batch, retention tower, and mixer unit were implemented in such a way that they use the same code as much as possible. As can be noted, batch reactor,

$$\frac{dn_i^E}{dt} = r_{i,ALL}^E\left(n_i^E, n_i^F, T, p\right) \tag{5.1}$$

retention tower,

$$\frac{d\dot{n}_{i,z}^E}{dz} = r_{i,ALL}^E\left(\dot{n}_{i,z}^E, \dot{n}_{i,z}^E, T_z, p_z\right) \Big/ v \tag{5.2}$$

and mixer/tank unit

$$\frac{d\dot{n}_{i,OUT}^E}{dt} = \left(\dot{n}_{i,IN}^E - \dot{n}_{i,OUT}^E\right) \Big/ \tau + r_{i,ALL}^E\left(\dot{n}_i^E, \dot{n}_i^F, T, p\right) \tag{5.3}$$

mass balance equations are quite simple, and differences are minor.

A separate implementation was made for the washer unit.

While solving the unit operation model, the following steps/actions take place in the program:

Independent variable loops from the initial value to the final value

a. DDASSL is called. One of the arguments is the name of the subroutine solving the numerical values of the derivatives. DDASSL uses the same routine for solving the numerical Jacobian.
b. DDASSL calls the derivative subroutine several times to find the evolution of the dependent variables. In that subroutine:
    i. Temperature is solved from the enthalpy using Newton-Raphson iteration (see Chapter 4.5)
    ii. For the derivative of each compound, the contribution from the reversible reaction equilibrium, liquid-liquid mass transfer, gas-liquid mass transfer, and irreversible reactions are determined and summed together (see Chapter 3.6).
c. After a successful step or problem encountered in solving the equations, DDASSL returns:
    i. Successful step: Donnan lambda is solved by solving the polynomial roots or with Newton-Raphson iteration (Equation 3.28)
    ii. Problem: tolerance is increased if the problem is encountered at the beginning (tolerance given by the simulator user was too tight), or decreased if the problem is encountered when many steps have been taken (tolerance was too loose and the system has become numerically unstable)
d. While solving the mixer unit, it needs to be checked whether steady state has been attained.
e. If the independent variable has not attained its final value, then go to step a, otherwise the unit operation model has been solved.

Initial values for the dependent variables are obtained by solving the reaction and phase equilibria of the flow entering the control volume. Otherwise, the composition of the flow coming from the previous unit is used as such.

Initial and final values for the independent variable (time or space) are obtained from the simulation specifications.

The dependent variables are scaled in the following manner:

- The molar amounts in the external liquid phase are scaled by the molar amount of the water in the external liquid phase, and the molar amounts in the fibre bound liquid are scaled by the molar amount of water in the fibre bound liquid.
- Enthalpy (J) is scaled by factor 10^9 and temperature by factor 10^8.

The scaling parameters for dependent variables were chosen so that the order of magnitude of the scaled values would be similar.

The independent variable was scaled by its final value.

Based on experience, a good value for the tolerance was usually 10^{-10}. When the Donnan effect changes a lot during simulation, then a tolerance of 10^{-12} has been proven to be suitable. A higher tolerance value speeds up the simulations, but the risk of numerical instability increases. Numerical instability may lead to the crashing of the simulations (DDASSL returns an error message) or, ironically, a significant slowdown of the simulation.

5.3 Solving reaction and phase equilibria

As mentioned above, each dependent variable needs to be initialized before solving the unit operation model. The assumption is that the composition of the flows entering the control volume satisfies both the reaction and phase equilibria.

Two approaches have been implemented for solving the equilibrium composition. The first implementation was based on solving the set of equations. The second approach, the rate-base approach, was developed, because the first approach was causing various problems quite often. The first approach, although no longer in use in the simulator, can be considered worth documenting. The classification of compounds into “reduced” and “non-reduced” compounds and the stoichiometric matrix for mass balance computations are also used in the present simulator implementation. The electroneutrality condition is needed in the initialization of the rate-based approach.

The methods presented in the literature are based on solving the system of equations or minimization of Gibbs energy (Lindgren et al. 2001). Towers and Scallan (1996) derived the equation for solving the Donnan equilibrium, and reaction equilibrium of acidic groups bound to the fibre wall. In order to use their equation, the pH in the external liquid phase needs to be known. Later, Räsänen et al. (2001) extended the equation so that the external liquid phase pH can also be solved in addition to the reaction equilibrium of the soluble compounds. In order to validate and demonstrate the rate-based approach, the pulp suspension equilibrium was

solved and compared to the results obtained with the equation presented by Towers and Scallan.

5.3.1 From the system of equations

Solving reaction and phase equilibria simultaneously results in the composition of all phases utilizing the following set of equations:

- Mass balances
- Reaction equilibrium
- Electroneutrality condition
- Equilibrium between fibre bound liquid and external liquid
- Gas-liquid equilibrium

Due to the high number of equations and variables, a systematic approach is needed in defining the equations and unknowns. First of all, compounds need to be considered as "reduced" or "non-reduced" according to Christian (2003). The main rule is that "non-reduced" compounds are formed solely using "reduced" compounds. For instance:

- "reduced" compounds: H^+, SO_4^{2-}, H_2O, Na^+
- "non-reduced" compounds: HSO_4^- ($H^+ + SO_4^{2-}$), OH^- ($H_2O - H^+$)

The fact that compounds are in these two categories helps in the construction of the stoichiometric matrix, Ξ:

- Each column (c) represents a "reduced" compound
- Each row (r) represents a compound (first "reduced" and then "non-reduced")

The upper sub-matrix (number of "reduced" × number of "reduced") is the unit matrix. The lower sub-matrix (number of "non-reduced" × number of "reduced") consists of stoichiometric coefficients of reaction and phase equilibria.

For example:

	H^+	SO_4^{2-}	H_2O	Na^+
H^+	1	0	0	0
SO_4^{2-}	0	1	0	0
H_2O	0	0	1	0
Na^+	0	0	0	1
HSO_4^-	1	1	0	0
OH^-	-1	0	1	0

Both mass balances and

$$total_n_c = w_{H_2O} \sum_{r \neq H_2O} \Xi(r,c) \cdot m_r + \Xi(r_{H_2O}, c) \cdot n_{H_2O} \tag{5.4}$$

reaction equilibria can be written using a stoichiometric matrix:

$$K_r = \prod_c m_c^{\Xi(r,c)} \tag{5.5}$$

The additional condition in electrolyte systems is the electroneutrality condition:

$$\sum_r z_r m_r = 0 \tag{5.6}$$

In the above example, there are:

- 6 unknowns
- 4 mass balance equations, 2 reaction equilibria, and the electroneutrality condition, i.e. in total 7 equations

Since there are more equations than unknowns, the equations cannot be solved until one of the equations is removed from the system. The mass balance for the hydrogen ion is left out, and a solution for the equations can be obtained.

In a two liquid phase system (with one acidic group bound to the fibre wall), the stoichiometric matrix is:

For example:

	H^+	SO_4^{2-}	H_2O	Na^+	**AF^-**
H^+	1	0	0	0	0
SO_4^{2-}	0	1	0	0	0
H_2O	0	0	1	0	0
Na^+	0	0	0	1	0
AF^-	0	0	0	0	1
HSO_4^-	1	1	0	0	0
OH^-	-1	0	1	0	0
HAF	1	0	0	0	1

$$total_n_c = w_{H_2O}^E \sum_{r \neq H_2O} \Xi(r,c) \cdot m_r^E + \Xi(r_{H_2O},c) \cdot n_{H_2O}^E + w_{H_2O}^F \sum_{r \neq H_2O} \Xi(r,c) \cdot m_r^F + \Xi(r_{H_2O},c) \cdot n_{H_2O}^F \tag{5.7}$$

$$K_r = \prod_c \left(m_c^E\right)^{\Xi(r,c)} \tag{5.8}$$

$$K_r = \prod_c \left(m_c^F\right)^{\Xi(r,c)} \tag{5.9}$$

$$\sum_r z_r m_r^E = 0 \tag{5.10}$$

$$\sum_r z_r m_r^F = 0 \tag{5.11}$$

The additional condition is the Donnan equilibrium for all mobile solutes:

$$\lambda^{z_i} = \frac{m_i^F}{m_i^E} \tag{5.12}$$

The amount of water in the fibre bound liquid is obtained from FSP:

$$w_{H_2O}^F = FSP \cdot w_{Fibres}^F \tag{5.13}$$

In the above example, there are:

- 6 unknowns for the external liquid phase composition, 8 unknowns for the fibre bound liquid composition, and Donnan λ i.e. in total 15 unknowns.
- 5 mass balances, 2 electroneutrality conditions, 5 Donnan equilibria, 2 reaction equilibria in the external liquid, 3 reaction equilibria in the fibre bound liquid, and an equation for the amount of water in the fibre bound liquid phase, i.e. in total 18 equations.

For equilibrium reactions involving only mobile compounds, it can be noted that:

$$K_r = \prod_c \left(m_c^E\right)^{\Xi(r,c)} = \prod_c \left(\frac{m_c^F}{\lambda^{z_c}}\right)^{\Xi(r,c)} = \prod_c \left(\lambda^{z_c}\right)^{-\Xi(r,c)} \prod_c \left(m_c^F\right)^{\Xi(r,c)} = \prod_c \left(m_c^F\right)^{\Xi(r,c)} \tag{5.14}$$

The final form of Equation (5.14) is obtained, because each equilibrium reaction preserves electroneutrality:

$$\prod_c \left(\lambda^{z_c}\right)^{-\Xi(r,c)} = \lambda^{-\sum_c z_c \Xi(r,c)} = \lambda^0 = 1 \tag{5.15}$$

Thus, the reaction equilibrium needs to be solved only in the fibre bound liquid. That reduces the number of equations to 16. Furthermore, the hydrogen ion mass balance is left out. Thus, the number of equations is 15, which equals the number of unknowns.

Finally, a compound, O_2, having a gas-phase equilibrium is added to the example:

	H^+	SO_4^{2-}	H_2O	Na^+	AF^-	**O_2 (aq)**
H^+	1	0	0	0	0	0
SO_4^{2-}	0	1	0	0	0	0
H_2O	0	0	1	0	0	0
Na^+	0	0	0	1	0	0
AF^-	0	0	0	0	1	0
O_2 (aq)	0	0	0	0	0	1
HSO_4^-	1	1	0	0	0	0
OH^-	-1	0	1	0	0	0
HAF	1	0	0	0	1	0
O_2 (g)	0	0	0	0	0	1

In comparison to the previous example:

- 3 more unknowns: amount of oxygen in the gas phase, molality of oxygen in the external liquid, molality of oxygen in the fibre bound liquid.
- 3 more equations: equilibrium between the gas phase and the external liquid, Donnan equilibrium, and mass balance for oxygen.

To summarize, when solving reaction and phase equilibria simultaneously, the following equations are needed:

- Mass balances for all other “reduced” compounds except for the hydrogen ion.
- Electroneutrality condition in the external liquid phase, and in the fibre bound liquid phase if fibres are present in the system.
- Reaction equilibrium only in the fibre bound liquid if fibres are present in the system. In a one-liquid phase system, the reaction equilibrium is solved in the external liquid phase.
- If fibres are present, the Donnan equilibrium for all mobile solutes.
- If fibres are present, the amount of water in the fibre bound liquid phase is obtained from the FSP value.
- The gas-liquid equilibrium is solved only in the external liquid phase. No gas is present in the fibre bound liquid.

The implementation of the above set of equations is simple. However, from the numerical point of view they are quite difficult to solve. The values for the molalities might be different by several orders of magnitude and the equations are non-linear. Accurate initial values obviously help in finding the solution, but usually such initial values are hard to generate.

One way to circumvent the order of magnitude problem is to use logarithmic molalities as variables to be solved (Christian 2003). This leads to the linearization of the equilibrium equations, but on the other hand, the electroneutrality and the mass balance equations become non-linear.

In addition, one trick is to use pH control in solving the equations. This also turned out to be the only way to solve the Donnan equilibrium in most cases. In the pH control approach, the hydrogen ion molality in the external liquid phase is forced to the value given in the simulation specifications. “pH control” ion is also chosen. The total amount of “pH control” ion is allowed to change. When this kind of “pH control” is applied, there is one additional equation (hydrogen ion molality is forced to the set pH) and one additional variable (the total amount of “pH control” ion). The pH control ion can be chosen from the set of “reduced” compounds.

Unfortunately, the various tricks to solve the set of non-linear equations did not always work. Furthermore, the usage of “pH control” in solving the Donnan equilibrium was not always practical, since the external liquid phase pH is not necessarily known. Thus, a rate-based approach to solve the reaction and phase equilibria was developed.

5.3.2 With rate-based approach

The rate-based approach was introduced in (Kuitunen and Alopaeus 2013). A similar approach has been applied for instance in solving material balances in distillation columns (Rose et al. .1958).

The molar amount of compounds and Donnan lambda given in the simulation specifications are used for the initialization of the composition of the phases. In the external liquid phase, the hydrogen and hydroxide ion molalities are set according to the deviation from the electroneutrality condition. The hydrogen ion molality is adjusted to compensate the excess negative charge, and the hydroxide ion molality to compensate the excess positive charge. The Donnan equilibrium equation is then applied in the computation of the hydrogen and hydroxide ion molalities in the fibre bound liquid. Finally, if there is an excess positive or negative charge in the fibre wall, a new imaginary component, *hydrogen ions attached into the fibres*, is added into the simulation. Its amount in the fibre wall is adjusted so that the fibre wall liquid is electroneutral.

By setting the initial values as described above, the electoroneutrality and mass balance conditions are fulfilled.

When the equilibrium composition is solved, the amount of *hydrogen ions attached to the fibres* is driven to zero. When the hydrogen ion is cleaved from the fibre wall, it becomes a "normal" hydrogen ion in the fibre bound liquid.

$$\frac{dm^{F}_{H_in:fibres^{+}}}{dt} = -10^{8} m^{F}_{H_in:fibres^{+}} = -\frac{dm^{F}_{H^{+}}}{dt} \tag{5.16}$$

Before using the batch reactor unit model to solve the ODEs, the liquid-liquid mass transfer area is set to 10^{15} m²/kg fibres in order to speed up the liquid-liquid mass transfer to be as fast as the equilibrium reactions. This modification reduces the stiffness of the equations. Giving unrealistic value for liquid-liquid mass transfer area is in this case acceptable, since the aim is to solve the equilibrium. The batch reactor is first solved only for 10^{-10} s. Simulation time is gradually increased, and finally it is equal to 1 hour, which is assumed to be long enough for the system to attain phase and reaction equilibria.

In order to validate and demonstrate the rate-based approach, the equilibrium of case "Pulp 1" presented by Towers and Scallan (1996) was solved with their equation and with the rate-based approach. The equation presented by Towers&Scallan is:

$$\begin{aligned} &\frac{2\left(\lambda^{3}-1\right)}{V+F\left(\lambda^{2}-1\right)}\sum M^{2+} + \frac{\left(\lambda^{2}-1\right)}{V+F\left(\lambda-1\right)}\sum M^{+} \\ &+\left(\lambda^{2}-1\right)\left[H^{+}\right]_{S} - \sum \frac{\lambda\left(C_{i}/F\right)K_{i}}{\lambda\left[H^{+}\right]_{S}+K_{i}} = 0 \end{aligned} \tag{5.17}$$

The symbols used in Equation (5.17) are given in Table 2 (N.B! not included in the nomenclature). M^{2+} stands for the total amount of divalent

cations (as mol/kg fibres), and M^+ for the total amount of monovalent cations (as mol/kg fibres).

Table 2. The symbols used in Equation (5.17) and the pulp suspension composition.

Total liquid (V)	dm^3/kg fibres	134.7
Water content of wall (F)	dm^3/kg fibres	1.4
Acid group content in the fibre wall (C)	mol/kg fibres	0.109
Dissociation constant (K)	mol/dm^3	10^{-4}
Total calcium	mol/kg fibres	0.0568
Total magnesium	mol/kg fibres	0.0177
Total manganese	mol/kg fibres	0.00096
Total sodium	mol/kg fibres	0.0436

The resulting equilibrium compositions estimated with the Towers&Scallan model and with rate-based approach are presented in Table 3. The major difference between these models is the fact that the ion product of water was not included in Equation (5.17). The most visible effect of this, reflected in the results, is the difference in the pH in the external liquid phase. In the Towers&Scallan approach, the pH was set to 8, but when the ion product of water is taken into account, the pH in the external liquid phase is 10.77. With the rate-based approach, there is a very minor error in electroneutrality ($<10^{-12}$) and mass balances ($<10^{-4}$ %). These errors are due to the usage of a numerical method (DDASSL) in solving the ODEs.

Table 3. Results from the equilibrium computations with the Towers&Scallan equation and with the rate-based approach. A^- is the dissociated fibre bound acid and HA is the non-dissociated fibre bound acid.

	Towers & Scallan	**Rate-based approach**	**Towers & Scallan**	**Rate-based approach**
Compound	**In fibre bound liquid (m^F, mmol/kg water)**		**In external liquid phase (m^E, mmol/kg water)**	
Ca^{2+}	27.74	27.78	0.13	0.13
Mg^{2+}	8.64	8.66	0.04	0.04
Mn^{2+}	0.47	0.47	2.28E-03	2.27E-03
Na^+	4.08	4.09	0.28	0.28
H^+	**1.43E-04**	**2.29E-07**	**1.00E-05**	**1.60E-08**
OH^-	4.48E-02	4.46E-02	0.64	0.64
A^-	77.75	77.86	-	-
HA	1.12E-01	1.79E-04	-	-
	λ		**pH in external liquid**	
	14.3488	14.3809	8.00	10.77

The key factor in using the rate-based method for solving the equilibrium is to set the initial values for the composition in both liquid phases (Table

4). The equilibrium was solved with the rate-based method using two different initial values for Donnan lambda, namely 1 (default guess) and 10 (rather close to the equilibrium value). According to the Donnan lambda value, ions are distributed between the liquid phases. Then, the hydroxide ion molality in the external liquid phase was adjusted according to the electroneutrality condition. The hydroxide ion concentration in the fibre bound liquid was then obtained from the Donnan equilibrium for the hydroxide ion. The fibre bound liquid electroneutrality condition was then adjusted by introducing the new variable, the hydrogen ion attached to the fibre wall. The molality of this imaginary compound can be negative or positive. As the equilibrium is solved, the molality of the hydrogen ion attached to the fibre wall is driven to zero (Equation 5.16).

Table 4. Initial values when solving the equilibrium with the rate-based approach.

	Initial guess for λ			
	1		**10**	
Compound	**In fibre bound liquid (m^F, mmol/kg water)**	**In external liquid phase (m^E, mmol/kg water)**	**In fibre bound liquid (m^F, mmol/kg water)**	**In external liquid phase (m^E, mmol/kg water)**
Ca^{2+}	0.42	0.42	20.78	0.21
Mg^{2+}	0.13	0.13	6.48	0.06
Mn^{2+}	0.01	0.01	0.35	0.00
Na^{+}	0.32	0.32	2.96	0.30
H^{+}	-	-	-	-
OH^{-}	1.44	1.44	0.08	0.85
A^{-}	-		-	
HA	77.86		77.86	
H^{+} attached to the fibre wall	-		- 58.10	

In Figure 10, the evolution of molalities in the fibre bound and external liquid is shown. As the fibre bound acid dissociates, it produces hydrogen ions. These are neutralized by hydroxide ions. As the stagnant negative charge in the fibre wall increases, the molalities of positively charged ions increase in the fibre bound liquid. Consequently, their molalities slightly decrease in the external liquid (Figure 11).

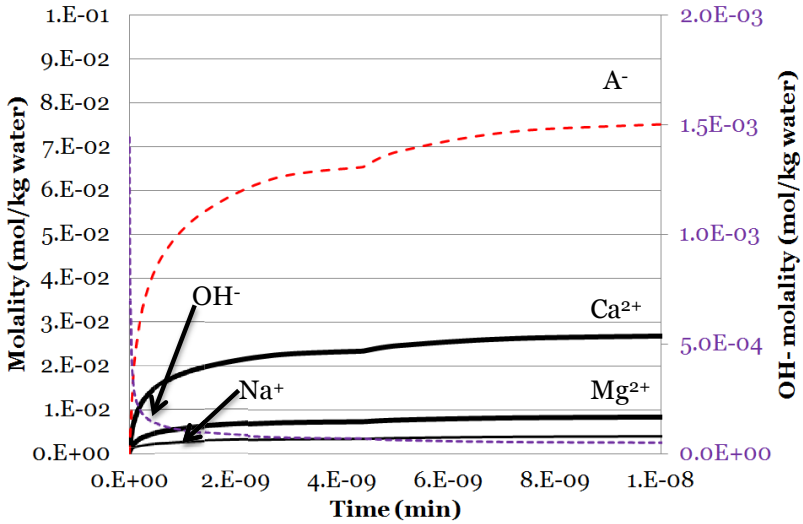

Figure 10. Evolution of molalities in the fibre bound liquid phase. Initial Donnan λ= 1. Dissociated fibre bound acid (A^-): dashed red line; Hydroxide ion (OH^-): dashed violet line; Calcium (Ca^{2+}) and magnesium (Mg^{2+}): thick black line; Sodium (Na^+): thin black line.

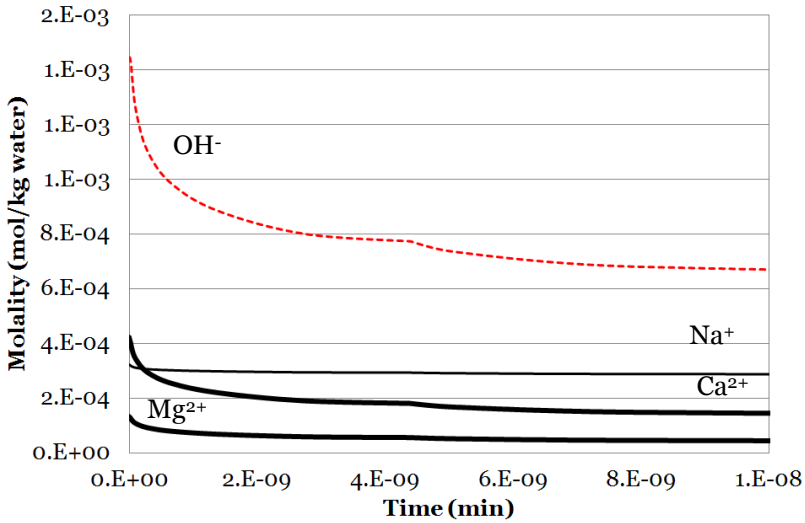

Figure 11. Evolution of molalities in the external liquid phase. Initial Donnan λ= 1. Hydroxide ion (OH^-): dashed red line; Calcium (Ca^{2+}) and magnesium (Mg^{2+}): thick black line; Sodium (Na^+): thin black line.

As the initial guess for Donnan lambda was 10, the changes in cation and hydroxide ion molalities were quite minor as shown in Figure 12. In this case, as the fibre bound acid dissociates, the hydrogen ions produced are converted to the imaginary hydrogen ions in the fibre wall until the molality of this imaginary compound equals zero.

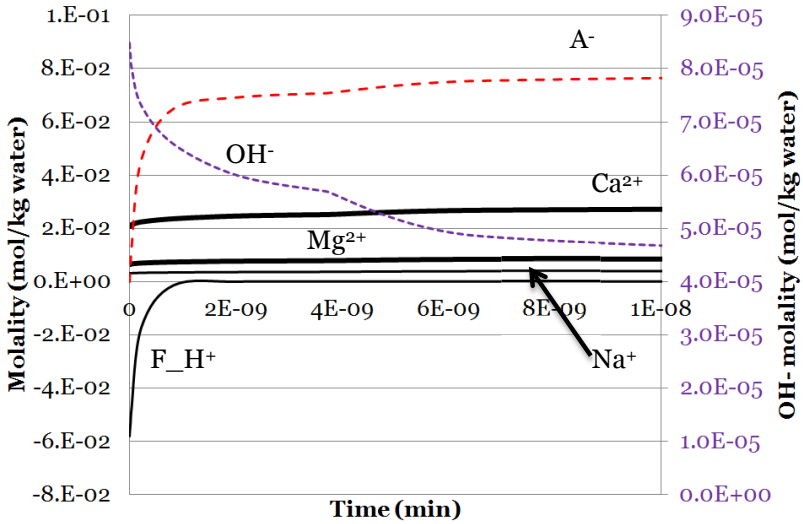

Figure 12. Evolution of molalities in the fibre bound liquid phase. Initial Donnan λ= 10. Dissociated fibre bound acid (A^-): dashed red line; Hydroxide ion (OH^-): dashed violet line; Calcium (Ca^{2+}) and magnesium (Mg^{2+}): thick black line; Sodium (Na^+): thin black line; Imaginary hydrogen ion bound to the fibre wall (F_H+): thin black line.

6. Case studies

The experimental setups modelled in this thesis are introduced in Table 5. The cases were chosen based on the needs set by the different projects:

- Accurate prediction of pH evolution in hot water extraction is important for the overall modelling of the hot water extraction kinetics
- Kraft cooking liquor impregnation (deacetylation in alkaline conditions) was part of the work done for modelling the kraft pulping process
- Lignin oxidation by oxygen was part of the work done for modelling the oxygen delignification stage
- An alkaline extraction model was needed so that the whole bleaching line could be simulated.

During this work, the following important factors that affect the success of the modelling outcome were identified:

1. The experimental setup needs to be mimicked in the simulation as precisely as possible. For instance, reactor pressure evolution needs to be modelled if gaseous compounds are participating reactions (Case 3).
2. Usually, homogenous phases are assumed in modelling. This has to be taken into account when designing the experiments. In Case 3, the batch reactor did not initially contain baffles. Thus, there was a big gas bubble around the rotating impeller and no bubbles travelled to the corners of the reactor. When baffles were added, the gas was homogenously dispersed as small bubbles in the liquid phase.
3. A sufficient number of different analyses of the raw materials needs to be performed. If it turns out that the characterization has not been complete enough, then the initial amount of that non-analysed compound or structure becomes an additional model parameter that needs to be regressed or otherwise estimated. This was discussed in papers [II] and [IV].

4. Samples need to be analysed in sufficient detail so that the reaction scheme can be developed. In principle, only the evolution of analysed compounds can be modelled with confidence.

Table 5. Experimental conditions in the case studies.

	Case 1	**Case 2**	**Case 3**	**Case 4**
	Hot water extraction	**Kraft cooking liquor impregnation**	**Lignin oxidation by oxygen**	**Alkaline extraction of Do pulp**
Raw material	Birch wood meal	Thin eucalypt wood chips	Softwood kraft lignin	Softwood OD pulp
Temperature (°C)	180	20/45/90	90/110	80
Pressure (bars)	Higher than vapour pressure of water	Atmospheric	6/9	2/4
Chemicals	Water	Water, NaOH, NaCl	Water, NaOH, O_2	Water, NaOH, H_2O_2, O_2
Reactor	Batch	Batch	Batch reactor connected to oxygen bottle	Batch reactor or batch reactor connected to oxygen bottle
Mixing conditions			Good	Mixing was not on all the time
Analysis results used in the parameter optimization	pH, acetyl groups in filtrate, acetic acid in filtrate	Acetyl groups in wood	Pressure, pH, lignin structure analysis, methanol, low molecular weight acids, H_2O_2	Kappa number, brightness, intrinsic viscosity, TOC, AOX, liquid absorbance, formic acid, carbonate, residual alkali and H_2O_2
Analysis results not used in the parameter optimization	-	-	Lignin acids	Yield, glycolic acid, COD, and pH.
References	Borrega et al. (2011)	Inalbon et al. (2009)	Kalliola et al. (2011)	Paper [IV]

7. Model parameters

A number of parameters are required in the models. Table 6 lists the parameter sources used in the case studies. The goal was to favour literature sources as much as possible.

The reaction kinetic parameters reported for the model compounds were not always found to be suitable. In Case 4 in particular, some reaction kinetic parameters were regressed although the parameters from the model compound studies were available in the literature. Regression ensures that the model behaviour is correct in the relevant model application conditions.

The optimization of the model parameters was conducted with Kinfit software (Jakobsson and Aittamaa 2012). The objective function was minimized by the Levenberg-Marquardt method (Press et al. 1989). In all cases, the objective function was:

$$SSE = \sum_i \sum_j \frac{\left(measured_{i,j} - simulated_{i,j}\right)^2}{measured_{i,j}^2} w_j \tag{7.1}$$

The weighting factors (w) deviated from unity only in Case 4, (paper [IV]).

Table 6. Parameter sources utilized for each case.

	Case 1	**Case 2**	**Case 3**	**Case 4**
	Hot water extraction	**Kraft cooking liquor impreg-nation**	**Lignin oxidation by oxygen**	**Alkaline extraction of Do pulp**
Raw material composition	Analysis (acetyl groups), literature (metals), based on the pH evolution in HWE (uronic acids)	Analysis, literature (phenolic units in lignin)	Analyses	Computations based on the engineering parameters*, analysis (HexA), regression (iron and concentration of a cellulose unit containing carbonyl functionality)
Properties of lignin units used in the engineering parameter estimation	-	-	-	Literature concerning model compound studies, own measurement
Thermo-dynamic parameters	Literature	Literature	Literature	Literature, pKa value of carbohydrates regressed
Reaction kinetic parameters	Regression	Regression	Literature (model compound studies), Arrhenius parameter regressed for 6 reactions	Case 3 parameters, Arrhenius frequency factor regressed for 8 reactions, dissolution stoichiometry was regressed for 3 reactions
Mass transfer parameters	Case 2	Regression of liquid film thickness, literature	Gas-liquid mass transfer parameter from a separate experimental setup	Gas-liquid mass transfer parameter from literature correlation, liquid-liquid mass transfer parameters from literature

* Engineering parameter = Kappa number, brightness, intrinsic viscosity

Regression = parameter regressed with Kinfit software.

8. Results and discussion

In this chapter, the effect of inert compounds and buffering on pH evolution are discussed first. This is followed by a brief introduction to the effect of temperature and pressure on the reversible reactions, irreversible reactions, and solubility of gases. Finally, everything is combined, and the importance of modelling the reaction and phase equilibria simultaneously with the irreversible reactions is demonstrated in the context of the case studies. In particular, the role of pH in modelling the irreversible reaction kinetics is emphasized.

The last topic of this chapter concerns the overall reaction kinetic libraries developed for lignin oxidation by oxygen and alkaline extraction of chlorine dioxide delignified pulp.

8.1 Effect of inert compounds on pH

Inert compounds are those that do not participate in irreversible reactions. However, as demonstrated in this chapter, they have an indirect effect on the reactions through changing the pH in both the fibre bound liquid and external liquid phase.

The Donnan effect in wood and in pulp suspensions has been the topic of numerous experimental and modelling studies (Grignon and Scallan 1980; Scallan 1983; Pu et al. 1993; Towers and Scallan 1996; Lindgren et al. 2001; Susilo et al. 2005). Based on these studies, it can be summarized that:

- When the pH in the external liquid phase is increased, Donnan lambda has higher values
- When ionic strength is low, Donnan lambda has higher values
- When there are more acids bound to the fibre wall and accessible to ion exchange, Donnan lambda has higher values.

Previously, the Donnan effect has been coupled with the modelling of HexA acid hydrolysis (Räsänen et al. 2005), and HexA formation and degradation in kraft pulping (Bogren et al. 2008). Räsänen et al. studied the effect of extensive washing on HexA removal kinetics experimentally, and in the modelling part of the study, they found that the Donnan theory explained the experimental observations. In the study by Bogren et al., the ionic strength varied as well due to the variation in NaHS concentration.

However, they did not model the fact that removal of HexA reduces the Donnan effect.

Of the cases discussed in this thesis, Case 1 (hot water extraction) and Case 2 (kraft cooking liquor impregnation) demonstrate the indirect effect of inert species on the reaction kinetics.

No literature discussing the Donnan effect or ion exchange in the context of hot water extraction could be found. The experimental results of Saltberg et al. (2006) concerning the leaching of metal ions from wood at varying pH values were similar to those of leaching metal ions from pulp (Towers and Scallan 1996). Thus, the existence of the Donnan effect is supported by Saltberg's results under neutral and slightly acidic conditions in a wood-water suspension. Previously, the Donnan effect on wood in alkaline conditions has been studied experimentally and modelled by Pu et al. (1993).

Unfortunately, probably because the Donnan effect has not been acknowledged in the context of hot water extraction, some relevant factors influencing the extent of the Donnan effect have not been reported for the raw materials used in the hot water extraction experiments. These factors are the amounts of metal ions and uronic acids in the wood to be extracted with hot water.

Consequently, in Case 1, the amount of metal ions and of uronic acids was estimated based on the literature. The metal ion content of wood might vary, thus, the effect of the varying calcium ion amount on the hydrogen ion concentration in the fibre wall was studied with the model (Table 7). The hydrogen ion concentration varies several orders of magnitude depending on the amount of calcium ions. Using the literature values for the composition (marked with * in Table 3), the pH in the fibre bound liquid phase is 3.2. The general hypothesis is that the onset of the hot water extraction reactions is due to the formation of hydrogen ions from the ionization of water at the high temperatures used in the extraction (Garrote et al. 1999). As the temperature of water is increased from 25 to 180 °C, its pKa value changes from 14 to 11.4. Thus the hydrogen ion concentration at 180 °C in plain water is $2 \cdot 10^{-6}$ mol/kg water. This is a much lower concentration than the predictions given in Table 7. Thus, based on the simulation results, the acidity in the fibre wall liquid caused by the uronic acids could be the reason for the onset of the hot water extraction reactions.

In this study, it has been assumed that calcium ions are in the soluble state. It has been suggested in the literature that the calcium in wood would be present as oxalate precipitate (Werkelin et al. 2010). The amount of oxalate extracted from spruce wood was 0.4 mmol/kg wood (Werkelin et al. 2010), which suggests that very low proportion of calcium (total amount 18

mmol/kg wood) is as oxalate precipitate. If calcium is as oxalate precipitate, then the free calcium ion concentration would be lower, and the pH in the fibre wall would be lower as well.

Table 7. The effect of Ca^{2+} amount (mmol/kg wood) on the initial composition of a wood-water suspension at 180°C. *The composition used in the modelling of hot water extraction.

	9	15	16.7*	21	37	43	47
$m^F_{H^+}$ (mmol kg^{-1} water)	1.14	0.70	0.60	0.44	0.10	0.04	0.01
pH^F	2.94	3.15	3.22	3.36	3.99	4.42	5.11
pH^E	6.5	6.6	6.63	6.7	7.0	7.2	7.5
λ	3602	2808	2585	2190	1028	604	247

In addition to the initial Donnan effect, the evolution of the Donnan effect as a function of time needs to be modelled as well (Figure 13). During hot water extraction, uronic acids dissolve from the wood, thus changing the Donnan effect. Simultaneously, metal ions are extracted from the wood due to the changes in the ion exchange property of the wood. At the end of the simulation, the pH values in the fibre wall liquid and external liquid phase are equal to each other.

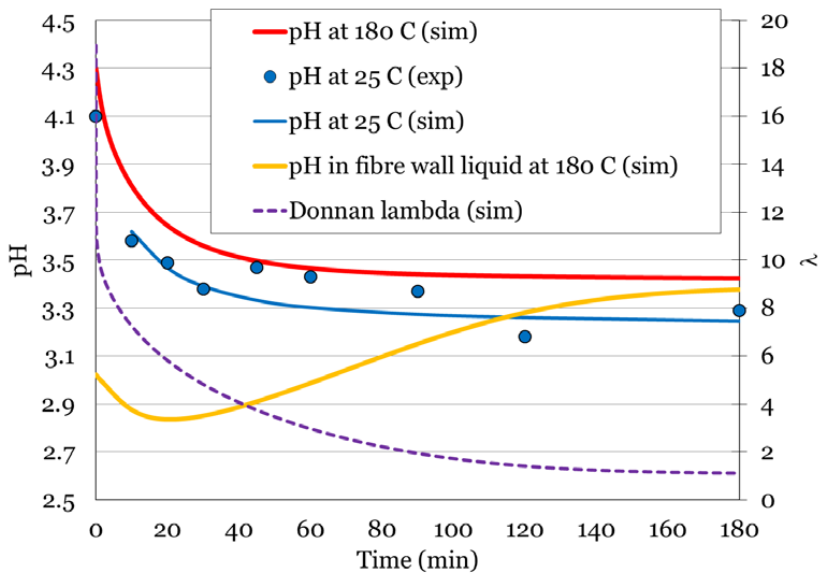

Figure 13. Simulated Donnan λ (dashed violet line), pH in external liquid at 180°C (red solid line), pH in fibre bound liquid at 180°C (orange solid line), and pH in external liquid at 25°C (blue solid line). Measured pH given with ●. Adopted from paper II.

In order to further demonstrate the effect of acetic acid, uronic acid, and metal ion concentration on the hydrogen ion molality, experimental data

published by Song et al. (2008) was studied. Based on the analysed amounts of uronic and acetic acid, and pH, the amount of metal ions in the filtrate samples was estimated. The result of the computation was that the Song et al. filtrate samples contained 28 – 38 mmol monovalent cations/kg wood. According to Saltberg et al. (2006), softwood contains 43 mmol monovalent cations/kg wood (divalent cation concentrations were multiplied by two). These two values are very close to each other, giving support to the assumption that pH is determined by the concentration of acetic acid, uronic acid, and metal ions in the filtrate.

The effect of inert salt on the alkaline impregnation kinetics was modelled with the Donnan theory in paper [II]. From Figure 14, it can be observed that, at lower alkali charges, the Donnan lambda is quite high, and it becomes smaller as the alkali charge is increased. This is due to the higher ionic strength. As salt is added into the suspension, the Donnan lambda has very similar values at all alkali charges, but the salt addition is not high enough to totally suppress the Donnan effect. As the reactions proceed, the Donnan effect becomes higher because the inaccessible uronic acids become accessible.

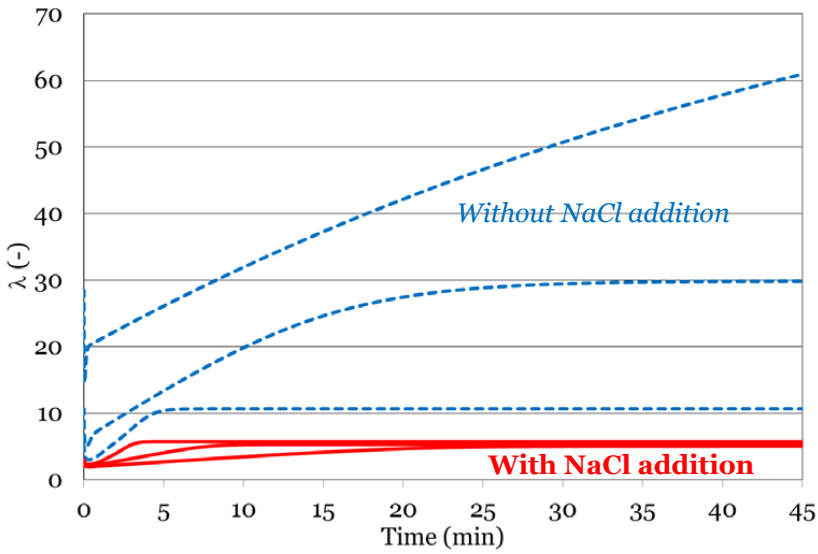

Figure 14. Evolution of Donnan lambda in the simulation of kraft cooking liquor impregnation at 90°C with NaCl addition (solid lines in red) and without NaCl addition (dashed lines in blue). NaOH molality from top to down: 0.01, 0.0316, and 0.1 mol/(kg water) and NaCl molality (only red): 0.19, 0.1684, and 0.1 mol/(kg water). Adopted from paper II.

As a conclusion, if the inert compound is an ion (cation or anion), it needs to be included in the model. The ions have an influence on the evolution of pH in both liquid phases through the Donnan effect or neutralizing or increasing the acidity. The pH, in turn, has an influence on the reaction kinetics as will be demonstrated below.

8.2 Effect of buffering on pH

Compounds that buffer the pH, i.e. prevent or slow down the evolution of pH, enter the processes with the raw materials or are formed in the reactions. In paper [I] it was shown that uronic acids and metal hydroxides entering the bleaching line with the pulp, buffer the pH in the D_o stage. According to the simulations, the pH at the end of the D_o stage would be one unit lower if the buffering effects were omitted.

Another example of buffering is Case 3. When lignin is oxidized by oxygen, a number of acids, detected by capillary electrophoresis, are formed: carbon dioxide, formic acid, oxalic acid, acetic acid, and glycolic acid. Another set of acids are those bound to the polymeric lignin, like muconic acid, maleic acid, and other acidic pseudo-units. Of all of these acidic compounds, only the reaction equilibrium of carbon dioxide was relevant in alkaline lignin oxidation conditions. The other acidic reaction products were assumed to be readily dissociated in alkaline conditions. The reversible reactions of carbon dioxide are:

$$CO_3^{2-} + H^+ \leftrightarrow HCO_3^- \quad (8.1)$$

$$HCO_3^- + H^+ \leftrightarrow CO_2 \text{ (liquid phase)} + H_2O \quad (8.2)$$

$$CO_2 \text{ (liquid phase)} \leftrightarrow CO_2 \text{ (gas phase)} \quad (8.3)$$

As the oxidation reactions proceed, more CO_3^{2-} and H^+ are formed. Following Le Chatelier's principle, the equilibrium shifts towards the right-hand side of Equation (8.1). In the harshest conditions, at 120 min, practically all the carbon dioxide is as HCO_3^- (Figure 15). After 120 min, further buffering takes place through the reactions given by Equations (8.2) and (8.3).

Initially, the equilibrium reactions given by Equations (8.2) and (8.3) were not included in the simulation, because, erroneously, it was thought that at such a high pH, these equilibria would not be relevant. As a result, the experimental pH curves could not be reproduced; instead, the pH attained too low values at the end of the simulation. Simulations with the model presented in paper [III] produce pH curves given in Figure 16.

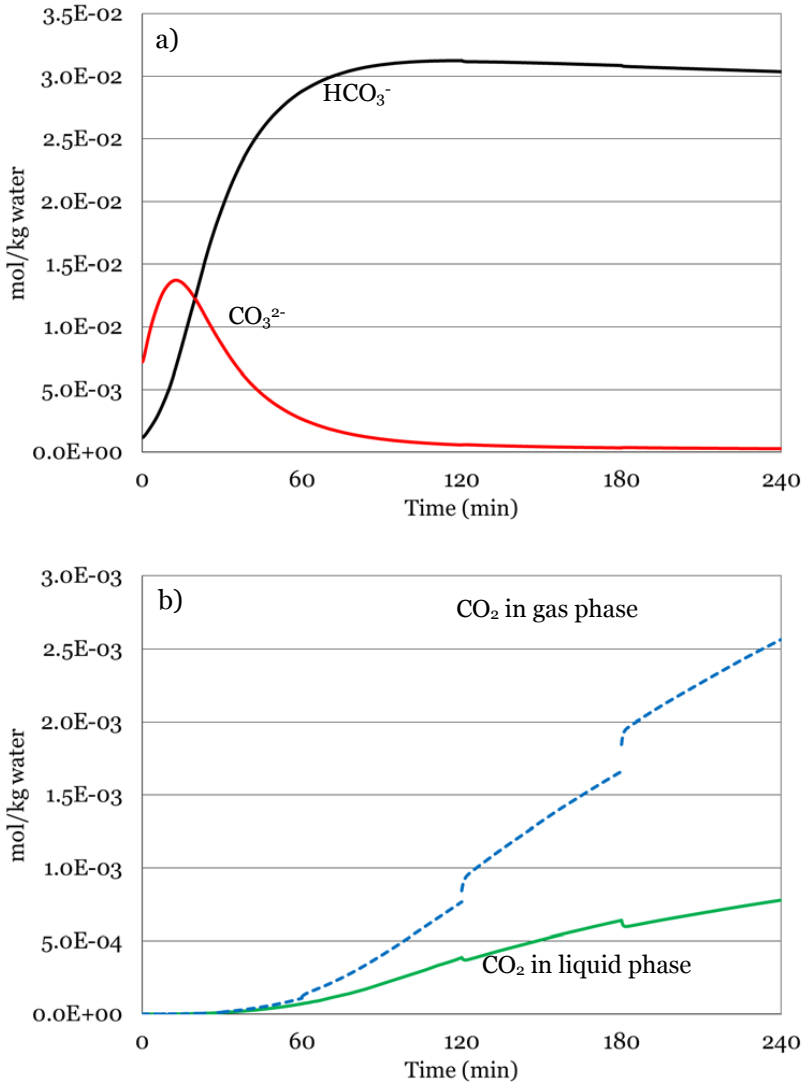

Figure 15. Simulated CO_2 species molalities (mol/kg water) at 0.9 MPa and 110 C. a) HCO_3^- (black line) and CO_3^{2-} (red line), b) CO_2 in gas phase (ticked blue line) and CO_2 in liquid phase (solid green line). Adopted from paper III.

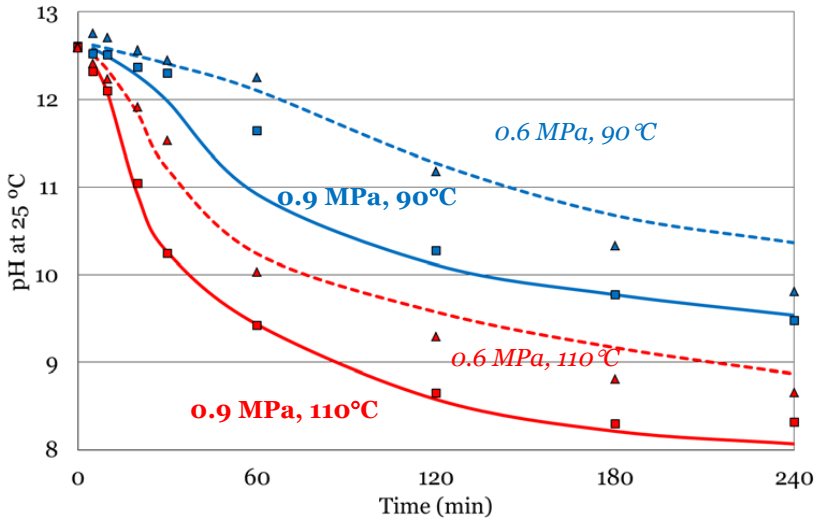

Figure 16. Measured and simulated evolution of pH in lignin oxidation experiments: 0.6 MPa, 90C (▲,---); 0.9 MPa, 90C (■,—); 0.6 MPa, 110C (▲,---); 0.9 MPa, 110C (■,—). Adopted from paper III.

8.3 Effect of temperature and pressure on the reaction kinetics

The effect of temperature on the reaction rates comes mainly through the Arrhenius equation. The higher the activation energy of the reaction, the greater the effect of the temperature on the reaction rate constant.

Temperature also has an effect on the equilibrium constants as discussed in Chapter 3.3. From Table 8 (Visuri et al. 2012), it can be seen that although chemical composition is the same, a variation in temperature changes the hydrogen ion concentration, because the values of the equilibrium constants change as a function of temperature. In all papers included into this thesis, the equilibrium constants are given at the temperatures used in the experiments.

Table 8. The estimated hydrogen ion molality in the kinetic experiments of galacto glucomannan acid catalyzed hydrolysis at 25°C and at reaction temperatures (Visuri et al. 2012).

	Estimated H^+ molality at temperatures			
pH at 25 °C	**25°C**	**150°C**	**160°C**	**170°C**
3.8	$1.58 \cdot 10^{-4}$	$1.25 \cdot 10^{-4}$	$1.23 \cdot 10^{-4}$	$1.21 \cdot 10^{-4}$
4.0	$1.00 \cdot 10^{-4}$	$7.83 \cdot 10^{-5}$	$7.72 \cdot 10^{-5}$	$7.62 \cdot 10^{-5}$
4.2	$6.31 \cdot 10^{-5}$	$4.91 \cdot 10^{-5}$	$4.85 \cdot 10^{-5}$	$4.78 \cdot 10^{-5}$

Temperature also has an influence on the solubility of gases through the equilibrium constants. This was considered when modelling Case 3. In the range of the conditions studied, the equilibrium constant for oxygen solubility did not change much. However, the variation in the water vapour-liquid equilibrium constant was high, which had an influence on the overall gas phase composition, and thus, the oxygen concentration in the liquid

phase. If the water vapour in the gas phase had been neglected, the oxygen concentration would have been 7 – 20 % too high at the beginning of the simulation. At the end of the simulation, as the reactor pressure had lowered due to the consumption of oxygen in reactions, the error would have been even higher: 10 – 75 %.

In addition to temperature, the solubility of gases is affected by pressure. In the lignin oxidation and in some alkaline extraction experiments, the pressure in the reactor varied. Thus, it was important to model the variation in the reactor pressure as well. In the lignin oxidation experiments, the pressure was recorded, thus enabling the validation of oxygen consumption in the modelled reactions.

8.4 Effect of phase and reaction equilibria on irreversible reactions

As noted above, the phase and reaction equilibria have an influence on the evolution of pH in an aqueous wood/pulp system. Due to ion exchange, the pH is lower in the fibre bound liquid, and the difference depends, for instance, on the ionic strength. Reversible and irreversible reactions produce or consume hydrogen or hydroxide ions. Buffering, in turn, prevents or slows down changes in pH.

Hydrogen and hydroxide ions are directly involved in a number of reaction mechanisms in the cases studied, as can been seen in Figure 17. All of these reactions take place in the fibre wall, except for reaction A. Reaction A takes place in both liquid phases since xylan, and simultaneously acetyl groups, dissolve into the liquid from the fibre wall, and are then able to diffuse into the external liquid phase.

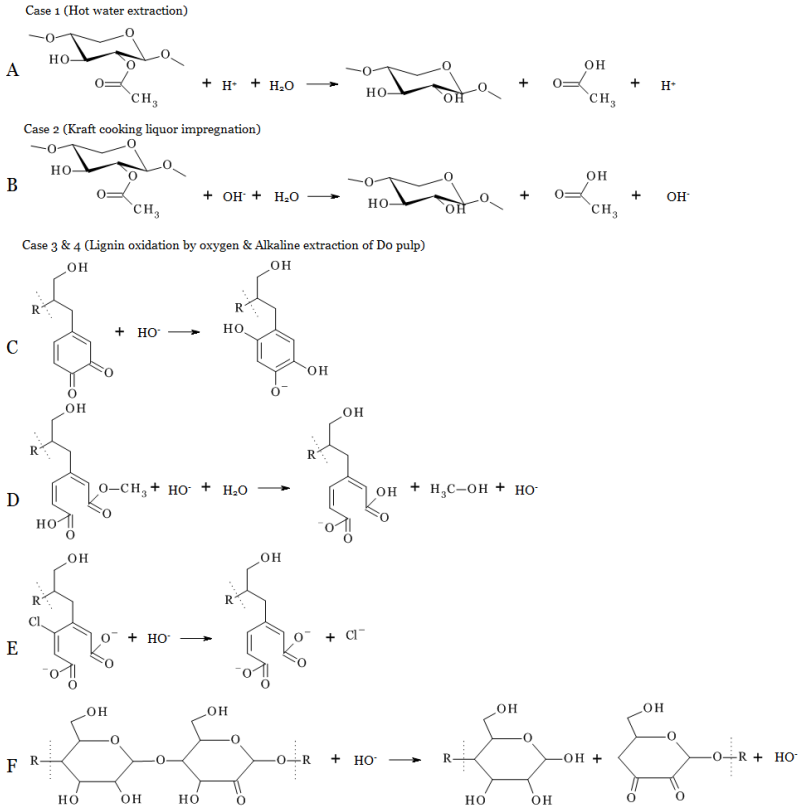

Figure 17. Irreversible reactions involving OH^- and H^+. **A**: hydrogen ion catalyzed hydrolysis of ester bond; **B**: hydroxide ion catalyzed hydrolysis of ester bond; **C**: 1,4-reductive Michael addition; **D**: hydroxide ion catalyzed hydrolysis of ester bond; **E**: hydrolysis of aliphatic chlorine; **F**: scission of glycosidic bond, which is next to the unit carrying the carbonyl group.

The best case for demonstrating the effect of liquid-liquid equilibrium on the reaction kinetics is Case 2. In some of the experiments, NaCl was added to set the total Na^+ molality into 0.2 mol/(kg water). While comparing the deacetylation rate with and without NaCl addition, the NaCl addition accelerated the deacetylation rate (Figure 18).

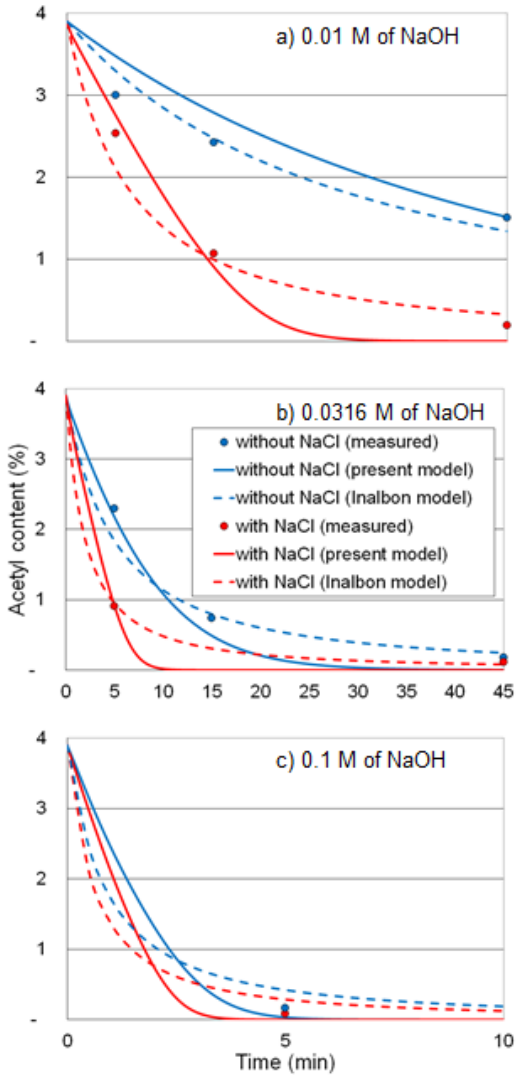

Figure 18. Deacetylation of wood during kraft cooking liquor impregnation at 90°C: Measured data (dashes) from (Inalbon et al. 2009), simulated acetyl group content with the model developed in this thesis (solid line), and with the model developed by (Inalbon et al. 2009) (dashed line), with NaCl addition (in red) and without NaCl addition (in blue). NaOH molality: a) 0.01, b) 0.0316, and c) 0.1 mol (kg water)$^{-1}$. NaCl molality: a) 0.19, b) 0.1684, and c) 0.1 mol/(kg water). Adopted from paper II.

The acceleration is due to the changes in the Donnan effect. With NaCl addition, the Donnan lambda is lower (Figure 14). In Equation (8.4), it can be concluded that the lower the Donnan separation coefficient, the higher the molality of the negatively charged ion in the fibre bound liquid phase:

$$\lambda^{z_i} = \frac{m_i^F}{m_i^E} \Rightarrow m_{OH^-}^F = m_{OH^-}^E \lambda^{-1} = \frac{m_{OH^-}^E}{\lambda} \tag{8.4}$$

Furthermore, the higher the molality of the hydroxide ion in the fibre bound liquid, the higher the rate of the deacetylation reaction:

$$k \cdot m_{OH-} \cdot m_{Acetyl} \tag{8.5}$$

Vos et al. (1966) have proposed the above rate law (Equation 8.5) for the deacetylation of cellulose acetate. Inalbon et al. (2009), on the other hand, ignored the ion exchange effect and derived the following rate law for the deacetylation reaction:

$$k \cdot c_{Acetyl}^{n} \cdot c_{OH^-}^{m} \cdot c_{Na^+}^{p} \tag{8.6}$$

The drawback of the rate law given by Equation (8.6) is the fact that it is suitable only for systems utilizing eucalypt raw material and 1-1 salt for adjusting the ionic strength. For instance, the uronic acid content varies among different raw materials (Sjöström 1989).

As demonstrated in paper [II], the deacetylation is so fast in industrial kraft liquor impregnation conditions that the exact modelling of the deacetylation reaction is not crucial. More important is the precise modelling of the mass transfer in the wood particles, as the mass transfer rate determines the rate of the kraft cooking liquor impregnation. However, there are many other reactions, like the peeling and stopping reactions of carbohydrates, HexA formation and degradation, and lignin reactions in kraft pulping, whose kinetics are directly or indirectly influenced by the hydrogen or hydroxide ions. These reactions are slower, thus their precise kinetic modelling is important.

Another example of the effect of phase equilibrium on the reaction kinetics is the gas-liquid equilibrium of oxygen in the context of Case 3 (oxidation of lignin by oxygen) and Case 4 (alkaline extraction of D0 pulp) (Figure 19).

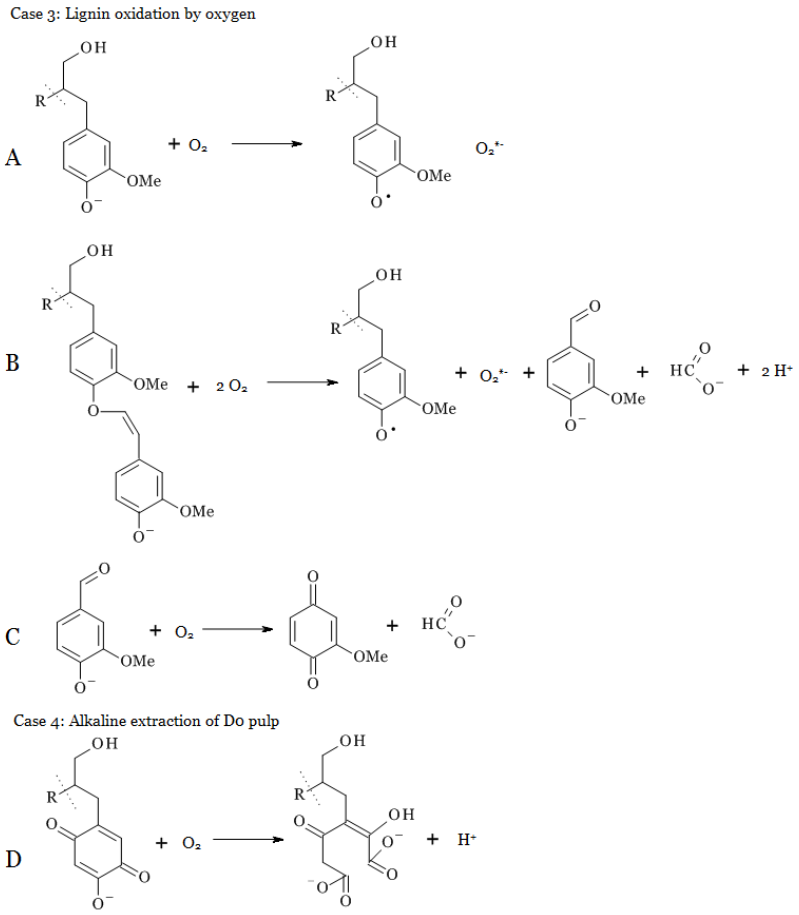

Figure 19. Reactions involving oxygen. **A**: oxidation of guaiacyl phenolate; **B**: oxidation of conjugated phenolate; **C**: oxidation of vanillin; **D**: oxidation of hydroxy-p-quinone.

By comparing the experimental curves of guaiacyl (Figure 20) and conjugated phenols (Figure 21) evolution at different pressures (but the same temperatures), it can be seen that the increase in the pressure results in faster degradation of these phenolic structures. These effects are reproduced by the model and support the idea that the gas-liquid equilibrium needs to be modelled simultaneously with the reaction kinetics.

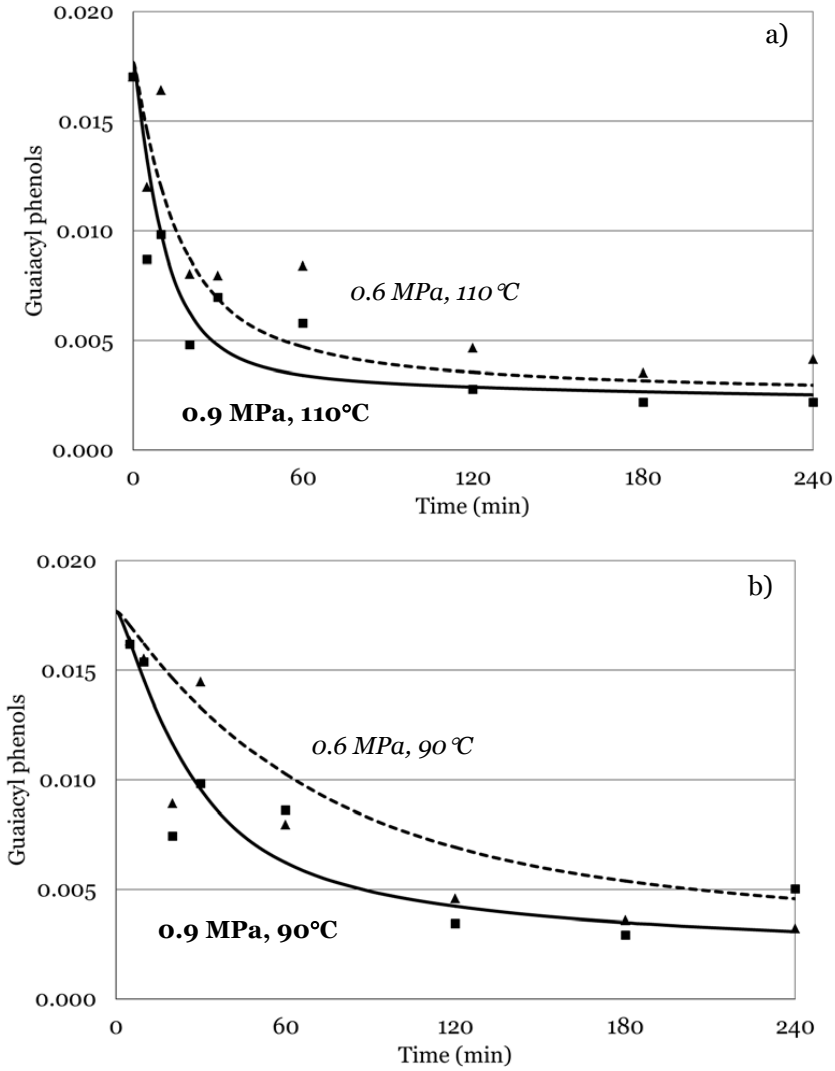

Figure 20. Simulated (lines) and measured (dashes) evolution of guaiacyl phenols (mol/kg water) as a function of time: a) 110°C at 0.6 MPa (dashed line, ▲) and 0.9 MPa (solid line, ■) pressure, b) 90°C at 0.6 MPa (dashed line, ▲) and 0.9 MPa (solid line, ■) pressure. Adopted from paper III.

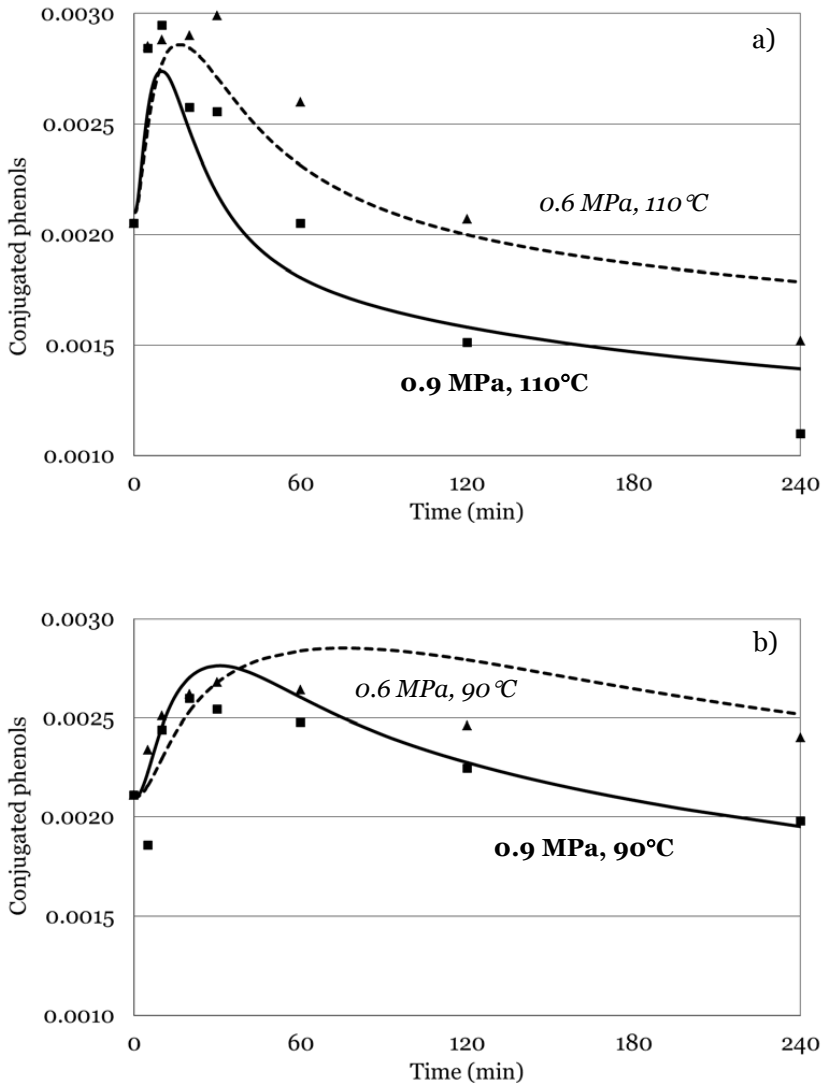

Figure 21. Simulated (lines) and measured (tick marks) evolution of conjugated phenols (mol/kg water) as a function of time: a) 110°C at 0.6 MPa (ticked line, ▲) and 0.9 MPa (solid line, ■) pressure, b) 90°C at 0.6 MPa (ticked line, ▲) and 0.9 MPa (solid line, ■) pressure. Adopted from paper III.

Finally, the reversible reaction equilibrium has an effect on irreversible reaction kinetics. First, the importance of the reversible reaction equilibrium of chemicals, and then that of the wood constituents is discussed.

The oxidation chemicals used in the different case studies were oxygen and hydrogen peroxide. In Case 3 (lignin oxidation by oxygen), hydrogen peroxide was not charged into the reactor, but was formed during the reactions as verified experimentally. In Case 4 (alkaline extraction of D_0 pulp), one or both of these chemicals were charged. When oxygen and

hydrogen peroxide are applied, oxygen radicals are formed as the oxygen and hydrogen peroxide react with organic compounds or with transition metals. Hydrogen peroxide and the oxygen radicals are involved in the reversible acid-base equilibrium reactions as given in Table 9.

Table 9. Reversible acid-base equilibrium of oxygen radicals and hydrogen peroxide and the pKa values estimated at temperatures used in case studies. Adopted from papers III and IV.

	Temperature (°C)				
	25	**80**	**88**	**91**	**107**
$HO_2^* \leftrightarrow O_2^{*-} + H^+$	4.79	-	4.49	4.48	4.42
$H_2O_2 \leftrightarrow HOO^- + H^+$	11.67	10.96	10.89	10.87	10.76
$HO^* \leftrightarrow O^{*-} + H^+$	11.54	10.85	10.78	10.74	10.59

Whether dissociated or non-dissociated, these compounds react as nucleophiles or electrophiles, i.e. they react with different functionalities in the organic compounds.

Of the equilibrium reactions listed in Table 9, the first is the least important. The pH in Cases 3 and 4 was so high that the dominating form is the superoxide anion (O_2^{*-}).

The dissociation of hydrogen peroxide is relevant in both Cases 3 and 4. Only the dissociated form, the hydroperoxide anion (HOO^-), is reactive with conjugated phenols (Case 3) and chromophores (Case 4). In Case 3, the degradation of conjugated phenols is quite rapid during the first 60 min, after which the degradation slows down (Figure 21). The reason for the slowdown is the fact that the pH (Figure 16) attains such a low value that hydrogen peroxide is no longer in dissociated form (Figure 22b).

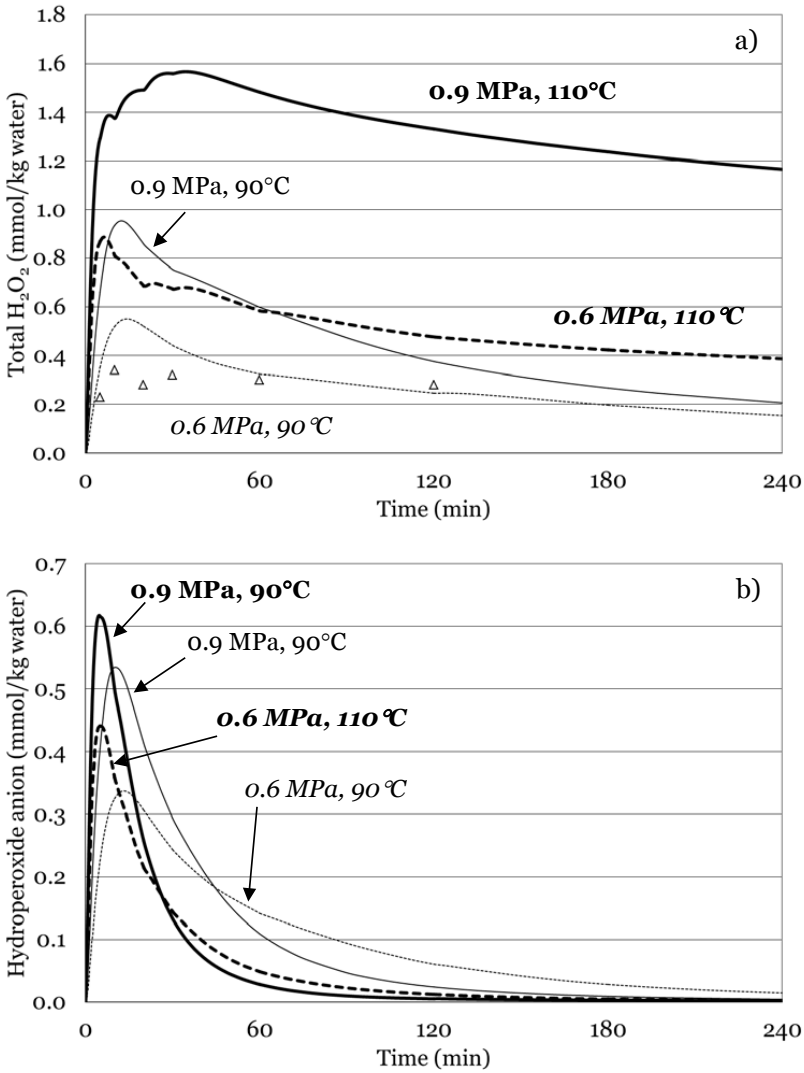

Figure 22. Simulated (lines) and measured (tick mark, 0.6 MPa, 90 °C) (a) total hydrogen peroxide and b) hydroperoxide anion in mmol/kg water. Adopted from paper III.

The dissociation of the hydroxyl radical is especially relevant in Case 3. At the beginning of the experiment, the hydroxyl radical is partly dissociated (Figure 23). The dissociated counterpart, the oxyl-anion radical, is responsible for the formation of new conjugated phenols (Figure 21). As the pH decreases (Figure 16), the oxyl-anion radical concentration becomes so low that the rate of new conjugated phenol formation becomes negligible in comparison to the degradation of conjugated phenols.

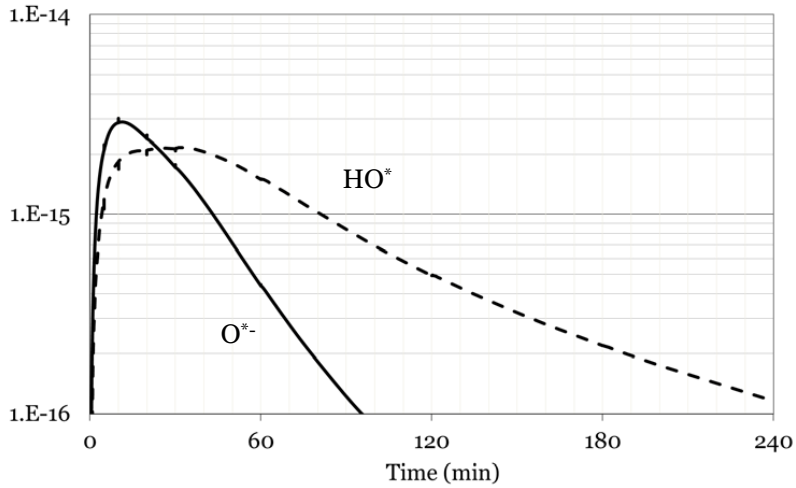

Figure 23. Molality of simulated hydroxyl (dashed line) and oxyl-anion (solid line) radicals (mol/kg water) at 0.9 MPa and 90°C. Adopted from paper III.

In studies concerning chlorine dioxide delignification, the importance of considering the equilibrium of chlorous acid in particular has been acknowledged by Lehtimaa et al. (2010).

Finally, considering the role of the reversible equilibrium reactions of organic compounds, the reaction of phenolate with oxygen is a relevant example. Only the dissociated phenol is able to react with oxygen whereas the non-dissociated form is non-reactive. From Figure 20, it can be concluded that when the pH drops below 10 (Figure 16), the guaiacyl phenols no longer degrade. In the conditions used in Case 3, the pKa value for guaiacyl phenol was ~ 10.5.

8.5 The reaction kinetic library for lignin and carbohydrate degradation with oxygen chemicals in alkaline conditions

For the simulation of Cases 3 and 4, in total 62 irreversible reactions were collected. The work consisted of determining the stoichiometry and reaction kinetic (Arrhenius) parameters of each reaction. The reactions were selected based on experimental observations. For instance, in Case 3, oxalic acid, formic acid, and carbon dioxide were detected in substantial amounts. Thus, the reactions in which these acids are formed were sought.

As can be noted from the figures presented in paper [III] and Figures 16, 20, 21, and 22, comparing Case 3 simulation results to the experimental results, the correspondence of the following measured and simulated values was:

- good for: pressure, pH, methanol, glycolic, acetic, guaiacyl phenol, conjugated phenol, formic acid, oxalic acid, and hydrogen peroxide

- relatively poor for: condensed phenols, liquid absorbance, lignin acids

Based on the mechanism proposed for lignin reactions in oxygen delignification conditions, the relevance of the different reactions for the actual oxygen delignification stage, in which the lignin is attached to the fibre wall and the aim is to solubilize the lignin, was discussed in paper [III]. A short summary of the main conclusions is given below.

Firstly, the breakage of the ether bonds between the lignin units was pointed out as important for two reasons:

1. cleavage of ether bonds results in the formation of phenolic units, thus improving the reactivity of lignin towards oxygen
2. the molecular weight of lignin polymers becomes smaller, enhancing lignin solubility

Especially the amount of acetic acid and glycolic acid formation correlate with the number of ether bonds cleaved during the oxygen delignification.

Another topic discussed in the context of oxygen delignification was the reactions that consume alkali. Especially if the alkali concentration becomes too low, the reactions will not proceed, since the guaiacyl phenols are no longer dissociated and cannot react with oxygen. A lot of alkali is consumed in the degradation of muconic acid by hydroxyl radicals. A beneficial feature of this reaction is that the muconic acids trap hydroxyl radicals and prevent their reaction with carbohydrates. Of all reactions defined for the hydroxyl radicals, the reaction of hydroxyl radical with muconic acid was the fastest.

Concerning Case 4 (alkaline extraction of D_o pulp), the correspondence of the following measured and simulated values was:

- good for: brightness, kappa number, and alkali consumption,
- relatively good for: intrinsic viscosity, TOC, AOX, formic acid, and liquid absorbance (Figure 24)
- rather poor for: hydrogen peroxide (Figure 25), carbon dioxide, glycolic acid, and oxalic acid

All measured and simulated values, together with relative error, are given for Case 4 in Tables 10-14.

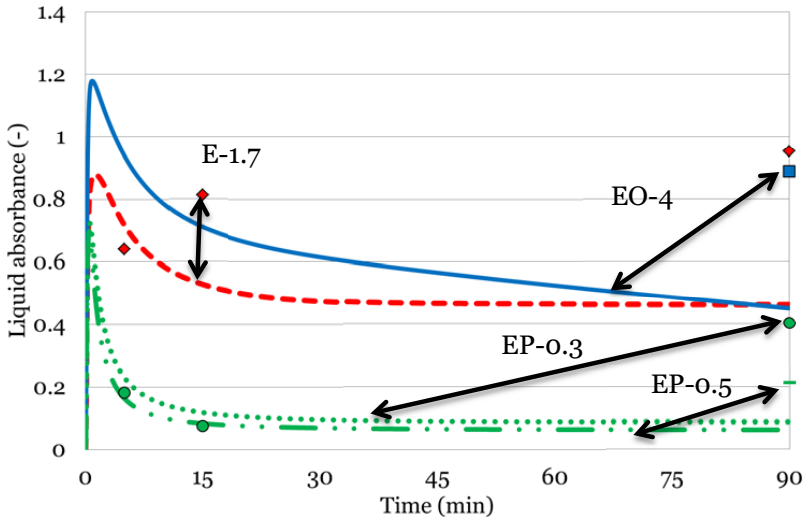

Figure 24. Simulated (lines) and measured (dash) liquid absorbance at in different experiments: E-1.7 (---, ♦), EO-4 (solid line, ■), EP-0.3 (····,●), and EP-0.5(·–·–,-).

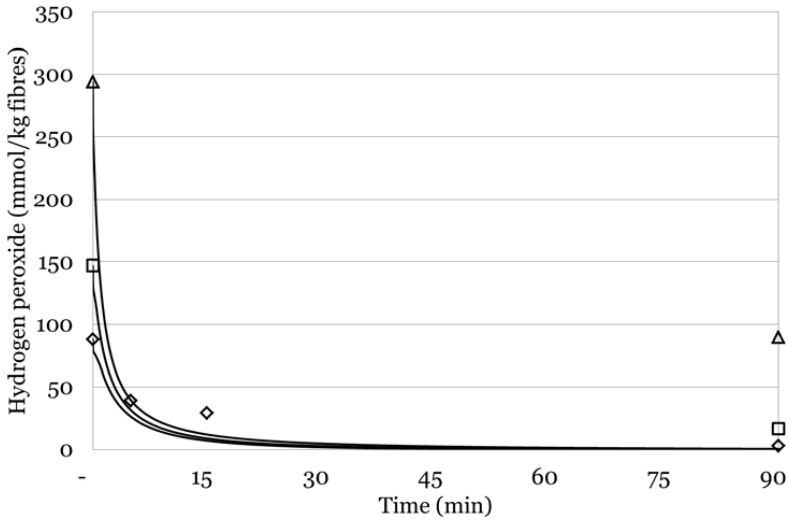

Figure 25. Simulated (solid line) and measured (dash) hydrogen peroxide concentration (as mmol/kg fibres) in alkaline extraction with different initial peroxide charges.

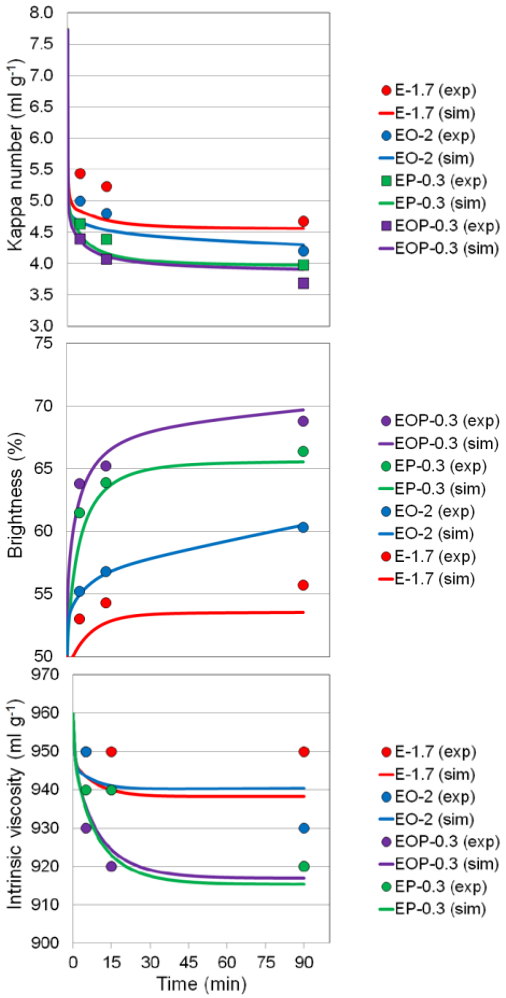

Figure 26. Comparison of the effect of oxygen and peroxide charge on a) kappa number, b) brightness, c) intrinsic viscosity evolvement. Oxygen pressure 2 bar, peroxide charge 0.3 w-%, and alkali charge 1.7 w-%. Adopted from paper IV.

Concerning the kinetics of the alkaline extraction, most of the changes take place during the first 5 minutes (Figure 26). For instance, the following reactions are rapid:

- hydroxide ion catalysed hydrolysis of chlorine bound to aliphatic carbon
- hydroxide ion catalysed hydrolysis of muconic acid esters leading to the solubilisation of lignin and decrease in kappa number
- hydroxide ion catalysed cleavage of glycosidic bonds next to the unit carrying carbonyl functionality in cellulose chains leading to intrinsic viscosity drop
- reaction of hydroperoxide anion with chromophore leading to increased brightness

After the rapid initial period, the kappa number decreases slightly, and brightness increases. Oxygen has been modelled to react with chromophores and this reaction is partly responsible for the slow kinetics. In the presence of hydrogen peroxide, the intrinsic viscosity decreases due to the formation of oxyl-anion from the hydrogen peroxide decomposition reactions.

Based on the developed model, a rather high amount of alkali is consumed in the ionization of hydroxyl groups in carbohydrates (~50%). In the model, it was assumed that this reversible reaction is responsible for part of the alkali consumption since in the course of modelling work it was noted that the other reversible and irreversible reactions did not consume enough alkali. However, this assumption should be validated in a separate experiment, for instance by measuring the alkali consumption of fully-bleached pulp. If it turns out that the hydroxyl groups in carbohydrates do not consume as much alkali as modelled in paper [IV], then there are some presently unknown reactions responsible for said alkali consumption.

Furthermore, it was noted that not all of the iron analysed from the pulp samples participated in the radical reactions degrading hydrogen peroxide. A likely explanation is the formation of a solid solution with magnesium precipitate. More details are given in paper [IV].

The parameter optimization program failed to provide a reaction rate constant for the reaction of a hydroxyl radical with a cellulose unit. According to the optimization result, the dissociated counterpart of the hydroxyl radical, the oxyl-anion radical, would be responsible for degrading the cellulose. It is possible that the hydroxyl radicals are consumed in various reactions with lignin and filtrate before they are able to diffuse into the cellulose-rich region.

Based on the modelling results, the lignin units that have undergone a reaction in the preceding D_o stage are more easily soluble in the alkaline extraction stage than those that have not encountered reactions in the D_o stage. Another interesting result was that it seems that when lignin is dissolved from the fibre wall it simultaneously takes some carbohydrate fragments along with it. This assumption is based on the observation that lignin dissolved from the fibre wall did not contribute enough on the TOC measured from the filtrate samples.

Table 10. Measured and simulated values together with relative error for alkaline extraction experiments (paper [IV]).

Experiment	k457/s457			kappa number (ml/g)			intrinsic viscosity (ml/g)		
	measured	simulated	Δ (%)	measured	simulated	Δ (%)	measured	simulated	Δ (%)
E-1.2-90 min	0.18	0.20	11	4.9	4.6	-7	940	938	0
E-1.7-5 min	0.20	0.24	17	5.4	4.8	-11	950	944	-1
E-1.7-15 min	0.19	0.21	12	5.2	4.7	-10	950	940	-1
E-1.7-90 min	0.18	0.20	14	4.7	4.6	-2	950	938	-1
E-3-90 min	0.18	0.20	13	4.7	4.5	-3	930	940	1
EP-0.3-5 min	0.12	0.14	22	4.6	4.5	-4	940	935	-1
EP-0.3-15 min	0.10	0.11	2	4.4	4.2	-5	940	923	-2
EP-0.3-90 min	0.09	0.09	6	4.0	4.0	0	920	915	-1
EP-0.5-90 min	0.06	0.07	7	3.8	3.8	0	920	907	-1
EP-1-90 min	0.04	0.04	5	3.5	3.7	5	880	892	1
E-2.5-P-0.5-15 min	0.09	0.07	-19	4.2	4.0	-6	910	916	1
E-2.5-P-0.5-90 min	0.06	0.06	-7	3.7	3.8	1	900	906	1
EO-2-5 min	0.17	0.18	6	5.0	4.7	-7	950	944	-1
EO-2-15 min	0.16	0.17	1	4.8	4.5	-6	940	941	0
EO-2-90 min	0.13	0.13	-2	4.2	4.3	2	930	940	1
EO-4-90 min	0.12	0.12	-5	4.0	4.2	6	920	941	2
EOP-0.3-5 min	0.10	0.11	8	4.4	4.4	-1	930	936	1
EOP-0.3-15 min	0.09	0.09	-6	4.1	4.1	1	920	924	0
EOP-0.3-90 min	0.07	0.07	-8	3.7	3.9	6	920	917	0
EOP-0.5-90 min	0.06	0.05	-5	3.4	3.8	11	920	907	-1

Table 11. Measured and simulated values together with relative error for alkaline extraction experiments (paper [IV])

	OH- (mol/kg water)			H2O2 (mol/kg water)			pH		
	measured	simulated	Δ (%)	measured	simulated	Δ (%)	measured	simulated	Δ (%)
E-1.2-90 min	0.016	0.017	10	n.d.	n.d.		10.4	10.6	2
E-1.7-5 min	0.032	0.028	-11	n.d.	n.d.		10.8	10.8	0
E-1.7-15 min	0.030	0.028	-8	n.d.	n.d.		10.8	10.8	0
E-1.7-90 min	0.027	0.028	2	n.d.	n.d.		10.8	10.8	0
E-3-90 min	0.057	0.055	-4	n.d.	n.d.		10.9	11.1	1
EP-0.3-5 min	0.028	0.025	-10	4.34E-03	3.40E-03	-22	10.8	10.7	-1
EP-0.3-15 min	0.028	0.025	-12	3.27E-03	9.12E-04	-72	10.8	10.7	-1
EP-0.3-90 min	0.023	0.024	6	3.27E-04	2.38E-06	-99	10.7	10.7	0
EP-0.5-90 min	0.023	0.023	1	1.86E-03	1.15E-05	-99	10.6	10.7	1
EP-1-90 min	0.019	0.022	14	9.96E-03	6.81E-05	-99	10.5	10.7	2
E-2.5-P-0.5-15 min	0.046	0.040	-14	7.28E-03	1.10E-03	-85	10.9	10.9	0
E-2.5-P-0.5-90 min	0.040	0.039	-1	1.73E-03	8.58E-06	-100	10.8	10.9	1
EO-2-5 min	0.031	0.028	-9	n.d.	n.d.		10.8	10.8	0
EO-2-15 min	0.029	0.028	-6	n.d.	n.d.		10.8	10.8	0
EO-2-90 min	0.024	0.027	12	n.d.	n.d.		10.7	10.8	1
EO-4-90 min	0.024	0.027	16	n.d.	n.d.		10.7	10.8	1
EOP-0.3-5 min	0.028	0.025	-12	4.12E-03	3.22E-03	-22	10.6	10.7	1
EOP-0.3-15 min	0.027	0.025	-10	2.71E-03	8.83E-04	-67	10.7	10.7	0
EOP-0.3-90 min	0.022	0.024	8	2.61E-04	3.10E-06	-99	10.6	10.7	1
EOP-0.5-90 min	0.020	0.023	15	1.83E-03	1.52E-05	-99	10.6	10.7	1

Table 12. Measured and simulated values together with relative error for alkaline extraction experiments (paper [IV])

	TOC (mg/kg water)			COD (mg/kg water)			AOX (mg/kg water)		
	measured	simulated	Δ (%)	measured	simulated	Δ (%)	measured	simulated	Δ (%)
E-1.2-90 min	730	717	-2	2100	1908	-9	8.3	7.7	-8
E-1.7-5 min	550	658	20	1800	1775	-1	6.5	7.4	13
E-1.7-15 min	600	689	15	1800	1842	2	6.9	7.6	10
E-1.7-90 min	750	719	-4	2200	1914	-13	7.7	7.7	0
E-3-90 min	900	722	-20	2300	1923	-16	7.4	7.8	6
EP-0.3-5 min	n.d.			n.d.	1917		8.0	8.2	2
EP-0.3-15 min	n.d.			n.d.	2042		8.3	8.8	6
EP-0.3-90 min	n.d.			n.d.	2130		8.7	9.0	4
EP-0.5-90 min	870	850	-2	2500	2168	-13	8.1	9.2	13
EP-1-90 min	900	873	-3	1800	2212	23	8.2	9.5	15
E-2.5-P-0.5-15 min	750	822	10	2000	2109	5	n.d.		
E-2.5-P-0.5-90 min	940	860	-9	2500	2190	-12	8.3	9.4	13
EO-2-5 min	620	683	10	1900	1833	-4	7.2	6.2	-14
EO-2-15 min	650	711	9	2000	1895	-5	7.7	6.4	-17
EO-2-90 min	860	763	-11	2500	2019	-19	8.0	6.7	-16
EO-4-90 min	860	775	-10	2500	2047	-18	8.2	6.8	-17
EOP-0.3-5 min	n.d.			n.d.	1942		7.1	7.3	3
EOP-0.3-15 min	n.d.			n.d.	2040		7.7	7.8	2
EOP-0.3-90 min	890	832	-6	2300	2133	-7	n.d.		
EOP-0.5-90 min	920	850	-8	2300	2164	-6	8.2	8.6	4

Table 13. Measured and simulated values together with relative error for alkaline extraction experiments (paper [IV])

	CO2 (mol/kg water)			Formic acid (mol/kg water)			Glycolic acid (mol/kg water)		
	measured	simulated	Δ (%)	measured	simulated	Δ (%)	measured	simulated	Δ (%)
E-1.2-90 min	4.69E-04	1.61E-04	-66	1.98E-04	9.00E-05	-54	8.28E-05	2.73E-06	-97
E-1.7-5 min	1.20E-03	3.58E-05	-97	9.56E-05	2.73E-05	-71	4.73E-05	3.16E-07	-99
E-1.7-15 min	1.13E-03	1.05E-04	-91	1.11E-04	5.83E-05	-47	5.65E-05	1.78E-06	-97
E-1.7-90 min	1.13E-03	1.47E-04	-87	1.89E-04	7.14E-05	-62	1.07E-04	2.85E-06	-97
E-3-90 min	n.d.	-1.00E+00		n.d.	4.46E-05		n.d.	2.52E-06	
EP-0.3-5 min	1.47E-03	4.04E-04	-73	1.96E-04	1.82E-04	-7	5.39E-05	9.30E-06	-83
EP-0.3-15 min	1.33E-03	7.69E-04	-42	2.13E-04	2.82E-04	33	9.34E-05	2.83E-05	-70
EP-0.3-90 min	1.08E-03	9.81E-04	-9	2.43E-04	3.39E-04	39	2.16E-04	4.45E-05	-79
EP-0.5-90 min	n.d.	-1.00E+00		n.d.	4.51E-04		n.d.	7.13E-05	
EP-1-90 min	n.d.	-1.00E+00		n.d.	6.60E-04		n.d.	1.29E-04	
E-2.5-P-0.5-15 min	2.33E-03	1.10E-03	-53	2.17E-04	3.10E-04	43	1.25E-04	5.64E-05	-55
E-2.5-P-0.5-90 min	2.33E-03	1.35E-03	-42	3.89E-04	3.76E-04	-3	3.79E-04	8.96E-05	-76
EO-2-5 min	1.39E-03	4.86E-05	-96	1.11E-04	3.15E-05	-72	6.31E-05	3.30E-07	-99
EO-2-15 min	1.11E-03	1.10E-04	-90	1.13E-04	5.38E-05	-52	6.84E-05	1.24E-06	-98
EO-2-90 min	1.51E-03	1.39E-04	-91	2.48E-04	6.14E-05	-75	2.41E-04	1.73E-06	-99
EO-4-90 min	1.14E-03	1.42E-04	-88	2.15E-04	6.13E-05	-71	1.84E-04	1.72E-06	-99
EOP-0.3-5 min	1.34E-03	4.59E-04	-66	1.80E-04	1.78E-04	-1	5.92E-05	8.57E-06	-86
EOP-0.3-15 min	1.33E-03	8.30E-04	-37	2.22E-04	2.76E-04	24	1.04E-04	2.58E-05	-75
EOP-0.3-90 min	9.77E-04	1.05E-03	8	2.45E-04	3.33E-04	36	2.10E-04	4.13E-05	-80
EOP-0.5-90 min	9.83E-04	1.33E-03	36	3.11E-04	4.56E-04	47	2.27E-04	7.11E-05	-69

Table 14. Measured and simulated values together with relative error for alkaline extraction experiments (paper [IV]).

	Chloride (mol/kg water)			Liquid absorbance (-)			Yield (w-%)		
	measured	simulated	Δ (%)	measured	simulated	Δ (%)	measured	simulated	Δ (%)
E-1.2-90 min	6.21E-04	3.47E-04	-44	0.98	0.47	-52	99.1	98.8	0
E-1.7-5 min	2.96E-04	3.47E-04	17	0.64	0.72	12	98.5	98.9	0
E-1.7-15 min	3.07E-04	3.47E-04	13	0.81	0.53	-35	98.5	98.9	0
E-1.7-90 min	3.47E-04	3.47E-04	0	0.95	0.46	-51	98.3	98.8	1
E-3-90 min	n.d.	3.46E-04		n.d.			98.0	98.8	1
EP-0.3-5 min	3.13E-04	3.46E-04	11	0.18	0.23	27	n.d.	98.8	
EP-0.3-15 min	3.55E-04	3.46E-04	-3	0.08	0.12	56	98.3	98.7	0
EP-0.3-90 min	3.75E-04	3.45E-04	-8	0.40	0.09	-78	98.2	98.6	0
EP-0.5-90 min	n.d.	3.45E-04		0.21	0.06		98.7	98.6	0
EP-1-90 min	n.d.	3.44E-04		n.d.			98.2	98.6	0
E-2.5-P-0.5-15 min	2.23E-04	3.45E-04	55	0.17	0.07	-61	98.9	98.7	0
E-2.5-P-0.5-90 min	3.07E-04	3.45E-04	12	0.13	0.06	-57	97.3	98.6	1
EO-2-5 min	3.02E-04	3.47E-04	15	0.67	0.94	41	n.d.	98.9	
EO-2-15 min	3.36E-04	3.47E-04	3	0.78	0.72	-8	n.d.	98.9	
EO-2-90 min	3.89E-04	3.47E-04	-11	0.94	0.51	-46	n.d.	98.8	
EO-4-90 min	3.89E-04	3.46E-04	-11	0.89	0.45	-49	n.d.	98.7	
EOP-0.3-5 min	3.30E-04	3.46E-04	5	0.18	0.26	49	n.d.	98.8	
EOP-0.3-15 min	3.33E-04	3.45E-04	4	0.11	0.12	13	n.d.	98.7	
EOP-0.3-90 min	3.86E-04	3.45E-04	-11	0.32	0.07	-77	n.d.	98.6	
EOP-0.5-90 min	3.58E-04	3.44E-04	-4	n.d.			n.d.	98.6	

9. Conclusions

In the introduction, it was indicated that there is both a need and an opportunity for the development of the physico-chemical model presented in this thesis. The need originates from the increasing complexity of processes. On the other hand, a vast amount of knowledge is needed in the development of physico-chemical models, and this knowledge is available.

The second chapter introduced the systematic approach chosen for modelling the chemical composition of systems containing wood fibres, water, chemicals, and reaction products. The chemical composition is modelled mainly with CAS-components. Polymers were modelled with monomeric pseudo-components. The monomeric pseudo-components resemble the real structures analysed from the fibres or from model compound studies. The conversion of chemical composition into generally used engineering parameters (kappa number, ISO brightness, intrinsic viscosity, etc.) was presented. Modelling of chemical composition with CAS-components and pseudo-components provides the opportunity to validate the model with advanced analytical tools, such as nuclear magnetic resonance spectroscopy or capillary electrophoresis (paper [III]). On the other hand, through the conversion of chemical composition into engineering parameters, simpler analytical methods can be used in model development as well (paper [IV]).

The third and fourth chapters presented the equations selected from the literature and derived in this thesis for modelling the relevant phenomena and unit operations. Different bleaching sequences can now be studied using the developed unit operation models. The fifth chapter presented the practical simulator implementation aspects. The rate-based method for solving phase and reaction equilibria, developed in this work, was presented. This method has proven to be more robust than the method based on solving the system of equations.

Chapter 6 introduced the cases studied in detail in this thesis. Remarks concerning the experimental setups and analyses were done from the

modelling point-of-view. It was pointed out that it is crucial to mimic the experimental conditions as precisely as possible in the simulations. On the other hand, it is important to make sure that the conditions in the experiments correspond to the assumptions done in the modelling. This especially applies to the mixing conditions in the experiments. The importance of performing a sufficiently detailed analysis of the raw material and the samples from the experiments was emphasized.

Chapter 7 demonstrated that in comprehensive modelling of the reaction kinetics of wood/pulp treatments in aqueous solutions, it is crucial to model the reaction and phase equilibria simultaneously. The influence of inert species and buffers on the pH evolution was discussed. pKa and pH together determine the degree of dissociation of the reactants. The role of phase equilibria, both the ion exchange between the liquid phases and the gas-liquid equilibrium, on the concentration of reactants in the actual reaction site was discussed. The degree of dissociation and the concentration of reactants have an effect on the reaction rates. The knowledge of the reaction rates is important, because the reaction rates determine the size of the equipment at a given production rate.

An important feature of the physicochemical modelling approach is that it enables the exploitation of data from various literature sources and almost all parameters have some kind of physical meaning. The physicochemical modelling approach provides a great opportunity for the quantitative testing of theories concerning reaction mechanisms. Most of the reaction mechanisms applied in this thesis were adopted from the literature and they seemed to fit the measurement data reasonably well.

10. Ideas for future research

Concerning future research, the most important result achieved in this thesis is the platform for the simulation of chemical treatments of wood fibres in aqueous solutions. It is fairly easy for experts in chemistry and modelling to add new compounds and reaction chemistries to the database and simulator. Thus, in the future the platform can be used for studies concerning existing and new chemistries and thus support the revitalization of the Finnish pulp and paper industry.

Concerning the cases presented in this thesis, the reaction libraries for the simulation of hot water extraction and oxygen delignification were not complete. In the modelling of hot water extraction, only the reactions affecting pH evolution were considered. However, the real interest in hot water extraction is the extraction of hemicelluloses, either in polymeric form or as sugar monomers. Thus, the reactions leading to the extraction of hemicelluloses and their hydrolysis into monomers should be combined with the reactions affecting the pH. The reactions of carbohydrates are not complete for oxygen delignification either. The mechanism leading to an intrinsic viscosity drop in oxygen delignification is similar to that developed for alkaline extraction. However, it is likely that the oxidation of the reducing end groups in carbohydrates should be modelled as well in order to obtain a realistic model for oxygen delignification. Substantial hemicelluloses degradation also takes place in the kraft pulping liquor impregnation stage.

It should be noted that the developed platform is not restricted to systems treating wood fibres. The platform could be extended to model a multi-solvent electrolyte system. This extension would be useful in studies concerning ionic liquids and amines. Ionic liquids have been studied a lot recently, and also pulp and wood has been treated with these solvents. Amine systems, in turn, are important in the field of sour gas absorption (cleaning of marine exhaust and the oil industry).

Besides the model development work, which aims to reveal the relevant phenomena to be modelled, more emphasis should be placed in the future on using the model in actual process optimization work.

References

Ala-Kaila, K. Modeling of mass transfer phenomena in pulp-water suspensions, Ph.D. Thesis, Helsinki University of Technology, Espoo, Finland, 1998.

Bogren, J., Brelid, H., Theliander, H. (2008) Effect of pulping conditions on the rates of formation and degradation of hexenuronic acid in Scots Pine. J. Pulp Paper Sci. 34:23-29.

Boroumand, F., Moser, J. E., van, d. B. (1992) Quantitative diffuse reflectance and transmittance infrared spectroscopy of nondiluted powders. Appl. Spectrosc. 46:1874-1886.

Borrega, M., Nieminen, K., Sixta, H. (2011) Degradation kinetics of the main carbohydrates in birch wood during hot water extraction in a batch reactor at elevated temperatures. Bioresour. Technol. 102:10724-10732.

Brogdon, B. N. (2001) Influence of oxidized lignin structures from chlorine dioxide delignified pulps on the kappa number test. J. Pulp Paper Sci. 27:364-369.

Bygrave, G., Englezos, P. (2000) Thermodynamics-based model and data for Ca, Mg, and Na ion partitioning in kraft pulp fibre suspensions. Nord. Pulp Paper Res. J. 15:155-159.

cepi, Key statistics: European Pulp and Paper Industry 2012 (cepi report), http://www.cepi.org/system/files/public/documents/publications/statistics/2013/Key%20Statistics%20Report%202012.pdf (accessed 11/19, 2013).

Christian, J. B. (2003) Simulating aqueous processes. Chem. Eng. Prog. 99:32-39.

FAO, Pulp and paper capacities (FAO report), http://www.fao.org/docrep/018/i3353t/i3353t.pdf (accessed 11/19, 2013).

Ganster, J.and Fink, H. -. (2005) Physical constants of cellulose. In: Polymer Handbook. Eds. Brandrup, J., Immergut, E.H., Grulke, E.A., Abe, A. and Bloch, D.R. John Wiley & Sons, New York, USA. pp. 135-157.

Garrote, G., Dominguez, H., Parajo, J. C. (1999) Hydrothermal processing of lignocellulosic materials. Holz. Roh. Werkst. 57:191-202.

Grenthe, I., Hummel, W., Puigdomenech, I. (1997) Chapter III: Chemical background for the modelling of reactions in aqueous systems. In: Modelling in Aquatic Chemistry. Eds. Grenthe, I. and Puigdomenech, I. OECD Publications, pp. 69-129.

Grenthe, I.and Puigdomenech, I. (1997) Chapter II: Symbols, standards, and conventions. In: Modelling in Aquatic Chemistry. Eds. Grenthe, I. and Puigdomenech, I. OECD Publications, pp. 35-67.

Grignon, J., Scallan, A. M. (1980) Effect of pH and neutral salts upon the swelling of cellulose gels. J Appl Polym Sci 25:2829-2843.

Helfferich, F. Ion Exchange. McGraw-Hill, New York, 1962.

Horvath, A. L. Handbook of Aqueous Electrolyte Solutions. John Wiley & Sons, Southampton, Great Britain, 1985.

Inalbon, M. C., Mocchiutti, P., Zanuttini, M. (2009) The deacetylation reaction in eucalyptus wood: Kinetics and effects on the effective diffusion. Bioresour. Technol. 100:2254-2258.

Jaatinen, T. , Finnish forest industry in January-June 2013: European market situation remains challenging - domestic costs must be kept in check, http://www.forestindustries.fi/newsroom/press-releases/Finnish-forest-industry-in-January-June-2013--European-market-situation-remains-challenging---domestic-costs-must-be-kept-in-check-1319.html (accessed 11/19, 2013).

Jain, S., Mortha, G., Calais, C. (2008) New predictive models for COD from all stages in full ECF bleaching sequences. In: 10th International Conference on Computer Modelling and Simulation, April 1-3, Cambridge. Institute of Electrical and Electronics Engineers Computer Society, Cambridge, United Kingdom, pp. 278-283.

Jakobsson, K., Aittamaa, J. , Kinfit parameter optimization software, http://chemtech.aalto.fi/en/research/groups/chemical_engineering/software/kinfit/ (accessed 11/24, 2013).

Ji, Y. Kinetics and mechanism of oxygen delignification, Ph.D. Thesis, The University of Maine, 2007.

Kalliola, A., Kuitunen, S., Liitiä, T., Rovio, S., Ohra-aho, T., Vuorinen, T., Tamminen, T. (2011) Lignin oxidation mechanisms under oxygen delignification conditions. Part 1. Results from direct analyses. Holzforsch. 65:567-574.

Kalliola, A., Kangas, P., Kuitunen, S. (2012) Simulating A/D stage bleaching chemistry. In: 12th European workshop on Lignocellulosics and pulp (EWLP), August 27-30, Espoo. pp. 308-311.

Koukkari, P., Pajarre, R., Pakarinen, H. (2002) Modeling of the ion exchange in pulp suspensions by Gibbs energy minimization. J. Solution Chem. 31:627-638.

Kubelka, P., Munk, F. (1931) Ein Beitrag zur Optik der Farbanstriche. Zeitschrift für technische Physik 12:593-601.

Kuitunen, S., Pulkkinen, I., Tarvo, V., Alopaeus, V. (2011) Modeling of fiber swelling. In: 5th International Colloquium on Eucalyptus Pulp, May 8-11, Porto Seguro.

Kuitunen, S., Alopaeus, V. (2013) Robust method for solving reaction and phase equilibrium in aqueous wood fiber systems. In: 9th European Congress of Chemical Engineering, April 21-25, Hague.

La Mer, V. K. (1932) Reaction velocity in ionic systems. Chem. Rev. 10:179-212.

Laliberte, M., Cooper, W. E. (2004) Model for calculating the density of aqueous electrolyte solutions. J. Chem. Eng. Data 49:1141-1151.

Laliberte, M. (2007a) Model for calculating the viscosity of aqueous solutions. J. Chem. Eng. Data 52:321-335.

Laliberte, M. (2007b) Model for calculating the viscosity of aqueous solutions, J. Chem. Eng. Data 52:1507-1508.

Lehtimaa, T. Reactions of chlorine (III) and their kinetics in the chlorine dioxide bleaching of kraft pulps, Ph.D. Thesis, Aalto University, Espoo, 2010.

Lehtimaa, T., Kuitunen, S., Tarvo, V., Vuorinen, T. (2010) Kinetics of aldehyde oxidation by chlorous acid. Industrial and Engineering Chemistry Research 49:2688-2693.

Levenspiel, O. Chemical Reaction Engineering. John Wiley & Sons, Singapore, 1972.

Li, J., Gellerstedt, G. (1997) The contribution to kappa number from hexeneuronic acid groups in pulp xylan. Carbohydr. Res. 302:213-218.

Li, J., Sevastyanova, O., Gellerstedt, G. (2002) The relationship between kappa number and oxidizable structures in bleached kraft pulps. J. Pulp Paper Sci. 28:262-266.

Li, J., Gellerstedt, G. (1998) On the structural significance of the kappa number measurement. Nord. Pulp Paper Res. J. 13:153-158.

Lide, D. R. CRC Handbook of Chemistry and Physics. CRC Press, Boca Raton, 1994.

Lindgren, J., Öhman, L. (2000) Characterization of acid/base properties for bleached softwood fibers as influenced by ionic salt medium. Nord. Pulp Pap. Res. J. 15:18-23.

Lindgren, J., Wiklund, L., Ohman, L. (2001) The contemporary distribution of cations between bleached softwood fibres and the suspension liquid, as a function of -log[H^+], ionic strength and temperature. Nord. Pulp Paper Res. J. 16:24-32.

Luyben, W. L. Process Modeling, Simulation and Control for Chemical Engineers. McGraw-Hill, Singapore, 1990.

Maja, S. Modeling Displacement Washing of Pulp, M.Sc. Thesis, Helsinki University of Technology, Espoo, Finland, 2006.

Morel, F. M. M., Hering, J. G. Principles and Applications of Aquatic Chemistry. John Wiley & Sons, New York, 1993.

Newman, J. S. Electrochemical Systems. Pretice-Hall, New Jersey, 1991.

Petzold, L. R. , DDASSL, http://pitagora.dm.uniba.it/~testset/solvers/dassl.php (accessed 11/24, 2013).

Pitzer, K. S. Activity Coefficients in Electrolyte Solutions. CRC Press, London, 1991.

Pöyry, Pulp market in transition (Pöyry Management Consulting report), http://www.poyry.com/sites/default/files/imce/0011_2013_v1_pulp_market_in_transition_final_small.pdf (accessed 11/19, 2013).

Press, W. H., Flannery, B. P., Teukolsky, S. A., Vetterling, W. T. Numerical Recipes - the Art of Scientific Computing (FORTRAN Version). Cambridge University Press, Cambridge, 1989.

Pu, Q., Gustafson, R., Sarkanen, K. (1993) Donnan equilibria in wood-alkali interactions Part 3. Theoretical modeling. J. Wood Chem. Technol. 13:1.

Puigdomenech, I., Rard, J. A., Plyasunov, A. V., Grenthe, I. (1997) Chapter X: Temperature corrections to thermodynamic data and enthalpy calculations. In: Modelling in Aquatic Chemistry. Eds. Grenthe, I. and Puigdomenech, I. OECD Publications, pp. 427-493.

Ragauskas, A. J., Nagy, M., Kim, D. H., Eckert, C. A., Hallett, J. P., Liotta, C. L. (2006a) From wood to fuels: Integrating biofuels and pulp production full access. Industrial Biotechnology 2:55-65.

Ragauskas, A. J., Williams, C. K., Davison, B. H., Britovsek, G., Cairney, J., Eckert, C. A., Frederick Jr, W. J., Hallett, J. P., Leak, D. J., Liotta, C. L., Mielenz, J. R., Murphy, R., Templer, R., Tschaplinski, T. (2006b) The path forward for biofuels and biomaterials. Science 311:484-489.

Ragnar, M., Lindgren, C. T., Nilvebrant, N. (2000) pK_a-values of guaiacyl and syringyl phenols related to lignin. J. Wood Chem. Technol. 20:277-305.

Räsänen, E., Stenius, P., Tervola, P. (2001) Model describing Donnan equilibrium, pH and complexation equilibria in fibre suspensions. Nord. Pulp Paper Res. J. 16:130-139.

Räsänen, E. Modelling ion exchange and flow in pulp suspension, Ph.D. Thesis, VTT Processes, Espoo, Finland, 2003.

Räsänen, E., Laitinen, A., Van Heiningen, A. R. P., Koukkari, P. (2005) Application of donnan equilibrium theory for improved bleaching process chemistry. In: 59th Appita Annual Conference and Exhibition, incorporating the 13th ISWFPC: International Symposium on Wood, Fibre and Pulping Chemistry. Appita Inc., Carlton, 3053, Australia, Auckland, New Zealand, pp. 321-327.

Reid, R. C., Prausnitz, J. M., Poling, B. E. The Properties of Gases and Liquids. McGraw-Hill, New York, USA, 1987.

Rewatkar, V. B., Bennington, C. P. J. (2000) Gas-liquid mass transfer in low- and medium-consistency pulp suspensions. Can. J. Chem. Eng. 78:504-512.

Rose, A., Sweeny, R. F., Schrodt, V. (.1958) Continuous distillation calculations by relaxation method. Ind. Eng. Chem. 50:737-740.

Salminen, J., Koukkari, P., Jäkärä, J., Paren, A. (2000) Thermochemical experiments and modelling of the PO bleaching stage. J. Pulp Paper Sci. 26:441-447.

Saltberg, A., Brelid, H., Theliander, H. (2006) Removal of metal ions from wood chips during acidic leaching 1: Comparison between Scandinavian softwood, birch and eucalyptus. Nord. Pulp Paper Res. J. 21:507-512.

Sandler, S. I. Chemical and Engineering Thermodynamics. John Wiley & Sons, New York, 1989.

Sankari, M., Ala-Kaila, K., Dahl, O., Perämäki, P. (2004) Real wash loss compounds in oxygen delignification of softwood kraft pulp. Nord. Pulp Paper Res. J. 19:264-270.

Scallan, A. M. (1983) Effect of acidic groups on swelling of pulps: A review. Tappi J. 66:73-75.

Scallan, A. M., Tigerstrom, A. C. (1992) Swelling and elasticity of the cell walls of pulp fibers. J. Pulp Paper Sci. 18:188-192.

Schmidt, J.and Heitner, C. (1999) Use of diffuse reflectance UV-visible spectroscopy to characterize chromophores in wood fibers. In: Advances in Lignocellulosic Characterization. Eds. Argyropoulos, D.S. Tappi Press, Atlanta. pp. 179-199.

Sixta, H., Potthast, A., Krotschek, A. W. (2006a) Chemical pulping processes. In: Handbook of Pulp. Eds. Sixta, H. Wiley-VCH Verlag GmbH, Weinheim. pp. 109-229.

Sixta, H., Suess, H., Potthast, A., Schwanninger, M., Krotscheck, A. W. (2006b) Raw material for pulp. In: Handbook of Pulp. Eds. Sixta, H. Wiley-VCH Verlag GmbH, Weinheim. pp. 21-68.

Sjöström, E. (1989) Origin of charge on cellulosic fibers. Nord. Pulp Paper Res. J. 4:90-93.

Song, T., Pranovich, A., Sumerskiy, I., Holmbom, B. (2008) Extraction of galactoglucomannan from spruce wood with pressurised hot water. Holzforschung 62:659-666.

Stone, J. E., Scallan, A. M. (1968) A structural model for the cell wall of water-swollen wood pulp fibers based on their accessibility to macromolecules. Cellulose Chem Tehnol. 2:343-358.

Stumm, W., Morgan, J. J. Aquatic Chemistry. John Wiley & Sons, New York, 1996.

Susilo, J., Bennington, C. P. J. (2007) Modelling kappa number and pulp viscosity in industrial oxygen delignification systems. Chem. Eng. Res. Design 85:872-881.

Susilo, R., Chandraghatgi, R., Englezos, P. (2005) Partitioning of iron, manganese, copper between fibres and liquor and the role of water chemistry. Pulp and Paper Canada 106:47-50.

Taloussanomat, PIX-Sellu (FOEX), Taloussanomat/Pörssi, http://porssi.taloussanomat.fi/commodities/startel_factsheet_overview.html?&STARTEL_SYM=SELLU.XXX&START=1 (accessed 11/19, 2013).

Tarvo, V. Modeling chlorine dioxide bleaching of chemical pulp, Ph.D. Thesis, Aalto University, Espoo, 2010.

Tarvo, V., Lehtimaa, T., Kuitunen, S., Alopaeus, V., Vuorinen, T., Aittamaa, J. (2010) A model for chlorine dioxide delignification of chemical pulp. J. Wood Chem. Technol. 30:230-268.

Towers, M., Scallan, A. M. (1996) Predicting the ion-exchange of kraft pulps using Donnan theory. J. Pulp Paper Sci. 22:J332-J337.

van der Stegen, J. H. G., Weerdenburg, H., van der Veen, A. J., Hogendoorn, J. A., Versteeg, G. F. (1999) Application of the Pitzer model for the estimation of activity coefficients of electrolytes in ion selective membranes. Fluid Phase Equilib. 157:181-196.

van Heiningen, A., Tunc, M. S., Gao, Y., Da, S. P. (2004) Relationship between alkaline pulp yield and the mass fraction and degree of polymerization of cellulose in the pulp. J. Pulp Paper Sci. 30:211-217.

van Heiningen, A., Krothapalli, D., Genco, J., Justason, A. (2003) A chemical reactor analysis of industrial oxygen delignification. Pulp and Paper Canada 104:96-101.

Visuri, J. A., Song, T., Kuitunen, S., Alopaeus, V. (2012) Model for degradation of galactoglucomannan in hot water extraction conditions. Ind Eng Chem Res 51:10338-10344.

Vos, K. D., Burris, F. O., Riley, R. L. (1966) Kinetic study of the hydrolysis of cellulose acetate in the pH range of 2-10. J Appl Polym Sci 10:825-832.

Werkelin, J., Skrifvars, B., Zevenhoven, M., Holmbom, B., Hupa, M. (2010) Chemical forms of ash-forming elements in woody biomass fuels. Fuel 89:481-493.

Zawadzki, M., Runge, T., Ragauskas, A. (1998) Chromophore properties of high brightness pulps. In: Pulping Conference, October 25 - 29, Quebec. TAPPI, Atlanta, USA, pp. 1551-1560.

Zhang, D. C., Hsieh, J., Chai, X. -., Ragauskas, A. J. (2007) Experimental and modeling of carbonate formation in the effluent of oxygen delignification. AlChE J. 53:669-677.

Zhang, X. Z., Ni, Y., Van Heiningen, A. R. P. (1998) Effect of consistency on chemical pulp ozonation; calculation of the effective capillary cross-sectional area (ECCSA) and tortuosity (l) of the fiber wall. In: 5th European Workshop on Lignocellulosics and Pulp. Portugal, pp. 413-416.

Errata

Paper [II] , 3rd page, 1st paragraph: OH_{phen} should be GOH.

Paper [III], Tables 2 and 3: The unit for Arrhenius frequency factor (A) is written as “mol/kg water/s”, but it should be “kg water/mol/s”.

Paper [III], Table 2: The stoichiometry for reaction R30 is written as “$oQ+HO^- \rightarrow hydQO^- + HO^-$“, but it should be “$oQ+HO^- \rightarrow hydQO^-$“.

Paper [III], Table 2: For reaction 34, the Arrhenius frequency factor $6.38\pm0.91\ 10^{10}$ should be $6.38\pm0.91\times10^{10}$.

Paper [III], Table 6: The text “Units presented as mmol kg/water” should be “Units presented as mmol/ kg water”

Paper [IV], 2nd page, 1st paragraph: “AE” should be replaced by “alkaline extraction”.

Paper [IV], Table 7: The unit for Arrhenius frequency factor (A) and rate constant (k) depends on the rate law. The unit given in the header is correct for all other reactions, except for R9 (the unit should be $mol^{-0.46}$ (kg water)$^{0.46}$ s^{-1}), R14 (s^{-1}), R15 (mol^{-3} (kg water)^3 s^{-1}), and R16 (mol^{-3} (kg water)^3 s^{-1}).

Aalto-DD 37/2014

ISBN 978-952-60-5617-3
ISBN 978-952-60-5618-0 (pdf)
ISSN-L 1799-4934
ISSN 1799-4934
ISSN 1799-4942 (pdf)

Aalto University
School of Chemical Technology
Department of Biotechnology and Chemical Technology
www.aalto.fi

BUSINESS +
ECONOMY

ART +
DESIGN +
ARCHITECTURE

SCIENCE +
TECHNOLOGY

CROSSOVER

DOCTORAL
DISSERTATIONS